농학박사학위논문

TRPM7 기능 억제가 삼중음성유방암 세포의 증식 및 전이에 미치는 영향 규명

Effects of TRPM7 Suppression on Invasion and Proliferation of TNBC Cells

2020년 8월

서울대학교 대학원
농생명공학부 응용생명화학전공
송 치 만

A Dissertation for the Degree of Doctor of Philosophy

Effects of TRPM7 Suppression on Invasion and Proliferation of TNBC Cells

August 2020

Chiman Song
Applied Life Chemistry Major
Department of Agricultural Biotechnology
Seoul National University

TRPM7 기능 억제가 삼중음성유방암 세포의 증식 및 전이에 미치는 영향 규명

Effects of TRPM7 Suppression on Invasion and Proliferation of TNBC Cells

지도교수 오 기 봉

이 논문을 농학박사학위논문으로 제출함
2020년 5월

서울대학교 대학원
농생명공학부 응용생명화학전공

송 치 만

송치만의 박사학위논문을 인준함
2020년 7월

위 원 장 이 상 기 (인)

부 위 원 장 오 기 봉 (인)

위 원 배 의 영 (인)

위 원 권 용 훈 (인)

위 원 심 태 보 (인)

Effects of TRPM7 Suppression on Invasion and Proliferation of TNBC Cells

Advisor: Ki-Bong Oh

A Dissertation Submitted in Partial Fulfillment
of the Requirement for the Degree of

DOCTOR OF PHILOSOPHY

to the Faculty of
Applied Life Chemistry Major,
Department of Agricultural Biotechnology

at

SEOUL NATIONAL UNIVERSITY

by

Chiman Song

Date Approved

July. 2020

Chair Sangkee Rhee (Seal)

Vice Chair Ki-Bong Oh (Seal)

Examiner Euiyoung Bae (Seal)

Examiner Yonghoon Kwon (Seal)

Examiner Taebo Sim (Seal)

Abstract

Triple-negative breast cancer (TNBC) is the worst breast cancer subtype because it has the highest metastatic potential and rate of recurrence. However, there are no effective therapies for TNBC, which lacks receptors such as estrogen receptors, progesterone receptors, and human epidermal growth factor receptor 2. Transient receptor potential cation channel subfamily M member 7 (TRPM7), composed of an ion channel and a kinase domain, regulates TNBC cell migration, invasion, and metastasis in its kinase domain-dependent manner. At present, little is known about the effects of TRPM7 kinase inhibitor on TNBC due to lack of potent TRPM7 kinase inhibitors. In part II of this study, I report a novel TRPM7 kinase inhibitor (TG100-115), that suppresses migration of TNBC cells. TG100-115 inhibits TRPM7 kinase activity in an ATP competitive fashion with over 70-fold stronger activity than that of rottlerin, known as a TRPM7 kinase inhibitor. Moreover, TG100-115 inhibits phosphorylation of the myosin IIA heavy chain and focal adhesion kinase, which is one of the metastasis markers. TG100-115 can be used as a potent TRPM7 kinase inhibitor and a potent inhibitor of TNBC cell migration. In contrast to its involvement in TNBC cell invasion, TRPM7 has not been found to be associated with TNBC proliferation. However, part III demonstrates that suppression of TRPM7 via TRPM7 knockdown or pharmacological inhibition (NS8593 as a TRPM7 channel inhibitor and TG100-115 as a TRPM7 kinase inhibitor) synergistically increases Tumor-necrosis factor-related apoptosis-inducing ligand (TRAIL)-induced antiproliferative effects and apoptosis in TNBC cells. Furthermore, the findings demonstrate that the synergistic interaction might be associated with TRPM7 channel activities. It was also found that downregulation of cellular FLICE-inhibitory protein through inhibition of Ca^{2+} influx might be involved in the synergistic interaction. This study provides both a new role of TRPM7 in TNBC cell apoptosis and a potential combinatorial therapeutic strategy using TRPM7 inhibitors with TRAIL in treatment of TNBC.

Keywords: TRPM7, triple-negative breast cancer, TG100-115, c-FLIP, TRAIL, cell migration, apoptosis

Student number: 2014-30385

Contents

List of Figures

List of Tables

List of Abbreviations

2-APB	2-Aminoethyl diphenyl borinate
Actomyosin	Actin and myosin
AKT	Ak strain transforming
AMPK	AMP-activated protein kinase
ANOVA	Analysis of variance
ATM/ATR	Ataxia-telangiectasia mutated
ATP	Adenosine triphosphate
BAPTA-AM	1,2-Bis(o-aminophenoxy)ethane-N,N,N′,N′-tetraacetic acid, tetraacetoxymethyl ester
BRCA	Breast cancer gene
BTK	Bruton's tyrosine kinase
CaMKII	Calcium/calmodulin-dependent protein kinase II
Caspase	Cysteine-aspartic proteases
CDK	Cyclin-dependent kinase
c-FLIP	cellular FLICE-inhibitory protein
c-FLIP$_L$	Long isoform of c-FLIP
c-FLIP$_S$	Short isoform of c-FLIP
Chk	Checkpoint kinase
CK	Cytokeratin
c-Met	Mesenchymal-epithelial transition factor
CREB	cAMP response element-binding protein
CSF-1R	Colony stimulating factor 1 receptor
DISC	Death inducing signaling complex
DMEM	Dulbecco’s modified Eagle’s medium
DNA	Deoxyribonucleic acid
Dox	Doxycycline hyclate
DPBS	Dulbecco's phosphate-buffered saline
DTT	Dithiothreitol
ECL	Enhanced chemiluminescence
EDTA	Ethylenediamine tetraacetic acid
eEF2	Eukaryotic elongation factor 2
eEF-2K	Eukaryotic elongation factor-2 kinase
EGF	Epidermal growth factor

EGFR	Epidermal growth factor receptor
EGTA	Ethylene glycol-bis(β-aminoethyl ether)-N,N,N′,N′-tetraacetic acid
EMT	Epithelial-mesenchymal transition
ER	Estrogen receptor
ERK	Extracellular receptor kinase
FAK	Focal adhesion kinase
FBS	Fetal bovine serum
FDA	U.S. Food and Drug Administration
FGFR	Fibroblast growth factor receptor
FITC	Fluorescein isothiocyanate
FLT3	FMS-like tyrosine kinase 3
GSK-3	Glycogen synthase kinase-3
hBDA	human Breast ductal adenocarcinoma
HEK-293	Human embryonic kidney-293
HEPES	4-(2-Hydroxyethyl)piperazine-1-ethanesulfonic acid
HER	Human epidermal growth factor receptor
HRP	Horseradish peroxidase
HTS	High-throughput screening
IGF-1R	Insulin-like growth factor type 1 receptor
IgG	Immunoglobulin G
IKK	IκB kinase
JAK	Janus kinase
JNK	c-Jun N-terminal kinase
LRRK2	Leucine rich repeat kinase 2
MAPK	Mitogen-activated protein kinase
MBP	Myelin basic protein
MEK/MAP2K1	Mitogen-activated protein kinase kinase
MHC	Myosin heavy chain
MHR	Melastatin homologous region
mTOR	mammalian Target of rapamycin
P2RX7	P2X purinoceptor 7
PAGE	Polyacrylamide gel electrophoresis
PARP	Poly (ADP-ribose) polymerase
PBS	Phosphate buffered saline
PCR	Polymerase chain reaction

PDGFR	Platelet-derived growth factor receptor
PDK-1	3-Phosphoinositide-dependent kinase 1
PFKFB3	6-Phosphofructo-2-kinase
PI	Propidium iodide
PI3K	Phosphoinositide 3-kinase
PKC	Protein kinase C
PLCγ2	Phospholipase Cγ2
PLK	Polo-like kinase
PR	Progesterone receptor
PVDF	Polyvinylidene fluoride
RIPA buffer	Radio-Immunoprecipitation Assay buffer
ROCK	Rho-associated protein kinase
RPMI	Roswell Park Memorial Institute
RT	Room temperature
RTK	Receptor tyrosine kinase
RT-PCR	Reverse transcription polymerase chain reaction
S1P	Sphingosine-1-phosphate
SD	Standard deviation
SDS	Sodium dodecyl sulfate
SGK	Serum and glucocorticoid-activated kinase
siRNA	small interfering Ribonucleic acid
SPA	Scintillation proximity assay
Src	Sarcoma
STAT	Signal transducer and activator of transcription
STIM1	Stromal interaction molecule 1
Syk	Spleen associated tyrosine Kinase
Tie-2	Tunica interna endothelial cell kinase 2
TNBC	Triple-negative breast cancer
TRAIL	Tumor necrosis factor-related apoptosis-inducing ligand
T-Rex	Tetracycline-Regulated Expression
TR-FRET	Time-resolved fluorescence resonance energy transfer
Tris	Tris(hydroxymethyl) aminomethane
TRP	Transient receptor potential
TRPM7	Transient receptor potential cation channel subfamily M member 7
Tween-20	Polyoxyethylene sorbitol ester 20

VEGFR	Vascular endothelial growth factor receptor
WNT	Wingless-related integration site

Part I

Literature Review

Absence of potent therapeutic strategies for TNBC

Breast cancer is the most common form of diagnosed cancer and the second leading cause of cancer-related death among women in the United States (Siegel et al., 2019). It is a highly heterogeneous disease that varies in histological features, therapeutic responses, and molecular profiles. Breast cancer cell types are classified as luminal A subtype (ER^+/PR^+ or $^-/HER\text{-}2^-$), luminal B subtype ($ER^+/PR^+/HER\text{-}2^+$), HER-2 enriched subtype (ER^- and or$/PR^-/HER\text{-}2^+$), basal-like subtype (ER^- and/or PR^-, $HER\text{-}2^-$, $CK5/6^+$, $CK14^+$, $CK17^+$, and $EGFR^+$), and normal breast-like type (ER^- and/or PR^-, $HER\text{-}2^-$, $CK5/6^-$, $CK14^-$, $CK17^-$, $EGFR^-$) (Mackay et al., 2011; Medina et al., 2020) (Figure 1.1). Luminal A breast cancers are often low grade with slow tumor growth and tend to be treatable with hormonal therapies such as tamoxifen (Eroles et al., 2012). Like luminal A subtype breast cancers, luminal B breast cancers are treatable with hormonal therapies, but are more aggressive and more frequently relapse (Wirapati et al., 2008; Ades et al., 2014). HER-2 enriched breast cancers tend to grow quickly and are often aggressive but are responsive to monoclonal antibodies such as trastuzumab or kinase inhibitors such as lapatinib (Ross et al., 2009). Breast cancers lacking ER, PR, and HER-2 are collectively referred to as Triple-negative breast cancers (TNBCs) and have higher metastatic potential and rates of recurrence compared to other breast cancer subtypes. Due to lack of ER, PR, and HER-2, TNBCs are not amenable to treatment with hormonal therapies or HER-2-targeted therapies. Primary systemic therapeutic strategies for patients with TNBC are conventional chemotherapeutics and radiation therapy because there are no potent FDA-approved targeted therapies for TNBC (Hwang et al., 2019). TNBC patients treated with the conventional chemotherapies have low response rates and short progression-free survival (Bardia et al., 2019).

Figure 1.1. Breast cancer subtypes. Republished with permission of Oxford University Press, from Microarray-Based Gene Expression Profiling for Molecular Classification of Breast Cancer and Identification of New Targets for Therapy, *Laboratory Medicine*, Rupninder Sandhu et al., Vol. 41(6), pp. 364-372, 2010; permission conveyed through Copyright Clearance Center, Inc.

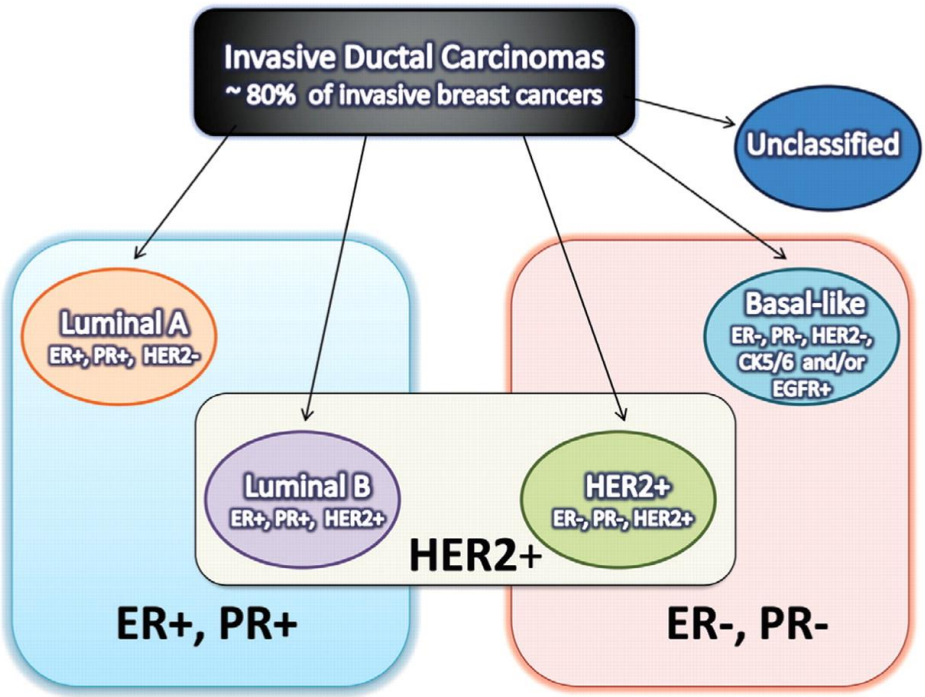
Invasive Ductal Carcinomas
~ 80% of invasive breast cancers
Unclassified
Luminal A
ER+, PR+, HER2-
Basal-like
ER-, PR-, HER2-, CK5/6 and/or EGFR+
Luminal B
ER+, PR+, HER2+
HER2+
ER-, PR-, HER2+
HER2+
ER+, PR+
ER-, PR-

Advances and limitations in targeted therapies for TNBC

TNBC accounts for approximately 15−20% of all breast cancers (Diana et al., 2018) and is more prevalent in younger premenopausal women (Foulkes et al., 2010). TNBCs are often high-grade invasive ductal carcinomas with a high proliferative activity and a large tumor size. These cancer types predominantly spread to the brain and lungs, while other breast cancer subtypes frequently disseminate to the soft tissues and bone (Dent et al., 2009). The median overall survival for patients with metastatic TNBC is approximately 18 months, while it exceeds 5 years for patients with ER^+, PR^+, and HER-2 enriched breast cancer (Swain et al., 2013; Vagia et al., 2020).

Multiple signaling pathways including RTK, non-RTK, and downstream molecules, have been proposed as therapeutic targets in TNBC (Figure 1.2). In detail, EGFR, PDGFR, VEGFR, FGFR, WNT, Hedgehog, Notch, RAS, JAK/STAT, and PI3K are established targets. For example, based on the reports that overexpression of EGFR in TNBC is involved in poor OS (Corkery et al., 2009), EGFR-targeting agents such as cetuximab and gefitinib have been approved for clinical treatments (Nakai et al., 2016). However, low efficacy has been observed in proliferation of TNBC cells treated with these agents because of the acquired resistance associated with AKT and HER-3 signaling pathways (Sergina et al., 2007; Corkery et al., 2009). Due to modest clinical outcomes in the combination therapies for TNBC patients, recent studies have focused on the combination of EGFR-targeting agents with other targeted therapies (Carey et al., 2012; Baselga et al., 2013). Meanwhile, PARP has been considered as a promising target for treatment of breast cancers with *BRCA* mutations. Approximately 70% of breast cancers with *BRCA1* mutations and about 16−23% of *BRCA2*-mutated breast cancers have TNBC phenotypes (Stevens et al., 2013). Tumors with mutation or inactivation of *BRCA* require PARP for DNA damage repair processes (Helleday, 2011; De Vos et al., 2012); thus, suppression of PARP-dependent DNA-damage repair processes could induce apoptosis and delay tumor development (Bryant et al., 2005; Farmer et al., 2005; To et al., 2014). Olaparib as a PARP inhibitor has been approved by FDA for patients with germline

BRCA-mutated, HER-2-negative metastatic breast cancers (Exman et al., 2019). Several clinical trials of olaparib as a single agent and combination therapies for TNBC are underway (Hwang et al., 2019). Nevertheless, advents of resistance to PARP inhibitors remain a limitation (Noordermeer and van Attikum, 2019). The FDA granted accelerated approval to two therapies including Trodelvy (sacituzumab govitecan-hziy) in 2020 and combination of Tecentriq (atezolizumab) with paclitaxel in 2019 for metastatic TNBC. However, treatment of Trodelvy is only approved for adults with metastatic TNBC who have received at least two previous treatments, and Tecentriq has limited potency for TNBCs whose tumors express PD-L1 ("Atezolizumab Combo Approved for PD-L1-positive TNBC", 2019). Despite advances in targeted therapies for TNBC, clinical outcomes remain unsatisfactory. Therefore, discovery of therapeutic targets and highly potent anti-cancer drugs remain necessary for treatment of TNBC.

Figure 1.2. Molecular targets and potential target inhibitors for TNBC. Republished with permission of Elsevier, from Targeted Therapies for Triple-Negative Breast Cancer: Combating a Stubborn Disease, *Trends in Pharmacological Sciences*, Murugan Kalimutho et al., Vol. 36(12), pp. 822-846, 2015; permission conveyed through Copyright Clearance Center, Inc.

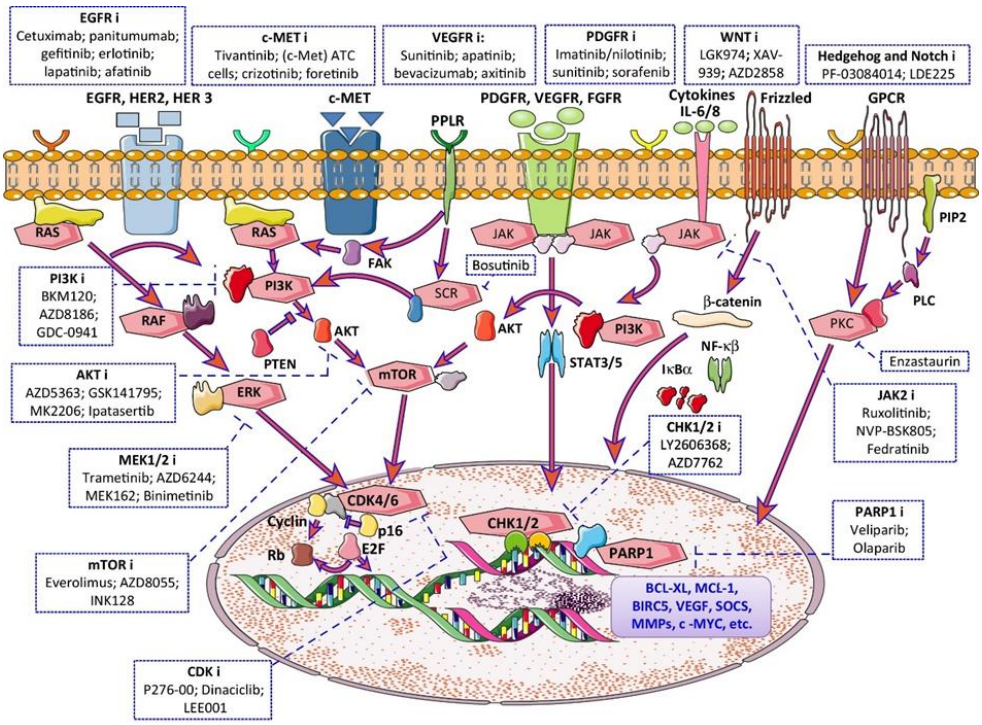
EGFR i
Cetuximab; panitumumab; gefitinib; erlotinib; lapatinib; afatinib
c-MET i
Tivantinib; (c-Met) ATC cells; crizotinib; foretinib
VEGFR i:
Sunitinib; apatinib; bevacizumab; axitinib
PDGFR i
Imatinib/nilotinib; sunitinib; sorafenib
WNT i
LGK974; XAV-939; AZD2858
Hedgehog and Notch i
PF-03084014; LDE225
EGFR, HER2, HER 3
c-MET
PPLR
PDGFR, VEGFR, FGFR
Cytokines IL-6/8
Frizzled
GPCR
PIP2
RAS
RAS
FAK
JAK
JAK
JAK
Bosutinib
PI3K i
BKM120; AZD8186; GDC-0941
PI3K
SCR
β-catenin
PLC
RAF
AKT
AKT
PI3K
PKC
PTEN
STAT3/5
NF-κβ
IκBα
Enzastaurin
AKT i
AZD5363; GSK141795; MK2206; Ipatasertib
mTOR
ERK
JAK2 i
Ruxolitinib; NVP-BSK805; Fedratinib
CHK1/2 i
LY2606368; AZD7762
MEK1/2 i
Trametinib; AZD6244; MEK162; Binimetinib
CDK4/6
Cyclin
p16
CHK1/2
PARP1 i
Veliparib; Olaparib
Rb
E2F
PARP1
mTOR i
Everolimus; AZD8055; INK128
BCL-XL, MCL-1, BIRC5, VEGF, SOCS, MMPs, c -MYC, etc.
CDK i
P276-00; Dinaciclib; LEE001

TRPM7 as a potent therapeutic target for TNBC

TRPM7 is a unique bifunctional protein composed of a non-selective cation channel domain and an alpha-kinase domain (Zou et al., 2019) (Figure 1.3). The ion channel pores of TRPM7 are permeable to cations such as Mg^{2+}, Ca^{2+}, and Zn^{2+} and its kinase domain phosphorylates annexin-1, myosin IIA heavy chain, eEF2, SMAD2, and PLCγ2 (Zou et al., 2019). The signaling pathways mediated by TRPM7 and its cellular effects in cancer have been elucidated (Yee, 2017) (Figure 1.4). In particular, TRPM7 is involved in proliferation and migration of various tumor cells such as breast cancer (Guilbert et al., 2009; Dhennin-Duthille et al., 2011; Middelbeek et al., 2012; Guilbert et al., 2013; Meng et al., 2013;), retinoblastoma (Hanano et al., 2004), gastric cancer (Kim et al., 2008; Kim et al., 2011), head and neck cancer (Jiang et al., 2007; J. P. Chen et al., 2010), pancreatic cancer (Yee et al., 2011; Rybarczyk et al., 2012; Yee et al., 2012), leukemia (Zierler et al., 2011), and prostate cancer (Sun et al., 2013). TRPM7 is overexpressed in hBDA and MCF-7 cells (Guilbert et al., 2009). Moreover, expression of TRPM7 is strongly correlated with Scarff−Bloom−Richardson grade, Ki67 proliferation index (mitosis marker), and tumor size (Guilbert et al., 2009). TRPM7 mediates cell proliferation through Ca^{2+} influx in MCF-7 cells (Guilbert et al., 2009). In contrast to hBDA and MCF7 cells, downregulation of TRPM7 seems not to affect proliferation in TNBC cells (Guilbert et al., 2013). However, in the present study, it was found that TRPM7 is associated with anti-proliferative effects in TNBC cells in the presence of TRAIL. In part III, whether suppression of TRPM7 via siRNA-mediated gene silencing and pharmacological approaches enhances TRAIL-induced apoptosis in TNBC cells is also investigated.

TRPM7 is required for cell migration and metastasis in breast cancer cells (Middelbeek et al., 2012; Guilbert et al., 2013; Meng et al., 2013), and it mediates cytoskeletal contractility and cell adhesion which are important to cell migration and invasion in MDA-MB-231 cells (TNBC cells) (Middelbeek et al., 2012). TRPM7 promotes cell migration and invasion through activation of the MAPK signaling pathway in MDA-MB-435 cells (TNBC cells) (Meng et al., 2013). It also mediates

breast cancer cell migration via phosphorylation of myosin IIA in a kinase-dependent manner (Guilbert et al., 2013). The TRPM7 kinase domain regulates actomyosin dynamics via phosphorylation of cytoskeletal proteins such as tropomodulin 1 and MHC isoforms A-C during cell migration (Clark et al., 2006; Clark et al., 2008; Dorovkov et al., 2009). Silencing of *TRPM7* decreases MDA-MB-231 cell migration in a kinase-dependent manner (Guilbert et al., 2013).

Based on the above studies, the TRPM7 kinase domain could be a potent therapeutic target in TNBC, but only two TRPM7 kinase inhibitors have been reported: rottlerin (Ryazanova et al., 2004), an inhibitor of PKCδ, and NH125, an inhibitor of eEF-2K (Devkota et al., 2012). Rottlerin has an IC_{50} value of 35 μM against the TRPM7 kinase domain (Ryazanova et al., 2004). This inhibitory activity is lower compared to the activity of rottlerin against PKC (Gschwendt et al., 1994). In addition, NH125 has TRPM7 kinase inhibitory activity with an IC_{50} value of 55 μM (Devkota et al., 2012), which is much higher than that of rottlerin. Therefore, further discovery of TRPM7 kinase inhibitors is still needed.

In order to investigate possibilities of TRPM7 as a potent therapeutic target for TNBC, in part II, a potent TRPM7 kinase inhibitor (TG100-115) is reported, and it was found that TG100-115 significantly inhibits migration and invasion of TNBC cells. Furthermore, in part III, I examined that suppression of TRPM7 ion channel via siRNA-mediated gene silencing and a TRPM7 ion channel inhibitor (NS8593) enhances TRAIL-induced apoptosis in TNBC cells. Consequently, it is demonstrated that inhibition of TRPM7 via pharmacological approaches significantly suppresses invasion and proliferation of TNBC cells. This could provide insight into new therapeutic approaches to the treatment of TNBC.

Figure 1.3. A schematic diagram to illustrate the structure of TRPM7. TRPM7 has four MHRs, six transmembrane segments, the TRP region, and the alpha-kinase domain (Zou et al., 2019).

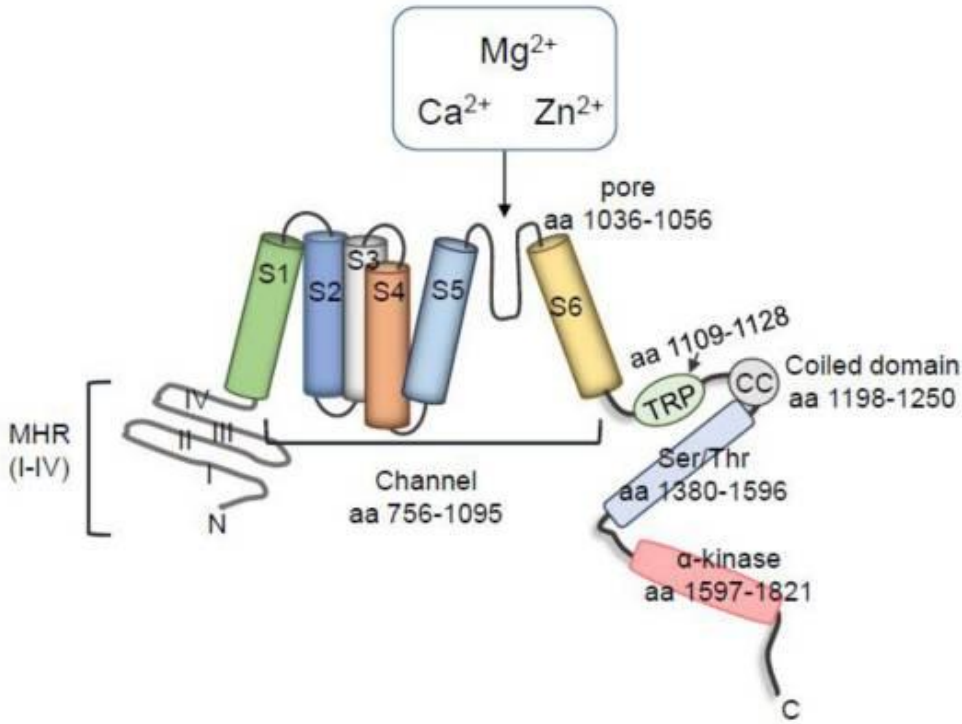
Mg2+
Ca2+ Zn2+
pore
aa 1036-1056
S1
S2
S3
S4
S5
S6
aa 1109-1128
TRP
CC
Coiled domain
aa 1198-1250
MHR
(I-IV)
IV
II
III
I
N
Channel
aa 756-1095
Ser/Thr
aa 1380-1596
α-kinase
aa 1597-1821
C

Figure 1.4. A schematic diagram of TRPM7-mediaed signaling pathways. (Yee, 2017)

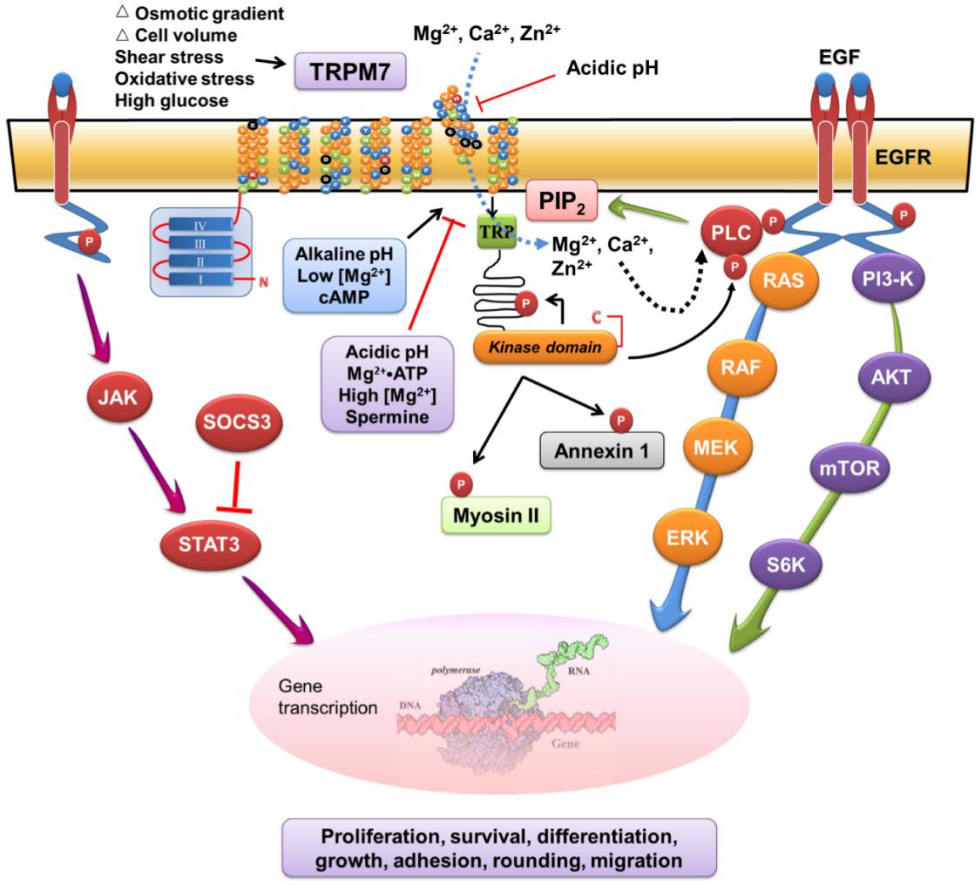
△ Osmotic gradient
△ Cell volume
Shear stress
Oxidative stress
High glucose
TRPM7
Mg2+, Ca2+, Zn2+
Acidic pH
EGF
EGFR
PIP2
TRP
Mg2+, Ca2+, Zn2+
PLC
RAS
PI3-K
Alkaline pH
Low [Mg2+]
cAMP
Acidic pH
Mg2+•ATP
High [Mg2+]
Spermine
Kinase domain
JAK
SOCS3
STAT3
Annexin 1
Myosin II
RAF
MEK
ERK
AKT
mTOR
S6K
Gene transcription
polymerase
RNA
DNA
Gene
Proliferation, survival, differentiation, growth, adhesion, rounding, migration

Part II

Identification of TG100-115 as a New and Potent TRPM7 Kinase Inhibitor Suppressing TNBC Cell Migration and Invasion

Part II of the present study has been published as Song et al., (2017) "Identification of TG100-115 as a New and Potent TRPM7 Kinase Inhibitor, Which Suppresses Breast Cancer Cell Migration and Invasion", *Biochim Biophys Acta Gen Subj*, *1861*(4):947-957.

Abstract

TRPM7 regulates breast cancer cell proliferation, migration, invasion, and metastasis in its ion channel- and kinase domain-dependent manner. The pharmacological effects of TRPM7 ion channel inhibitors on breast cancer cells have been studied, but little is known about the effects of TRPM7 kinase inhibitors due to lack of potent TRPM7 kinase inhibitors. In this study, it was found that CREB peptide is a potent substrate for the TR-FRET based TRPM7 kinase assay. Using this method, a new and potent TRPM7 kinase inhibitor, TG100-115, is reported here. TG100-115 inhibits TRPM7 kinase activity in an ATP competitive fashion with over 70-fold stronger activity than that of rottlerin, which is known as a TRPM7 kinase inhibitor. TG100-115 has little effect on proliferation of MDA-MB-231 cells but significantly decreases migration and invasion in both MDA-MB-231 and MDA-MB-468 cells. Moreover, TG100-115 inhibits TRPM7 kinase regulated phosphorylation of the myosin IIA heavy chain and phosphorylation of FAK. TG100-115 also suppresses TRPM7 ion channel activity and can be used as a potent TRPM7 kinase inhibitor and a potent inhibitor of TNBC cell migration. In addition, it could be a useful tool for studying the pharmacological effects of TRPM7 kinase activity aimed at providing insight into new therapeutic approaches to the treatment of TNBC.

Introduction

Breast cancer is the most common form of cancer in women and is expected to account for 29% of all new cancer related cases in the United States (Siegel et al., 2015). Although new techniques have been developed to detect this disease at an early stage and advanced therapies have been uncovered to increase patient survival, breast cancer promoted by metastasis of tumor cells is still the second leading cause of cancer deaths (Siegel et al., 2015). Metastasis is a complicated, multi-step process that involves cell detachment, migration, invasion, intravasation, transport, extravasation, and colonization (Tsai and Yang, 2013).

TRPM7 is required for breast cancer cell proliferation, migration, and metastasis (Guilbert et al., 2009; Middelbeek et al., 2012; Guilbert et al., 2013; Kim, 2013; Kim et al., 2013; Meng et al., 2013; Davis et al., 2014). TRPM7 mRNA levels in primary breast tumors correlate with breast cancer progression and metastasis (Middelbeek et al., 2012). As such, a decrease of TRPM7 expression lowers the metastatic properties of MDA-MB-231 cells (TNBC cells) *in vitro* and *in vivo* (Middelbeek et al., 2012). *TRPM7* knockdown increases cytoskeletal contractility and focal adhesions of MDA-MB-231 cells, and it decreases the migratory potential of MCF7 breast cancer cells (Middelbeek et al., 2012). Meng et al. found that TRPM7 regulates migration and invasion of MDA-MB-435 cells (TNBC cells) via a MAPK signaling pathway (Meng et al., 2013). In MDA-MB-468 cells (TNBC cells), TRPM7 also regulates EGF-induced STAT3 phosphorylation, as well as expression of the EMT marker-vimentin (Davis et al., 2014).

TRPM7 plays a crucial role in Ca^{2+}-dependent actomyosin contractility and cell adhesion and migration (Clark et al., 2006). Clark et al. found that activation of TRPM7 by bradykinin, a Gq-PLC coupled receptor agonist, is associated with actomyosin remodeling in a Ca^{2+} influx and kinase domain-dependent manner (Clark et al., 2006). Moreover, the kinase domain of TRPM7 promotes phosphorylation of the myosin IIA heavy chain (Clark et al., 2006). Ca^{2+} signaling is known to regulate cell adhesion, migration, and several ion channels, including ORAI1 and STIM1, are

responsible for entry of stored Ca^{2+}, which is critical for breast cancer metastasis and migration (Yang et al., 2009). Acting as a calcium flicker igniter and mechanical sensor at the leading edge of migrating fibroblasts, TRPM7 is required for localized Ca^{2+} signals (Wei et al., 2009). Inhibition of the ion channel property of TRPM7 by carvacrol suppresses U87 glioblastoma cell proliferation, migration, and invasion (Chen et al., 2015). Similarly, the TRPM7 ion channel inhibitor waixenicin A curtails proliferation of Jurkat T-cells and rat basophilic leukemia cells, but these inhibitory properties are Mg^{2+}- rather than Ca^{2+}-dependent (Zierler et al., 2011).

The kinase domain of TRPM7 is involved in the regulation of breast cancer cell migration through phosphorylation of myosin IIA heavy chain (Guilbert et al., 2013). Clark et al. showed that in N1E-115 neuroblastoma cells, TRPM7 is associated with the myosin IIA heavy chain in a kinase-dependent fashion (Clark et al., 2006) and that it regulates myosin IIA filament stabilization and localization through phosphorylation (Clark et al., 2008). The TRPM7 kinase domain also participates in regulating actomyosin dynamics via phosphorylation of cytoskeletal proteins such as tropomodulin 1 and MHC isoforms A-C during cell migration (Clark et al., 2006; Clark et al., 2008; Dorovkov et al., 2009). The results of pharmacological studies demonstrate that inhibition of cytoskeletal tension by Rho-kinase inhibitors (Y27632 and GSK429286) promotes recovery of migratory and metastatic properties caused by *TRPM7* knockdown (Middelbeek et al., 2012).

Although TRPM7 is involved in breast cancer migration and metastasis, pharmacological studies, have only been performed with TRPM7 ion channel inhibitors (Kozak et al., 2002; Prakriya and Lewis, 2002; Li et al., 2006; Parnas et al., 2009; H. C. Chen et al., 2010; X. Chen et al., 2010; Zierler et al., 2011; Chubanov et al., 2012; Qin et al., 2013). This limitation is a consequence of the lack of potent TRPM7 kinase inhibitors. Two studies of TRPM7 kinase inhibitors have been reported, one focusing on rottlerin (Ryazanova et al., 2004), a known inhibitor of PKCδ, and the other on NH125, a known inhibitor of eEF-2K (Devkota et al., 2012). By utilizing a radiolabel based *in vitro* TRPM7 kinase assay, it was shown that rottlerin has an IC_{50} value of 35 μM for inhibition of the kinase activity of TRPM7

(Ryazanova et al., 2004). This inhibitory activity is low compared to that of rottlerin against PKC (Gschwendt et al., 1994). In addition, Devkota et al. reported that NH125 has TRPM7 kinase inhibitory activity with a 55 μM IC_{50} value (Devkota et al., 2012), which is much higher than that of rottlerin.

A fura-2 fluorescence quenching based protocol was developed for HTS of TRPM7 kinase inhibitors by Castillo et al. (Castillo et al., 2010). Although conventional kinase assays, such as the filtration binding method using radiolabeled ATP and the SPA are highly sensitive, they have several limitations that make them difficult to use in HTS. For example, the filtration binding assay has low-throughput owing to the need for washing and separation steps, and the SPA creates radioactive waste (Ma et al., 2008). The LANCE *Ultra* assay, which relies on time-resolved fluorescence resonance energy transfer (TR-FRET), is a non-radiometric method that is highly sensitive and is less susceptible to interference associated with other substances (Ma et al., 2008). Despite these advantages, application of the LANCE *Ultra* assay for screening TRPM7 kinase inhibitors has not been described to date because of the absence of suitable kinase substrates.

In the study described below, it was found that the CREB peptide is an ideal substrate for the LANCE *Ultra* assay. In addition, this new assay procedure was used to screen a kinase inhibitors library obtained from Selleck Chemicals. The effort led to the discovery that TG100-115 is a highly potent TRPM7 kinase inhibitor, which decreases TNBC cell migration and invasion. Moreover, the present work explored the effects of TG100-115 on phosphorylation of myosin IIA heavy chain and focal adhesion kinase (FAK), which are metastasis markers (Sawhney et al., 2009). Finally, the capability of TG100-115 to inhibit the ion channel activity of TRPM7 was evaluated.

Materials and Methods

Antibodies and reagents

Anti-TRPM7 C-terminus antibody was purchased from NeuroMab (N74/25, USA), and anti-β actin (8H10D10), -CREB (86B10), -pCREB (1B6; Ser133), -Myosin IIA (3403), -pMyosin IIA (5026; Ser1943), -FAK (3285), and -pFAK (3283; Tyr397) antibodies were purchased from Cell signaling technology (USA). Anti-rabbit IgG-HRP (sc-2004), and -mouse IgG-HRP (sc-2005) antibodies were purchased from Santa Cruz Biotechnology (USA). A kinase inhibitors library (L1200) and TG100-115 were purchased from Selleck Chemicals (USA), and rottlerin was purchased from Tocris (UK). Dox and 2-APB were purchased from Sigma-Aldrich (MO, USA).

Cell culture

MDA-MB-231 (Korean Cell Line Bank, Republic of Korea) and MDA-MB-468 cells were cultured at RPMI 1640 media and DMEM media, respectively, supplemented with 10% (v/v) FBS, penicillin (100 U/mL) and streptomycin (100 μg/mL) in a humidified 5% CO_2 incubator at 37 °C. T-REx 293 cells stably expressing mouse TRPM7 were kindly provided by Professor Byung Joo Kim (Pusan National University, Busan, Republic of Korea). T-REx-293 cells expressing TRPM7 were cultured in DMEM supplemented with 10% (v/v) FBS, penicillin (100 U/mL), streptomycin (100 μg/mL), 5 μg/mL blasticidin and 0.5 mg/mL zeocin in a humidified 5% CO_2 incubator at 37 °C. Cells were passaged every two or three days.

In vitro kinase assay using CREB peptide

Kinase activities of recombinant human TRPM7 kinase domain (a.a. 1158-1865; Carna Biosciences, Japan) were measured using the LANCE *Ultra* TR-FRET assay (PerkinElmer, USA) with the FlexStation3 microplate reader (Molecular Devices,

USA). All kinase assays were performed using a final volume of 10 µL in white 384-well plates at RT. The microplates were sealed with microplate sealing tapes (Corning, PA, USA) during incubation. The TRPM7 kinase domain and ATP (Sigma-Aldrich, MO, USA) were prepared at 4× concentrations (40 nM and 40 µM/400 µM/4 mM, respectively) in LANCE reaction buffer (1 mM EGTA, 10 mM $MgCl_2$, 2 mM DTT, 0.01% Tween-20, and 50 mM HEPES; pH 7.5). U*Light*-CREBtide (Ser133), U*Light*- MBP (Thr232) Peptide, U*Light*-Histone H3 (Thr3/Ser10) Peptide, U*Light*-PLK (Ser137) Peptide, and U*Light*-p70 S6K (Thr389) Peptide (PerkinElmer, MA, USA) were used as substrates. Each substrate (final concentration of 50 nM) was incubated with 10 nM TRPM7 kinase domain in the absence or presence of ATP (10, 100, or 1,000 µM) for 1 h. The kinase reaction was terminated by addition of 10 mM EDTA in the LANCE Detection buffer (PerkinElmer, MA, USA) and the mixture was further incubated for 5 min. Each Eu-anti-phospho antibody (Eu-anti-phospho-CREBtide for CREBtide, Eu-anti-phospho-MBP for MBP peptide, Eu-anti-phospho-Histone H3 for H3 peptide, Eu-anti-phospho-PLK for PLK peptide, and Eu-anti-phospho-p70 S6K for p70 S6K peptide from PerkinElmer) in the LANCE Detection buffer was added to the mixture giving a final concentration of 2 nM and the mixture was incubated for 1 h. The intensity of the fluorescence signal was measured using the FlexStation3 microplate reader in TR-FRET mode (excitation wavelength of 320 nm, emission wavelength of 665 nm, time delay of 50 µs between excitation and emission detection, and an integration time of 100 µs). The signal-to-background ratio (S/B ratio) at 665 nm was determined by using the ratio of the fluorescent signal in the presence of ATP versus the fluorescent signal in the absence of ATP. In order to determine the divalent cation dependence, the kinase assays were performed in the presence of different concentrations $MgCl_2$ or $MnCl_2$ in LANCE reaction buffer (1 mM EGTA, 2 mM DTT, 0.01% Tween-20, 10 µM ATP, and 50 mM HEPES; pH 7.5). *In vitro* assays for screening of kinase inhibitors library (L1200, Selleck Chemicals, USA) were performed with 50 nM U*Light*-CREBtide (Ser133) and 10 µM ATP in LANCE reaction buffer (1 mM EGTA, 2 mM $MnCl_2$, 2 mM DTT, 0.01% Tween-20, 10 µM

ATP, and 50 mM HEPES; pH 7.5). *In vitro* kinase assays for elucidating the binding mode of TG100-115 were carried out in the presence of different concentrations of TG100-115 at different ATP concentrations (10, 100, and 1,000 μM). Concentration-response curves of TG100-115 were fitted to a four-parameter logistic nonlinear regression model to obtain IC_{50} (concentration at 50% activity inhibition) values.

In vitro kinase assay using recombinant full-length CREB

In vitro kinase assays were performed using recombinant human TRPM7 kinase domain and recombinant full-length human CREB (a.a. 1-327; Life technologies, USA) in kinase reaction buffer (1 mM EGTA, 2 mM $MgCl_2$, 2 mM DTT, 0.01% Tween-20, and 50 mM HEPES; pH 7.5). Reaction mixtures (200 ng of recombinant CREB, 100 ng of recombinant TRPM7 kinase domain in kinase reaction buffer) were incubated at 30 °C for 30 min in the absence or presence of 100 μM ATP. The reactions were terminated by addition of Laemmli sample buffer and the mixtures were shaken at 95 °C for 5 min. The mixtures were subjected to SDS- PAGE, and Western blot analysis was performed according to the procedures mentioned above. Pixel densities of bands on developed X-ray films were analyzed using Image J software. Subtraction of the average densitiy of the negative control band (pCREB bands in the absence of TRPM7 kinase domain) from the density of each band gave normalized densities of positive control bands (pCREB bands in the presence of TRPM7 kinase domain). Concentration-response curves of TG100-115 were fitted to a four-parameter logistic nonlinear regression model provided by Prism 6 (GraphPad software, Inc., CA, USA) to obtain IC_{50} values.

Molecular docking analysis

A docking model of TG100-115 on TRPM7 kinase was constructed using Glide tool as provided in Maestro ("Schrödinger Release 2015-4, Schrödinger, LLC, New York, NY", 2015; "Small-Molecule Drug Discovery Suite 2015-4: Glide, version 6.9, Schrödinger, LLC, New York, NY", 2015). The crystal structure of TRPM7 kinase

domain from Protein Data Bank [PDB code; 1IA9, a complex with the AMP-PNP (β-γ-imidoadenosine-5′-phosphate)] was utilized for docking simulation (Yamaguchi et al., 2001). The starting coordinates of the TRPM7 structure were minimized using the Protein Preparation Wizard by applying an OPLS-2005 force field (Shivakumar et al., 2010). The inhibitor of TRPM7, TG100-115, was built using a Maestro build panel and minimized using the Macromodel module of Maestro in the Schrödinger Suite Program. The minimized structure of TG100-115 was docked onto the prepared receptor grid around the ATP binding site of TRPM7. The best-docked poses with the lowest Glide docking score were selected as the final docking model.

Wound healing assay

MDA-MB-231 or MDA-MB-468 cells were seeded in 6-well plates (Thermo Fisher Scientific, MA, USA) at a density of 1×10^6 cells per well, and incubated overnight. Cell monolayers were wounded using a 1000 μL pipette tip, and washed with PBS twice to remove the detached cells. Cells were incubated with various concentrations (1, 10, and 50 μM) of TG100-115, rottlerin, or PIK-294 for 27 h (MDA-MB-231 cells) or 48 h (MDA-MB-468 cells). The images of scratched regions were recorded before and after 27 h (MDA-MB-231 cells) or 48 h (MDA-MB-468 cells) incubation, and migration ratios were calculated from migration areas determined using Image J software.

Invasion assay

The invasion assay was performed using CHEMICON QCM 24-well Invasion assay kit (ECM 554, Chemicon International, MA, USA). MDA-MB-231, MDA-MB-468, or T-REx-293 expressing TRPM7 cells were seeded in the 8-μm ECMatrix™-coated transwell chamber (Chemicon International, MA, USA) at a density of 2.5×10^5 cells per well after serum starvation for 24 h. The cells were incubated for 15 h (MDA-MB-231 and MDA-MB-468 cells) or 48 h (T-REx-293 expressing TRPM7) at 37 °C

in a humidified 5% CO_2 incubator. Invaded cells from the bottom of the chamber were detached using 225 μL of cell detachment solution (Chemicon International, MA, USA) for 30 min at 37 °C. The detached cells were lysed with 75 μL of lysis buffer (Chemicon International, MA, USA) containing CyQuant GR Dye solution (Chemicon International, MA, USA) for 15 min at RT and the fluorescence intensities of 200 μL of the mixtures in a 96-well black-wall plate were measured using a FlexStation3 microplate reader (excitation wavelength of 480 nm and emission wavelength of 520 nm). Invasion ratios were calculated from relative fluorescence intensities acquired at different concentrations (1, 10, and 50 μM) of TG100-115, rottlerin, or PIK-294.

Cell proliferation assay

MDA-MB-231 cells were seeded into a 96-well plate (BD biosciences, MA, USA) at a density of 5×10^3 cells per well, and then incubated for 24 h at 37 °C in a humidified 5% CO_2 incubator. After removing the culture medium, fresh media containing different concentrations of TG100-115, rottlerin, or PIK-294 were added, and incubated for 15, 27, or 48 h at 37 °C. After incubation, 20 μL of MTT [3-(4, 5-dimethylthiazol-2-yl)-2,5-diphenyltetrazolium bromide; Sigma-Aldrich, MO, USA] was added to each well and incubated for 2 h at 37 °C. Absorbance at 560 nm was measured using a FlexStation3 microplate reader. Concentration-response curves of TG100-115, rottlerin, and PIK-294 were fitted to a four-parameter logistic nonlinear regression model to obtain GI_{50} (concentration at 50% growth inhibition) values. The GI_{50} values of rottlerin and TG100-115 were determined from concentration-response curves at 48 h after treatment.

Western blot analysis

MDA-MB-231 cells were seeded into 60-mm dishes at a density of 2×10^6 cells per dish, and incubated for 24 h at 37 °C in a humidified 5% CO_2 incubator. The cells

were treated with different concentrations of test compounds, and incubated for indicated times at 37 °C in a humidified 5% CO_2 incubator. After incubation, the cells were washed twice with PBS and lysed in RIPA Buffer (Sigma-Aldrich, MO, USA) with protease inhibitor cocktail solution (Sigma-Aldrich, MO, USA) and phosphatase inhibitor cocktail solution (Sigma-Aldrich, MO, USA) for 30 min at 4 °C. Proteins from cell lysates were quantified using the BCA assay, and equivalent amounts of total proteins were loaded on 12% SDS-PAGE gels. The separated proteins from the polyacrylamide gel were transferred to PVDF membranes (EMD Millipore, Germany). The membrane was blocked with 5% skim milk in TBST buffer (137 mM NaCl, 20 mM Tris, and 0.1% Tween-20; pH 7.4) for 1 h. After blocking, the membrane was incubated with primary antibodies at 4 °C overnight, and HRP-conjugated antibodies were used as secondary antibodies. The complexes with HRP-linked secondary antibodies were detected using the ECL substrate kit (Thermo Fisher Scientific, MA, USA).

In vitro kinase assay against FAK

In vitro kinase assay for FAK, performed by the Reaction Biology Corporation (PA, USA), was carried out with recombinant FAK in the presence of different concentrations of TG100-115 and 10 μM ATP in kinase reaction buffer (10 mM $MgCl_2$, 1 mM EGTA, 0.02% Brij35, 0.02 mg/mL BSA, 0.1 mM Na_3VO_4, 2 mM DTT, 20 mM HEPES; pH 7.5). Poly [Glu:Tyr] (4:1; 0.2 mg/mL) was used as a substrate for FAK, and the reactions were initiated by addition of ^{33}P-ATP (specific activity: 10 μCi/μL). After incubation for 2 h, kinase activities were detected by filtration binding method.

Electrophysiology

T-REx-293 cells, stably expressing TRPM7, were plated onto glass coverslips and then maintained for at least 48 h before whole-cell recordings. Expression of TRPM7 was induced by addition of Dox at a final concentration of 1 μg/mL for 24 h. Whole-

cell currents were recorded with the intracellular solution containing (in mM units): 135 Cs-MES, 3.67 $CaCl_2$, 10 EGTA and 10 HEPES (pH 7.2 was adjusted with CsOH), and with the extracellular solution containing (in mM units): 135 Na-MES, 3 $CaCl_2$, 0.5 EDTA and 10 HEPES (pH 7.4 was adjusted with NaOH). Patch pipettes were made from borosilicate glass capillaries (Warner Instruments, Inc., CT, USA). The pipettes resistance had 5-6 MΩ. Whole-cell currents were recorded using a patch clamp amplifier (Axopatch 200B, Axon Instrument, Inc., CA, USA). The current–voltage relationships were measured by applying ramp pulses (from –120 mV to +100 mV during 1000-ms) at a holding potential of 0 mV. Whole-cell currents were acquired and digitized at 5 kHz using a Digidata 1440A (Axon Instrument, Inc., CA, USA) and filtered at 1 kHz. Currents were analyzed with Clampfit software (Axon instruments, Inc., CA, USA). All experiments were conducted at RT.

MDA-MB-231 cells were plated onto coverslips and maintained in RPMI media supplemented with 10% fetal bovine serum, penicillin (100 U/mL), streptomycin (100 μg/mL) for at least 48 h before electrophysiology experiments. The standard solution for pipette contained, in mM: 135 Cs-MES, 10 EGTA, 10 HEPES, 3.67 CaCl2 (pH 7.2 adjusted with CsOH) and bath solution contained in mM :135 Na-MES, 3 CaCl2, 0.5 EDTA, 10 HEPES, (pH 7.4 adjusted with NaOH) were used. Patch pipettes were made from borosilicate glass capillaries (Warner Instruments, Inc.). The pipettes resistance were 7-8 MΩ. Whole-cell currents were recorded using a patch clamp amplifier (Axopatch 700B, Axon Instrument, Inc.). The current–voltage relationships were measured by applying ramp pulses (from –100 mV to +100 mV during 1000-ms) from a holding potential of -40 mV. A Digidata 1550A interface was used to convert digital–analogue signals between amplifier and computer. Data were sampled at 5 kHz and filtered at 1 kHz. Currents were analyzed with Clampfit software (Axon instruments, Inc.). All experiments were performed at RT.

Statistical analysis

All data were analyzed using Prism 6 software (GraphPad, USA), and presented as mean ± S.D.. Statistical significances were evaluated by either two-tailed Student's t-test when differences between two groups or one-way ANOVA with Tukey's multiple comparison test when differences among three or more groups. Statistical values of $p < 0.05$ were considered to be statistically significant. *$p < 0.05$, **$p < 0.01$, ***$p < 0.001$, and ****$p < 0.0001$. Error bars represent S.D. (n = 3).

Results

***In vitro* TRPM7 kinase assays were established via the TR-FRET technique with CREB peptides.**

The LANCE *Ultra* TR-FRET assay was adopted to identify a proper substrate for *in vitro* TRPM7 kinase assay needed for high throughput screening. Five U*Light*-labeled peptides (CREB, histone H3, MBP, PLK, and p70S6K), known to generate signals for over 80% of 184 Ser/Thr kinases from PerkinElmer instruction manual in LANCE *Ultra* KinaSelect Ser/Thr kit, were used as substrates in the assays (Figure 2.1A). The S/B ratios using the CREB peptide in the TRPM7 kinase assays were higher than those using the other substrates. The S/B ratios using the CREB peptide in the presence of 100 μM and 1 mM ATP were 4.27 ± 0.19 and 10.85 ± 0.51, respectively. Importantly, the S/B ratios arising from *in vitro* TRPM7 kinase assays using the CREB peptide as substrate and in the presence of different concentrations of ATP were observed to increase in an ATP concentration dependent manner (Figure 2.1B). In order to decrease the concentrations of ATP utilized in the TRPM7 kinase assays for screening the type I kinase inhibitor library, *in vitro* kinase assays were carried out using 10 μM ATP and different concentrations of divalent cations (Mg^{2+} and Mn^{2+}) (Figure 2.1C). It is known that Mn^{2+} increases the level of TRPM7 kinase promoted-phosphorylation of MBP and histone H3 (Ryazanova et al., 2004). Optimal concentrations of Mg^{2+} and Mn^{2+} that gave maximum S/B ratios in the TRPM7 kinase assays were found to be 5 mM and 2 mM, respectively. These concentrations are similar to those of Mg^{2+} and Mn^{2+} that give maximum phosphorylation in the radiolabel based *in vitro* TRPM7 kinase assays (Ryazanova et al., 2004). The S/B ratio for an assay using 2 mM Mn^{2+} is 14.59 ± 0.23, while the maximum S/B ratio in the presence of 5 mM Mg^{2+} is only 3.02 ± 0.71. As seen in the earlier study (Ryazanova et al., 2004), the kinase activity in the presence of Mn^{2+} is higher than that in the presence of Mg^{2+}. These data suggest that *in vitro* TRPM7 kinase assays using the CREB peptide as a substrate give the same results as those using the radiolabel based *in vitro* TRPM7 kinase assays.

Figure 2.1. Establishment of *in vitro* TRPM7 kinase assay. (A) An optimal substrate for TRPM7 kinase assays was selected using KinaSelect Ser/Thr kit. (B) Effects of ATP on TRPM7 kinase activities. Kinase activities of recombinant human TRPM7 kinase domain were measured with U*Light*-CREBtide at different concentrations (10, 100, and 1000 μM) of ATP. (C) Effects of Mg^{2+} and Mn^{2+} on TRPM7 kinase activities. The reactions were performed using recombinant human TRPM7 kinase domain and U*Light*-CREBtide in the presence of 10 μM ATP.

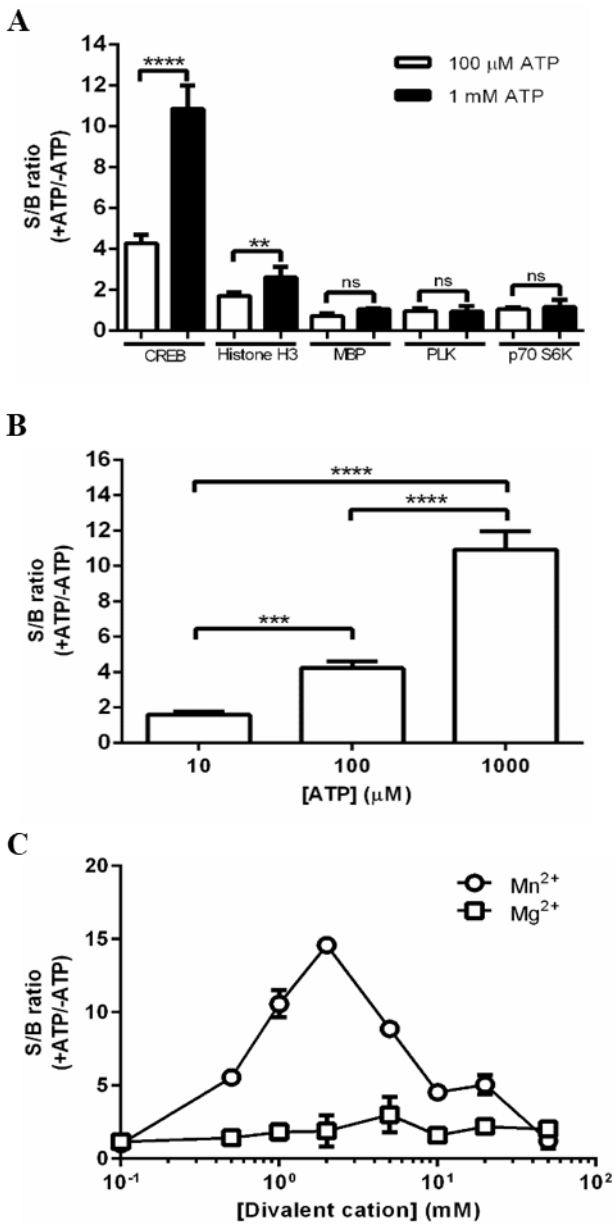
A
S/B ratio (+ATP/-ATP)
100 μM ATP
1 mM ATP
****
**
ns
ns
ns
CREB
Histone H3
MBP
PLK
p70 S6K
B
S/B ratio (+ATP/-ATP)
****
****
***
10
100
1000
[ATP] (μM)
C
S/B ratio (+ATP/-ATP)
Mn2+
Mg2+
[Divalent cation] (mM)

Known kinase inhibitors suppress TRPM7 kinase activities.

A kinase inhibitor library, comprised of 172 substances, was screened for activity against TRPM7 using the above described *in vitro* kinase assay (Table 2.1). Rottlerin was used as a positive control (Ryazanova et al., 2004). Kinase inhibitors that reduce the kinase activity of TRPM7 to 70% at 10 μM concentration were considered as hit compounds. The IC_{50} values against TRPM7 kinase of five substances (Figure 2.2A) that fit this criterion were determined (Figure 2.2B and Table 2.2). All five substances were found to have greater inhibitory activities than those of rottlerin. Significantly, TG100-115 is the most potent compound with an IC_{50} value of 1.07 ± 0.14 μM, which is much higher than that of rottlerin (IC_{50} = 79.06 ± 1.05 μM, which is within the range of the value reported earlier (Ryazanova et al., 2004)). These results indicate that the *in vitro* TRPM7 kinase assay is useful in carrying out a HTS.

Table 2.1. Inhibitory effects of 172 kinase inhibitors on TRPM7 kinase activities.

	Kinase inhibitors	Targets	Average (% of Control)	S.D.
1	TG100-115	PI3K	4.86	3.69
2	TG100713	PI3K	42.52	4.63
3	JNJ-7706621	CDK, Aurora kinase	50.11	18.11
4	PHA-665752	c-Met	61.61	7.05
5	Butein	EGFR	66.69	4.75
6	PRT062607 (P505-15, BIIB057) HCl	Syk	71.45	6.96
7	Sunitinib Malate	VEGFR, PDGFR, c-Kit	74.00	5.55
8	Bardoxolone Methyl	IκB/IKK	75.62	7.78
9	ETP-46464	mTOR, ATM/ATR	76.58	0.11
10	Skepinone-L	p38 MAPK	76.62	6.54
11	Piceatannol	Syk	76.93	16.43
12	Tyrphostin AG 1296	FGFR, c-Kit, PDGFR	77.97	7.33
13	PQ 401	IGF-1R	79.01	3.26
14	GNF-2	Bcr-Abl	79.12	2.50
15	NU6027	CDK	79.95	0.67
16	CX-6258 HCl	Pim	79.96	0.78
17	GDC-0349	mTOR	80.94	1.61
18	BKM120 (NVP-BKM120, Buparlisib)	PI3K	81.33	4.96
19	GDC-0980 (RG7422)	mTOR, PI3K	81.61	6.64
20	Mubritinib (TAK 165)	HER2	81.62	9.60
21	BMS-265246	CDK	81.81	17.53
22	NVP-BVU972	c-Met	82.84	10.86
23	PP121	DNA-PK, PDGFR, mTOR	82.99	0.49
24	KN-62	CaMKII, P2RX7	83.57	8.56
25	Zotarolimus (ABT-578)	mTOR	86.65	2.94
26	TPCA-1	IκB/IKK	86.66	14.04
27	Torin 2	ATM/ATR, mTOR	86.97	4.52
28	GSK2126458 (GSK458)	PI3K, mTOR	87.25	0.07
29	TGX-221	PI3K	87.55	10.32
30	MK-2461	c-Met, PDGFR, FGFR	87.76	3.33
31	AG-18	EGFR	88.02	12.13
32	MK-8776 (SCH 900776)	CDK, Chk	88.12	6.89
33	A-769662	AMPK	88.50	4.47

34	Chrysophanic acid	mTOR, EGFR	88.84	1.90
35	GDC-0941	PI3K	88.90	7.33
36	GNE-0877	LRRK2	89.67	5.06
37	IPI-145 (INK1197)	PI3K	89.91	19.64
38	AZD5438	CDK	89.97	1.00
39	EHT 1864	Rho	90.30	5.75
40	BYL719	PI3K	90.34	12.01
41	AZD8931 (Sapitinib)	HER2, EGFR	90.54	7.95
42	Indirubin	GSK-3	90.67	10.32
43	ZM 323881 HCl	VEGFR	90.72	13.72
44	NU7441 (KU-57788)	DNA-PK, PI3K	91.60	4.54
45	TAK-632	Raf	91.60	7.81
46	SC-514	IκB/IKK	91.72	9.10
47	TAK-285	EGFR, HER2	91.77	6.18
48	TCS 359	FLT3	91.78	18.67
49	PHA-767491	CDK	91.81	3.97
50	SMI-4a	Pim	91.85	3.98
51	GDC-0068	AKT	91.87	12.76
52	OSI-027	mTOR	91.95	14.34
53	AS-252424	PI3K	92.04	10.53
54	Tofacitinib (CP-690550, Tasocitinib)	JAK	92.06	8.61
55	KU-0063794	mTOR	92.07	8.63
56	Filgotinib (GLPG0634)	JAK	92.52	6.23
57	KU-55933	ATM/ATR	92.54	9.98
58	AG-1478 (Tyrphostin AG-1478)	EGFR	92.71	17.41
59	GSK2636771	PI3K	92.71	2.60
60	TAE226 (NVP-TAE226)	FAK	93.19	4.63
61	XMD8-92	ERK	93.49	0.03
62	XL147	PI3K	93.52	8.60
63	RKI-1447	ROCK	93.54	4.86
64	GSK429286A	ROCK	93.79	12.75
65	Dovitinib (TKI-258, CHIR-258)	FGFR, FLT3, c-Kit, VEGFR, PDGFR	93.97	0.10
66	TIC10	AKT	93.98	7.24
67	K-Ras(G12C) inhibitor 9	Rho	94.09	3.89
68	WHI-P154	JAK, EGFR	94.17	2.51
69	BIX 02188	MEK	94.25	0.79

70	GNE-7915	LRRK2	94.43	5.88
71	AZD3463	ALK	94.49	6.53
72	BX-912	PDK-1	94.61	5.57
73	Apatinib	VEGFR	94.75	6.76
74	MEK162 (ARRY-162, ARRY-438162)	MEK	94.86	15.47
75	Honokiol	MEK, AKT	94.98	7.86
76	GSK650394	SGK	95.03	16.91
77	LDC000067	CDK	95.17	4.93
78	OSI-906 (Linsitinib)	IGF-1R	95.68	8.24
79	Go 6983	PKC	95.77	9.01
80	PF-573228	FAK	95.85	6.81
81	AZD2014	mTOR	95.89	8.68
82	WZ3146	EGFR	95.92	0.98
83	Wortmannin	ATM/ATR, PI3K	95.97	6.86
84	SAR131675	VEGFR	95.98	12.20
85	Acadesine	AMPK	95.99	16.70
86	AZD8330	MEK	96.16	1.16
87	IM-12	GSK-3	96.24	6.25
88	Palomid 529 (P529)	mTOR	96.27	10.03
89	VS-5584 (SB2343)	PI3K	96.27	0.65
90	AT9283	JAK, Aurora kinase, Bcr-Abl	96.39	11.16
91	Telatinib	VEGFR, PDGFR, c-Kit	96.51	15.18
92	NMS-P937 (NMS1286937)	PLK	96.56	2.27
93	HER2-Inhibitor-1	HER2, EGFR	96.97	4.07
94	LY2228820	p38 MAPK	96.98	5.63
95	SB202190 (FHPI)	p38 MAPK	97.08	18.61
96	AZD8055	mTOR	97.09	7.09
97	Fingolimod (FTY720) HCl	S1P receptor	97.10	4.39
98	GNF-5	Bcr-Abl	97.40	7.70
99	CAY10505	PI3K	97.58	13.36
100	VX-745	p38 MAPK	97.67	14.83
101	RAF265 (CHIR-265)	VEGFR, Raf	97.68	4.51
102	Enzastaurin (LY317615)	PKC	97.71	1.47
103	WAY-600	mTOR	97.93	3.39
104	Semaxanib (SU5416)	VEGFR	97.96	13.56

105	AR-A014418	GSK-3	98.12	8.66
106	PD168393	EGFR	98.31	3.98
107	R406 (free base)	Syk	98.39	1.42
108	LY2603618	Chk	98.56	10.83
109	CCT137690	Aurora kinase	98.77	14.18
110	Erlotinib HCl (OSI-744)	Autophagy, EGFR	99.06	14.38
111	INK 128 (MLN0128)	mTOR	99.15	11.00
112	ZCL278	Rac	99.29	0.39
113	WYE-125132 (WYE-132)	mTOR	99.42	3.97
114	Cabozantinib malate (XL184)	VEGFR	99.70	10.88
115	HMN-214	PLK	99.83	13.44
116	Amuvatinib (MP-470)	FLT3, c-RET, PDGFR, c-Kit	100.08	6.74
117	AZ 628	Raf	100.09	16.75
118	GW5074	Raf	100.25	15.26
119	WH-4-023	Src	100.27	5.37
120	CZC24832	PI3K	100.32	7.77
121	Roscovitine (Seliciclib, CYC202)	CDK	100.43	10.12
122	TG003	CDK	100.58	0.23
123	Foretinib (GSK1363089)	VEGFR, c-Met	101.04	8.52
124	DCC-2036 (Rebastinib)	Bcr-Abl	101.05	18.26
125	Fasudil (HA-1077) HCl	ROCK	101.11	7.95
126	AZ20	ATM/ATR	101.14	5.78
127	Refametinib (RDEA119, Bay 86-9766)	MEK	101.20	2.97
128	R406	Syk, FLT3	101.35	5.20
129	Ridaforolimus (Deforolimus, MK-8669)	mTOR	101.43	10.24
130	S-Ruxolitinib (INCB018424)	JAK	101.57	2.93
131	CGK 733	ATM/ATR	101.63	3.77
132	AZ 960	JAK	101.70	13.00
133	BIRB 796 (Doramapimod)	p38 MAPK	101.76	5.19
134	AP26113	ALK	101.77	1.89
135	GNE-9605	LRRK2	101.77	6.08
136	AT7519	CDK	101.81	12.95
137	GF109203X	PKC	101.94	3.30
138	BX-795	IκB/IKK, PDK-1	102.04	4.31

139	AVL-292	BTK	102.04	13.28
140	Trametinib (GSK1120212)	MEK	102.20	5.78
141	SB203580	p38 MAPK	102.36	6.83
142	OSI-930	c-Kit, CSF-1R, VEGFR	102.46	11.14
143	PP2	Src	102.53	7.56
144	Tofacitinib (CP-690550) citrate	JAK	102.66	3.89
145	KU-60019	ATM/ATR	102.73	8.21
146	CYC116	Aurora Kinase, VEGFR	102.76	1.55
147	PD0325901	MEK	102.85	13.51
148	MGCD-265	Tie-2, VEGFR, c-Met	103.16	14.71
149	Sorafenib tosylate	PDGFR, Raf, VEGFR	103.19	14.97
150	LDK378	ALK	103.19	18.24
151	Danusertib (PHA-739358)	c-RET, FGFR, Bcr-Abl, Aurora kinase	103.41	0.55
152	PHT-427	PDK-1, AKT	103.43	3.36
153	CHIR-99021 (CT99021) HCl	GSK-3	103.51	5.42
154	SKI II	S1P receptor	103.55	5.02
155	U0126-EtOH	MEK	103.77	8.48
156	PF-477736	Chk	103.83	2.54
157	A66	PI3K	103.98	8.83
158	Tivozanib (AV-951)	VEGFR, PDGFR, c-Kit	103.99	6.98
159	CEP-32496	CSF-1R, Raf	104.00	10.25
160	PIK-294	PI3K	104.18	9.39
161	MLN8054	Aurora kinase	104.19	15.67
162	MK-8745	Aurora kinase	104.25	6.68
163	PFK15	PFKFB3	104.31	14.66
164	Sorafenib	Raf	104.34	1.07
165	VE-821	ATM/ATR	104.41	5.20
166	Linifanib (ABT-869)	CSF-1R, PDGFR, VEGFR	104.46	5.99
167	YM201636	PI3K	104.46	5.97
168	Thiazovivin	ROCK	104.66	13.33
169	Ibrutinib (PCI-32765)	BTK	104.67	16.78
170	PF-04217903	c-Met	104.80	16.43
171	Pazopanib HCl (GW786034 H)	VEGFR, PDGFR, c-Kit	104.94	6.38
172	ZSTK474	PI3K	104.97	7.47

Figure 2.2. Inhibitory effects of kinase inhibitors on TRPM7 kinase activities.

(A) Five compounds (TG100-115, TG100713, JNJ-7706621, PHA-665752, and Butein) among the kinase inhibitor library were found to reduce TRPM7 kinase activity to 70% at 10 μM concentration. (B) Concentration-response curves of five compounds against TRPM7 kinase domain through the *in vitro* kinase assay using LANCE *Ultra* TR-FRET assays.

A

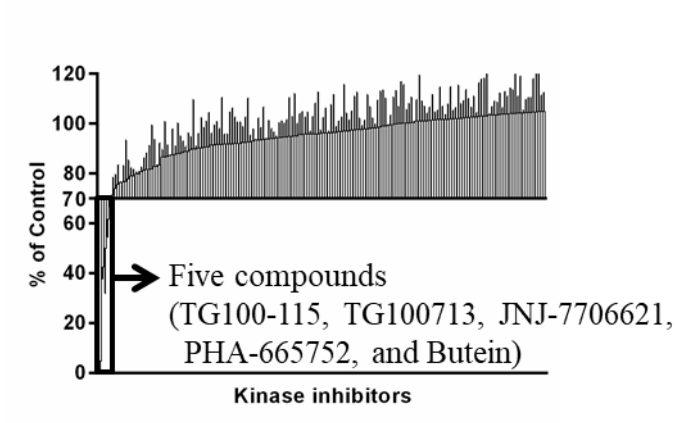
120
100
80
70
60
40
20
0
% of Control
Five compounds
(TG100-115, TG100713, JNJ-7706621,
PHA-665752, and Butein)
Kinase inhibitors

B

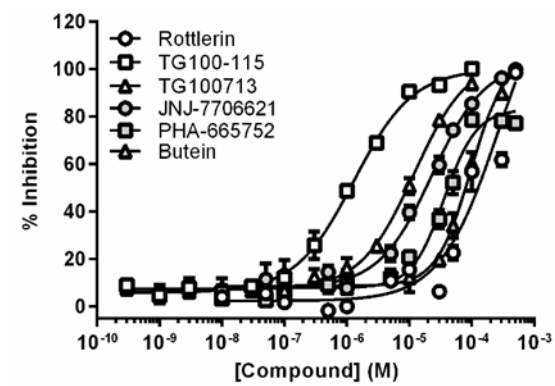
Rottlerin
TG100-115
TG100713
JNJ-7706621
PHA-665752
Butein
% Inhibition
120
100
80
60
40
20
0
10-10
10-9
10-8
10-7
10-6
10-5
10-4
10-3
[Compound] (M)

Table 2.2. Inhibitory activities of the hit compounds against TRPM7 kinase domain.

Compound	%Inhibition at 10 μM	IC_{50} (μM)	Literature IC_{50} (μM)
Rottlerin	12.10 ± 2.29	79.06 ± 1.05	35 [a]
TG100-115	95.14 ± 3.69	1.07 ± 0.14	
TG100713	57.48 ± 4.63	9.06 ± 0.92	
JNJ-7706621	49.89 ± 18.11	16.24 ± 0.38	
PHA-665752	38.39 ± 7.05	42.18 ± 5.91	
Butein	33.31 ± 4.75	71.28 ± 7.28	

[a] The IC_{50} value was determined through radiolabeled *in vitro* TRPM7 kinase assays (Ryazanova et al., 2004).

TG100-115 inhibits phosphorylation of recombinant full-length CREB by TRPM7 kinase domain.

To confirm the TRPM7 kinase inhibitory activity of TG100-115, I performed *in vitro* kinase assays using recombinant full-length CREB as a substrate. Like the results obtained from using the assay that employs the CREB peptide, Ser133 of full-length CREB was phosphorylated by the TRPM7 kinase domain (Figure 2.3A). The level of phosphorylation at Ser133 of the full-length CREB was diminished in the presence of TG100-115 in a concentration-dependent fashion (Figure 2.3B). The bands corresponding to phosphorylated CREB were quantified by using densitometry analysis and each was normalized to the density of the band arising from reaction of CREB promoted by the TRPM7 kinase domain in the absence of TG100-115. The IC_{50} value of TG100-115 against the TRPM7 kinase domain, determined using full-length CREB (Figure 2.3C), was found to be 1.96 μM. This value is similar to that obtained from the *in vitro* TRPM7 kinase assays using the CREB peptide (Table 2.2). These observations demonstrate that TRPM7 kinase assays using full-length CREB as the substrate give results that are as accurate as those arising from *in vitro* TRPM7 kinase assays using CREB peptide, and TG100-115 have potent inhibitory activity against the TRPM7 kinase domain.

Figure 2.3. Recombinant human full-length CREB is phosphorylated by TRPM7 kinase domain and its phosphorylation is inhibited by TG100-115. (A) Recombinant human TRPM7 kinase domain was incubated with recombinant human full-length CREB. Formation of phosphorylated Ser133 of CREB was analyzed by using Western blot analysis. (B) Phosphorylation of CREB was determined in the presence of TG100-115 via Western blot analysis. (C) Bands of phosphorylated CREB in (B) were quantified by using densitometry analysis.

A

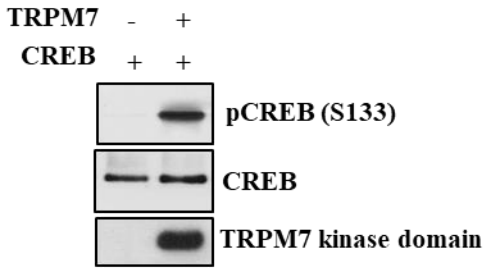
TRPM7 - +
CREB + +
pCREB (S133)
CREB
TRPM7 kinase domain

B

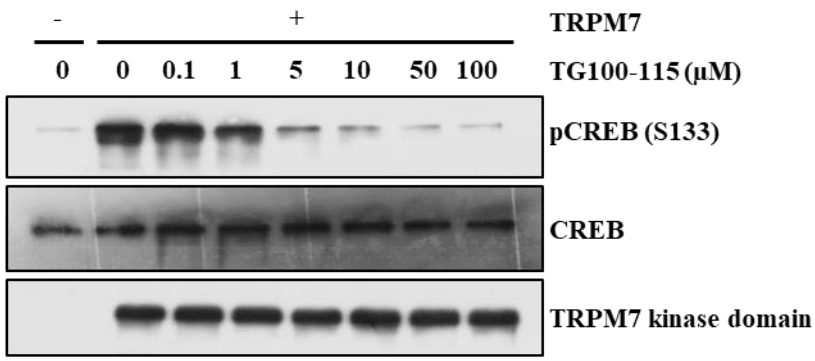
- +
TRPM7
0 0 0.1 1 5 10 50 100
TG100-115 (μM)
pCREB (S133)
CREB
TRPM7 kinase domain

C

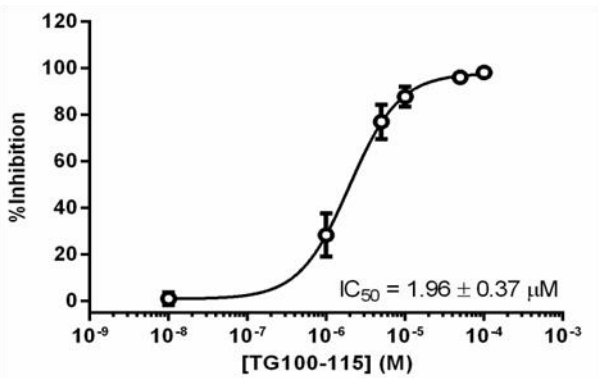
120
100
80
60
40
20
0
%Inhibition
IC50 = 1.96 ± 0.37 μM
10-9 10-8 10-7 10-6 10-5 10-4 10-3
[TG100-115] (M)

Molecular docking study and inhibition of TG100-115 on TRPM7 kinase activity in an ATP competitive fashion.

Molecular docking was performed using the crystal structure of the TRPM7 kinase domain to gain information about the mode of binding of TG100-115 to TRPM7. The interactions involved in determining the mode (Figures 2.4A and 2.4B) of TG100-115 binding in the ATP binding site of TRPM7 kinase domain are as follows. The pteridine-2,4-diamino groups of TG100-115 form hydrogen bonds with the side chain of Glu1718, backbone of Met1721 and Glu1719 in the TRPM7 kinase domain. The bis(3-hydroxylphenyl) group of TG100-115 forms additional hydrogen bonds with the side chains of Lys1626 and Glu1615 in the p-loop of the TRPM7 kinase domain. The results of the docking studies show that TG100-115 fits nicely in the ATP binding pocket of the TRPM7 kinase domain. To gain experimental evidence for the mode of binding, the kinase inhibitory activity of TG100-115 on TRPM7 was determined as a function of different concentrations of ATP. The concentration-response curves were fitted to a four-parameter logistic nonlinear regression model to obtain IC_{50} values (Figure 2.4C). According to Cheng-Prusoff equation (Cheng and Prusoff, 1973), a phenomenon that an increase in the ATP concentrations causes an increase in IC_{50} values, demonstrates that inhibition by TG100-115 is a consequence of competitive binding to the TRPM7 kinase domain (Figure 2.4D).

Figure 2.4. Docking studies predicting interactions of TG100-115 with TRPM7 kinase domain. (A) Molecular docking analysis between TRPM7 kinase domain and TG100-115. Hydrogen bonds are shown as red dashed lines. (B) Binding site to depict the key interactions of TG100-115 with the TRPM7 kinase domain. Hydrogen bonds are shown as red dashed lines. (C) Representative concentration-response curves of TG100-115 against TRPM7 kinase domain in the presence of the various concentrations of ATP. (D) IC_{50} values of TG100-115 against TRPM7 kinase domain in the presence of the various concentrations of ATP. The molecular docking analysis was performed by Dr. Kim, Nam Doo (New Drug Development Center, Daegu-Gyeongbuk Medical Innovation Foundation, Republic of Korea).

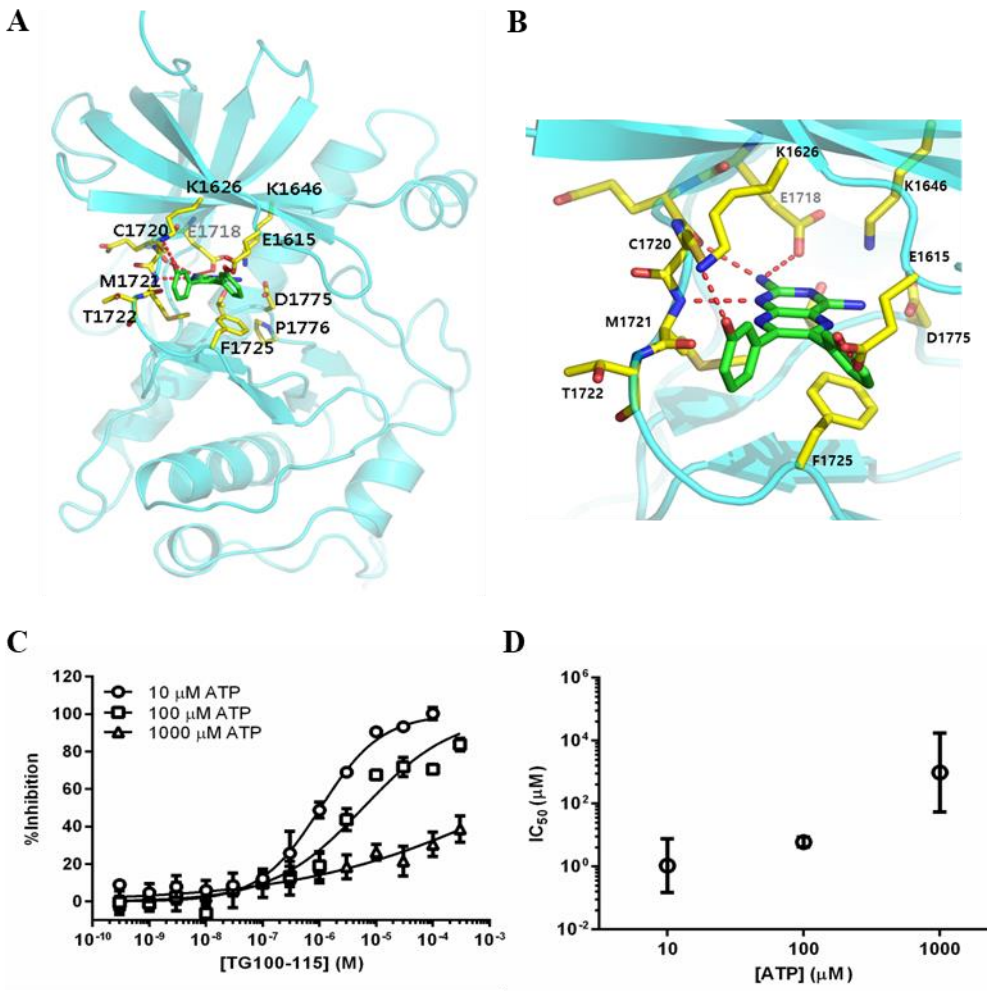
A
K1626
K1646
C1720
E1718
E1615
M1721
D1775
T1722
P1776
F1725
B
K1626
E1718
K1646
C1720
E1615
M1721
D1775
T1722
F1725
C
10 μM ATP
100 μM ATP
1000 μM ATP
%Inhibition
[TG100-115] (M)
D
IC50 (μM)
[ATP] (μM)

TG100-115 suppresses migration and invasion of MDA-MB-231 cells.

Based on the fact that the TRPM7 kinase domain is involved in migration and invasion of breast cancer cells (Guilbert et al., 2013), I investigated the effect of TG100-115 on migration and invasion of aggressive MDA-MB-231 cells. As the data in Figure 2.5A show, migration of MDA-MB-231 cells treated with TG100-115 is significantly reduced in a concentration-dependent manner. Especially interesting is the observation that the migration ratio in the presence of 50 μM TG100-115 decreases by 42.41 ± 1.03% (Figure 2.5B). Invasion of MDA-MB-231 cells was also found to be significantly reduced by treatment of 50 μM TG100-115 (Figure 2.5C). Indeed, invasiveness of cells in the presence of 50 μM TG100-115 decreases by 59.71 ± 3.66% compared to cells treated with DMSO. Rottlerin reduces migration of cells by 41.81 ± 0.08% (Figure 2.5B) and invasion of cells by 55.91 ± 3.78% at 50 μM (Figure 2.5C).

Figure 2.5. TG100-115 suppresses cell migration and invasion in MDA-MB-231 cells. (A) MDA-MB-231 cells, treated with different concentrations of TG100-115 or rottlerin, were incubated for 27 h after scratching cell monolayers. Scale bar represents 2 mm. (B) Migration ratios were calculated using migration areas. MDA-MB-231 cells treated with different concentrations of TG100-115 or rottlerin were incubated for 27 h. (C) Invasion assays were performed using CHEMICON QCM 24-well Invasion assay kit. Invasion ratios were calculated using fluorescence intensities.

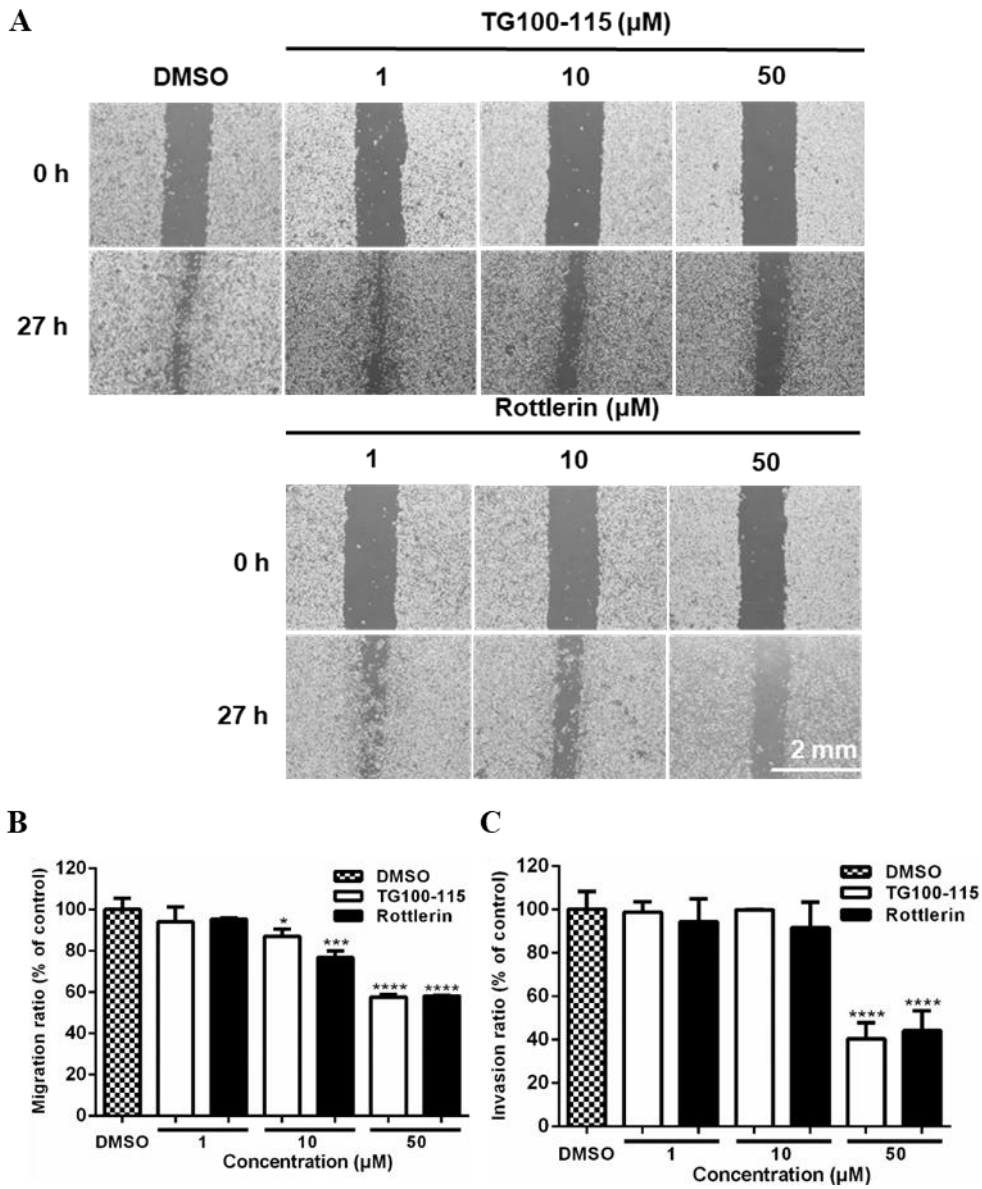
A
TG100-115 (μM)
DMSO
1
10
50
0 h
27 h
Rottlerin (μM)
1
10
50
0 h
27 h
2 mm
B
Migration ratio (% of control)
DMSO
TG100-115
Rottlerin
Concentration (μM)
C
Invasion ratio (% of control)
DMSO
TG100-115
Rottlerin
Concentration (μM)

TG100-115 has low cytotoxicity against MDA-MB-231 cells.

To determine whether cytotoxicity is the cause of the reduction of cell motility, the effects of TG100-115 and rottlerin on proliferation of MDA-MB-231 cells were elucidated (Figures. 2.6A, 2.6B, and 2.6C). TG100-115 at 50 μM concentration did not affect proliferation of MDA-MB-231 cells at both 15 h and 27 h, which are the treatment times used for invasion and migration assays, respectively. At 48 h after treatment, TG100-115 at 50 μM concentration was observed to reduce cell proliferation by 20.32 ± 1.28%, which is relatively low compared to the antiproliferative activity of rottlerin at the same concentration. GI_{50} values obtained from concentration-response curves show that rottlerin (GI_{50} = 1.76 ± 0.34 μM versus the reported value of 1.22 μM (Lu et al., 2014) has a 103-fold higher antiproliferative activity than that of TG100-115 (Table 2.3). Moreover, the results show that TG100-115 significantly inhibits breast cancer cell migration and invasion but it has a low cytotoxicity. In contrast, the inhibitory activity of rottlerin on cell invasion could be related to its cytotoxicity.

Figure 2.6. Representative concentration-response curves against MDA-MB-231 cells. The cells treated with different concentrations of TG100-115 or rottlerin were incubated for (A) 15, (B) 27, or (C) 48 h. Proliferation of MDA-MB-231 cells was measured via MTT assays.

A

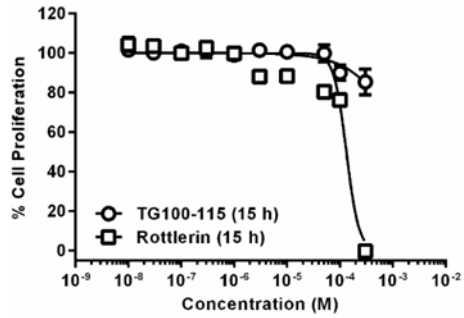
% Cell Proliferation
120
100
80
60
40
20
0
TG100-115 (15 h)
Rottlerin (15 h)
10-9 10-8 10-7 10-6 10-5 10-4 10-3 10-2
Concentration (M)

B

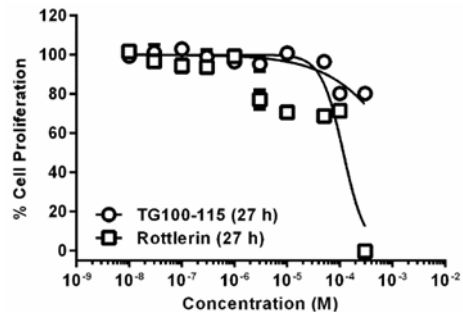
% Cell Proliferation
120
100
80
60
40
20
0
TG100-115 (27 h)
Rottlerin (27 h)
10-9 10-8 10-7 10-6 10-5 10-4 10-3 10-2
Concentration (M)

C

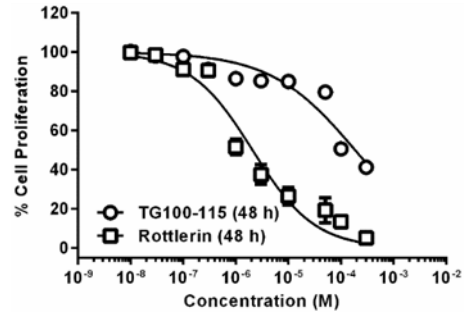
% Cell Proliferation
120
100
80
60
40
20
0
TG100-115 (48 h)
Rottlerin (48 h)
10-9 10-8 10-7 10-6 10-5 10-4 10-3 10-2
Concentration (M)

Table 2.3. GI_{50} values of TG100-115 and rottlerin against MDA-MB-231 cells

Compounds	GI_{50} (μM)	Literature GI_{50} (μM)
Rottlerin	1.76 ± 0.34	1.22 [a]
TG100-115	180.47 ± 13.71	

[a] The GI_{50} value was determined through Cell Titer Glo assay (Lu et al., 2014).

TG100-115 suppresses migration and invasion of MDA-MB-468 cells.

To assess the effect of TG100-115 on migration and invasion of other TNBC cells, I adopted MDA-MB-468 cells. Like MDA-MB-231 cells, the migration of MDA-MB-468 cells was decreased by TG100-115 (Figure 2.7A). TG100-115 and rottlerin reduced the migration of MDA-MB-468 cells in a concentration-dependent manner, and the migration ratios decreased by 50.62 ± 9.21% and 48.82 ± 1.01% at 50 μM concentration, respectively (Figure 2.7B). I also observed that invasion of MDA-MB-468 cells was significantly reduced by TG100-115 and rottlerin in a concentration-dependent fashion (Figure 2.7C). Invasion ratios of MDA-MB-468 cells in the presence of TG100-115 or rottlerin were decreased by 53.06 ± 1.06% and 47.34 ± 4.26% at 50 μM concentration, respectively.

Figure 2.7. TG100-115 and rottlerin suppress migration and invasion of MDA-MB-468 cells. (A) MDA-MB-468 cells in the presence of different concentrations of TG100-115 or rottlerin were incubated for 48 h after scratching cell monolayers. Scale bar represents 2 mm. (B) Migration ratios were calculated using migration areas. (C) Invasion assays were performed using CHEMICON QCM 24-well Invasion assay kit. Invasion ratios were calculated using fluorescence intensities. The cells treated with DMSO were used as a control.

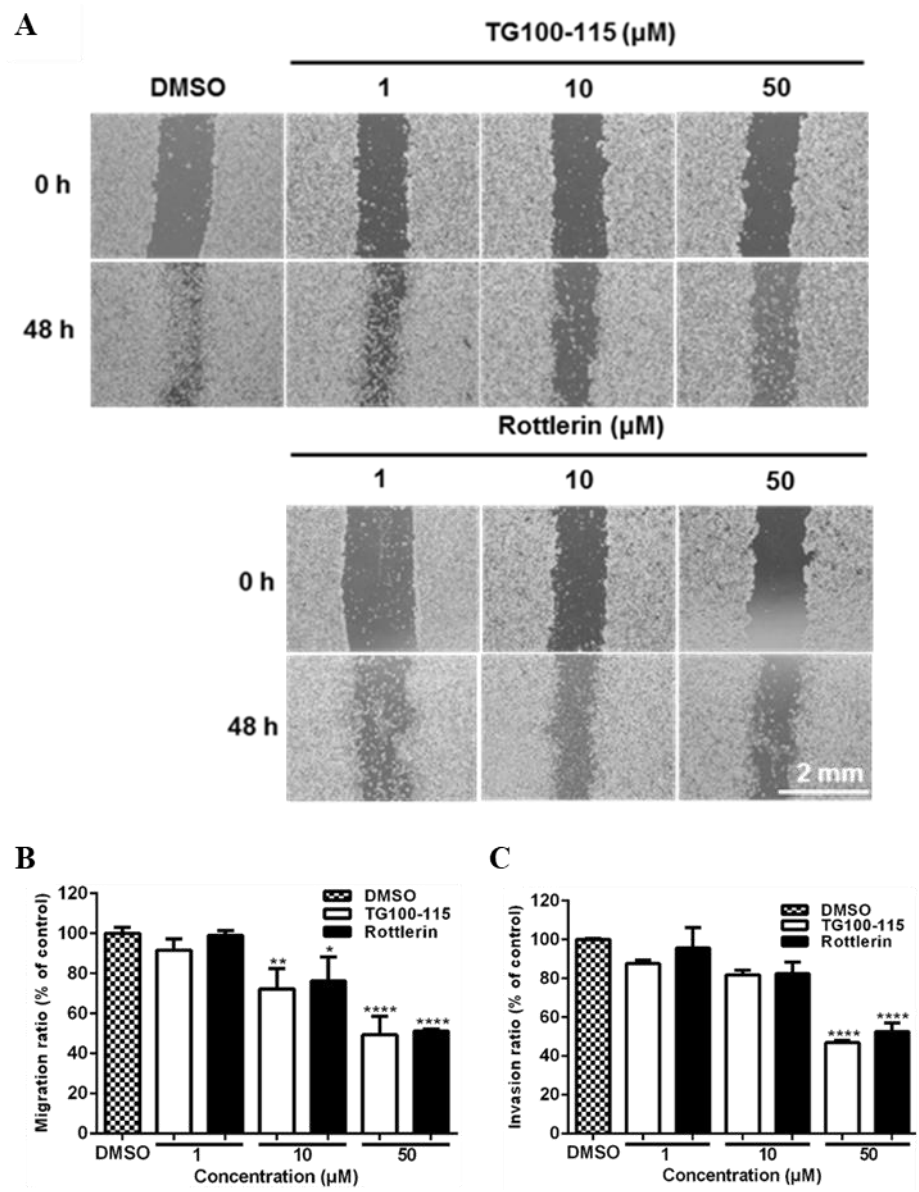
A
TG100-115 (μM)
DMSO
1
10
50
0 h
48 h
Rottlerin (μM)
1
10
50
0 h
48 h
2 mm
B
Migration ratio (% of control)
DMSO
TG100-115
Rottlerin
Concentration (μM)
C
Invasion ratio (% of control)
DMSO
TG100-115
Rottlerin
Concentration (μM)

PI3k inhibitory activity of TG100-115 partially contributes to the reduction of cell motility.

To investigate whether PI3K inhibitory activity of TG100-115 contributes to the reduced cell motility caused by TG100-115, I performed wound-healing assays and transwell invasion assays using PIK-294, a selective PI3K p110δ inhibitor, as TG100-115 has kinase-inhibitory activity against PI3K p110δ (Doukas et al., 2006). Like TG100-115, PIK-294 decreased the migration of MDA-MB-231 cancer cells in a concentration-dependent manner (Figure 2.8A). Migration ratio in the presence of 50 μM PIK-294 decreased by 27.69 ± 6.90% (Figure 2.8B), which is less than the reduction of that in the presence of 50 μM TG100-115. PIK-294 also reduced invasion of the cells by 43.31 ± 1.45% at 50 μM concentration (Figure 2.8C). Indeed, the effect of PIK-294 on the cell invasion was less than that of TG100-115. These data indicate that PI3K inhibitory activity of TG100-115 could partially affect the reduction of cell motility. I also examined the anti-proliferative activity of PIK-294 to determine whether cytotoxicity of PIK-294 contributes to the reduction of cell motility (Figure 2.8D). PIK-294 at 50 μM concentration reduced cell proliferation by 15.47 ± 9.60%, 24.42 ± 2.26%, and 28.10 ± 7.98% at 15 h, 27 h, and 48 h, respectively. The anti-proliferative activity of PIK-294 was higher than that of TG100-115. This might result from higher PI3K p110δ inhibitory activity of PIK-294 (IC_{50} = 10 nM, (Knight et al., 2006)) than that of TG100-115 (IC_{50} = 235 nM, (Doukas et al., 2006)) because it has been reported that knockdown of *PI3K p110δ* by small interfering RNA induced significant growth inhibition of multiple myeloma cells (INA-6) (Ikeda et al., 2010). These results suggest that cytotoxicity of PIK-294 could partially contribute to the reduction of cell motility.

Figure 2.8. PIK-294 suppresses migration and invasion of MDA-MB-231 cells. (A) MDA-MB-231 cells in the presence of different concentrations of PIK-294 were incubated for 27 h after scratching cell monolayers. Scale bar represents 2 mm. (B) Migration ratios were calculated using migration areas. (C) Invasion assays were performed using CHEMICON QCM 24-well Invasion assay kit and MDA-MB-231 cells in the presence of 50 μM TG100-115, rottlerin, or PIK-294. Invasion ratios were calculated using fluorescence intensities. (D) Representative concentration-response curves against MDA-MB-231 cells. The cells treated with different concentrations of PIK-294 were incubated for 15, 27, or 48 h.

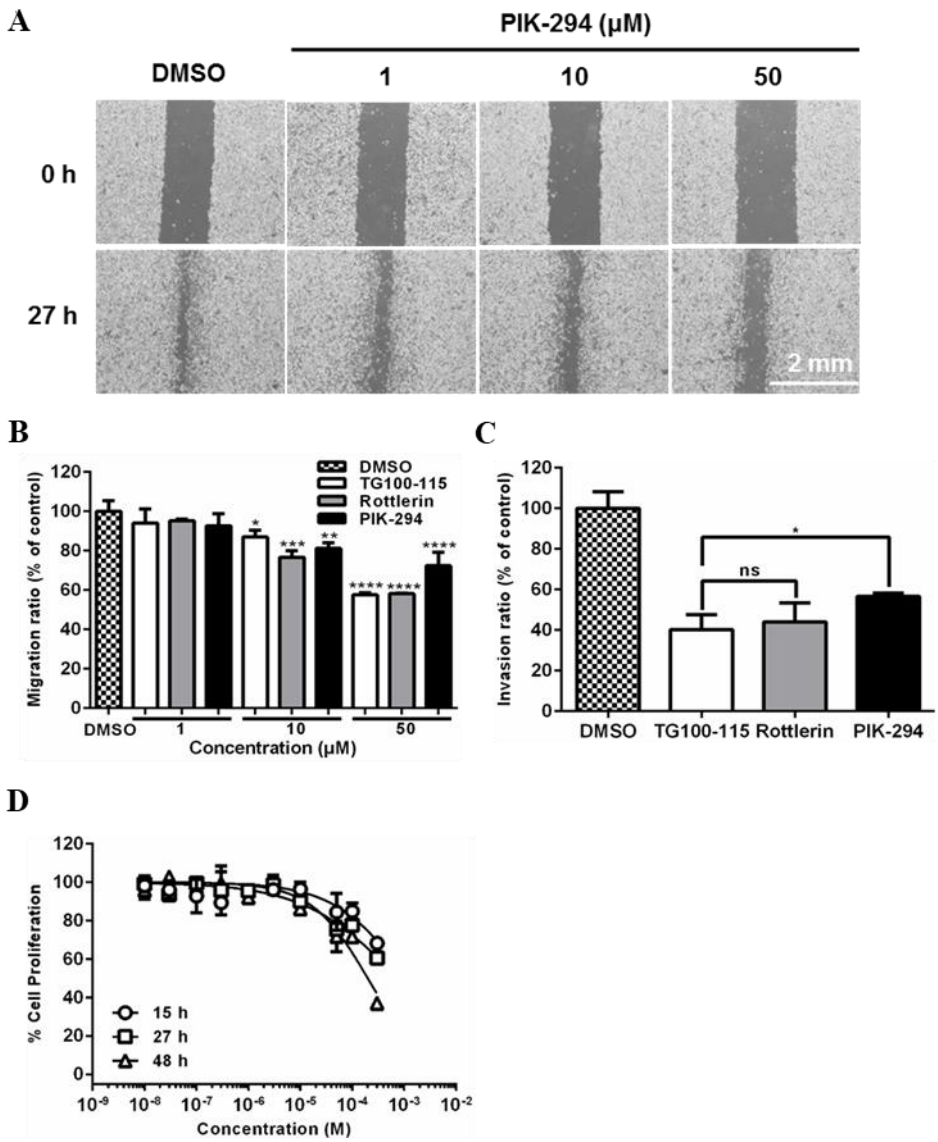
A
PIK-294 (μM)
DMSO
1
10
50
0 h
27 h
2 mm
B
DMSO
TG100-115
Rottlerin
PIK-294
Migration ratio (% of control)
Concentration (μM)
C
Invasion ratio (% of control)
ns
DMSO
TG100-115
Rottlerin
PIK-294
D
% Cell Proliferation
15 h
27 h
48 h
Concentration (M)

Reduction of cell motility by TG100-115 is associated with calcium ion.

Calcium ion is required for breast cancer cell migration (Yang et al., 2009). To examine whether the effects of TG100-115 on cell migration and invasion is associated with calcium ion, wound-healing assays and transwell invasion assays were performed with BAPTA-AM, a cell permeable calcium chelator. As a previous study (Di et al., 2015), migration of MDA-MB-231 cells was reduced by treatment of BAPTA-AM. TG100-115 inhibited the cell migration in the presence of BAPTA-AM in a concentration-dependent fashion (Figures 2.9A and 2.9B). The differences in migration ratio in the presence or absence of BAPTA-AM at 0 μM and 50 μM TG100-115 were 30.96% and 14.86%, respectively. Treatment of BAPTA-AM also reduced cell invasion (Figure 2.9C). The differences in invasion ratio in the presence or absence of BAPTA-AM at 0 μM and 50 μM TG100-115 were 33.91% and 5.76%, respectively. As a result, the effect of calcium chelation by treatment of BAPTA-AM on cell motility was decreased in the presence of high concentrations of TG100-115. These data suggest that TG100-115 suppresses the motility of MDA-MB-231 cells through a Ca^{2+}-dependent mechanism.

Figure 2.9. Effects of TG100-115 on migration and invasion of MDA-MB-231 cells in the presence of BAPTA-AM. (A) MDA-MB-231 cells treated with different concentrations of TG100-115 were incubated in the presence of 15 μM BAPTA-AM for 27 h after scratching cell monolayers. Scale bar represents 2 mm. (B) Migration ratios were calculated using migration areas. (C) Invasion assays were performed using CHEMICON QCM 24-well Invasion assay kit and MDA-MB-231 cells treated with different concentrations of TG100-115 in the presence of 15 μM BAPTA-AM. Invasion ratios were calculated using fluorescence intensities.

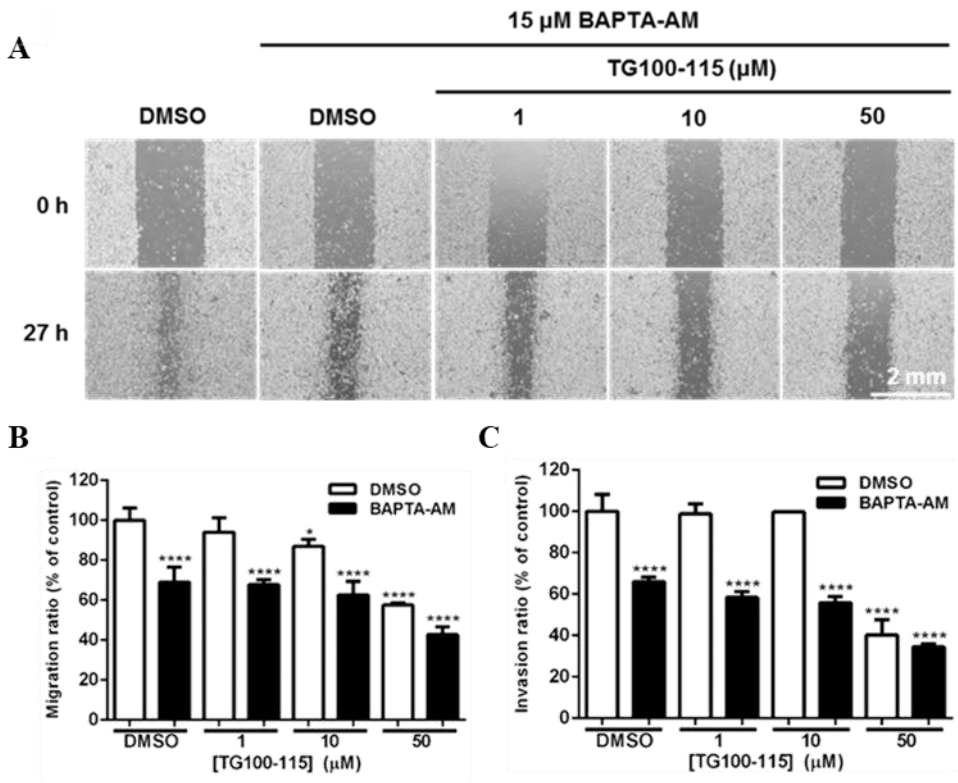
A
15 μM BAPTA-AM
TG100-115 (μM)
DMSO
DMSO
1
10
50
0 h
27 h
2 mm
B
Migration ratio (% of control)
DMSO
BAPTA-AM
[TG100-115] (μM)
C
Invasion ratio (% of control)
DMSO
BAPTA-AM
[TG100-115] (μM)

Reduction of cell motility by TG100-115 is associated with inhibition of TRPM7. To determine whether the effects of TG100-115 on cell motility is associated with inhibition of TRPM7, I performed transwell invasion assays using T-REx-293 cells stably expressing TRPM7 (Figure 2.10). TRPM7 overexpression induced by treatment of Dox increased cell invasion by 34.91 ± 1.88% compared to cells that are not treated with Dox. This phenomenon is consistent with a previous study showing that TRPM7 overexpression increased migration of MCF-7 and MDA-MB-231 cells (Guilbert et al., 2013), while Su et al. have reported that overexpression of TRPM7 caused cell rounding and loss of adhesion and knockdown of *TRPM7* increased cell adhesion, spreading and motility of HEK-293 cells (Su et al., 2006). This discrepancy might be due to different cell types or different motility assay types. Cell invasion induced by TRPM7 overexpression was reduced by 48.05 ± 8.32% in the presence of 50 μM TG100-115 compared to cells overexpressing TRPM7 that are not treated with TG100-115. These results show that TG100-115 suppresses cell motility through inhibition of TRPM7.

Figure 2.10. TG100-115 suppresses invasion of T-REx-293 cells expressing TRPM7. Invasion assays were performed using CHEMICON QCM 24-well Invasion assay kit and T-REx-293 cells expressing TRPM7 treated with different concentrations of TG100-115 in the presence or absence of 1 μg/mL Dox. Invasion ratios were calculated using fluorescence intensities. The cells treated with DMSO in the absence or presence of Dox were used as controls.

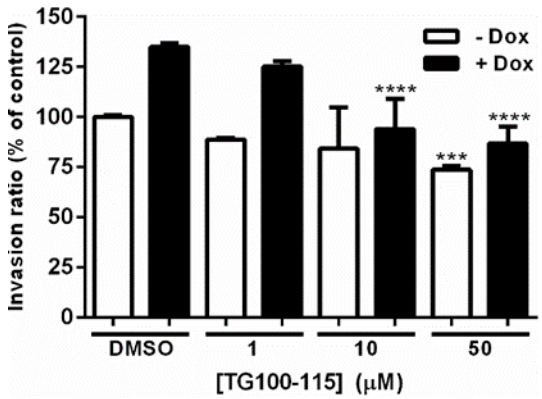
Invasion ratio (% of control)
150
125
100
75
50
25
0
- Dox
+ Dox
****
****
***
DMSO
1
10
50
[TG100-115] (μM)

TG100-115 inhibits phosphorylation of myosin IIA heavy chain and FAK.

The myosin IIA heavy chain plays a role in TRPM7 kinase domain-mediated migration of MDA-MB-231 cells (Guilbert et al., 2013). To investigate whether TG100-115 affects the phosphorylation of myosin IIA heavy chain, I performed Western blot analysis in MDA-MB-231 cells in the presence of TG100-115 or rottlerin (Figure 2.11A). Treatments of TG100-115 and rottlerin decreased the phosphorylation of myosin IIA heavy chain by 34.04 ± 2.01% and 13.27 ± 3.09% at 100 μM, respectively (Figure 2.11B). The partial decrease in phosphorylation of myosin IIA heavy chain caused by TG100-115 is in accord with observations made in earlier efforts which show that *TRPM7* knockdown decreases myosin IIA phosphorylation by 41% in MDA-MB-231 cells (Guilbert et al., 2013). The phosphorylation level of FAK, an adhesion marker in MDA-MB-231 cells (Sawhney et al., 2009), was also elucidated. The results of Western blotting experiments show that phosphorylation of FAK in the presence of 100 μM TG100-115 or rottlerin is reduced by 70.36 ± 2.00% and 82.44 ± 1.51%, respectively (Figure 2.11C). The migration inhibition of rottlerin through reduced phosphorylation of FAK in cells was coincided with the previous report that rottlerin decreases migration of CGTH W-2 cells through downregulation of phosphorylated FAK (pFAK), integrin β-1, phosphorylated paxillin, RhoA, and Rac-1 in a PKCδ-independent manner (Lin et al., 2010). The results of biochemical kinase assays (Figure 2.11D) show that FAK kinase activity is decreased by 25% in the presence of 100 μM TG100-115. The overall data indicate that TG100-115 and rottlerin decrease the level of phosphorylation of the myosin IIA heavy chain and FAK in MDA-MB-231 cells, and that TG100-115 does not directly inhibit phosphorylation of FAK.

Figure 2.11. TG100-115 suppresses phosphorylation of myosin IIA and FAK in MDA-MB-231 cells. (A) Representative Western blots. MDA-MB-231 cells were incubated with different concentrations of TG100-115 or rottlerin for 24 h. Protein lysates were analyzed by using Western blot analysis with indicated antibodies. Bands of (B) phosphorylated myosin IIA and (C) phosphorylated FAK obtained from (A) were quantified by densitometry analysis. (D) A concentration-response curve of TG100-115 against FAK through a filtration binding assay based biochemical kinase assay.

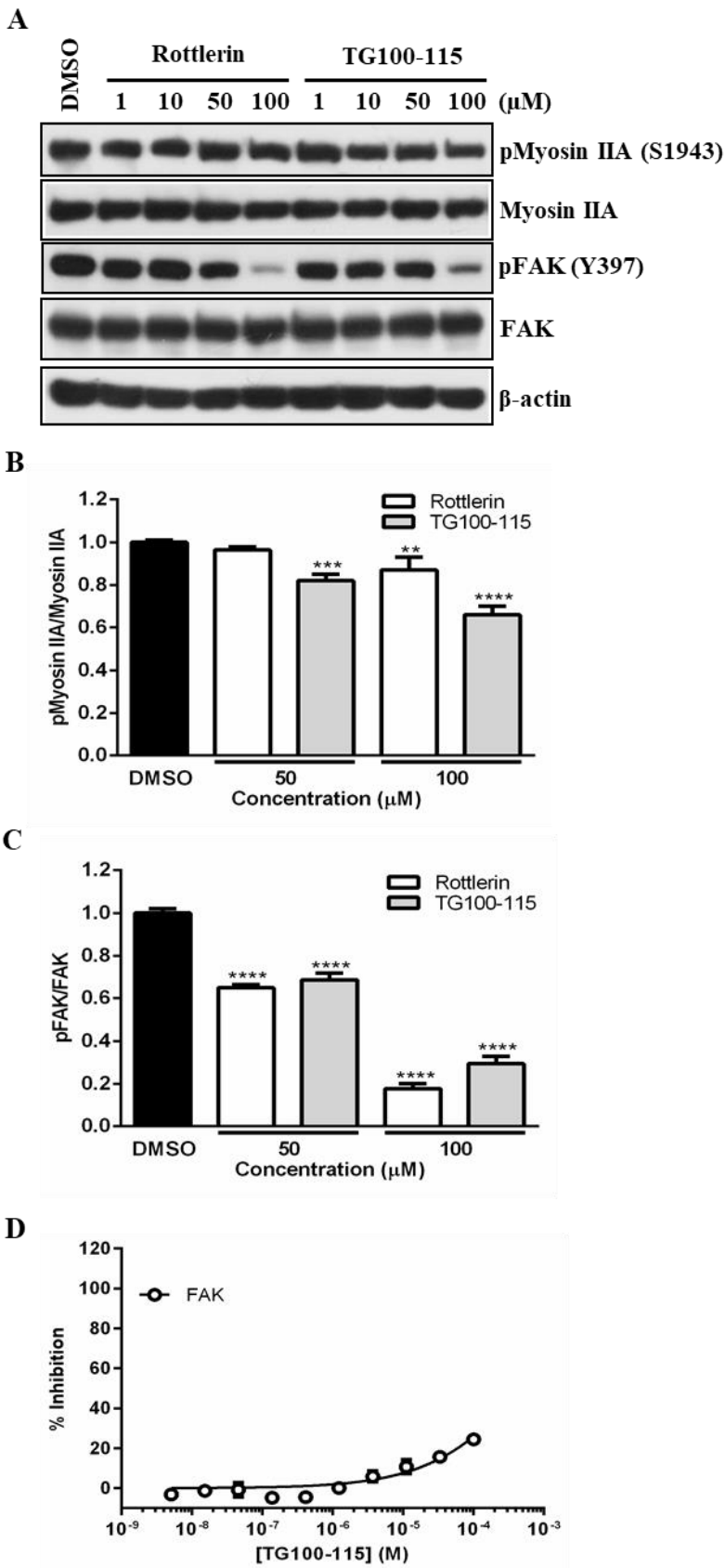
A
DMSO
Rottlerin
TG100-115
1 10 50 100 1 10 50 100 (μM)
pMyosin IIA (S1943)
Myosin IIA
pFAK (Y397)
FAK
β-actin
B
pMyosin IIA/Myosin IIA
Rottlerin
TG100-115
DMSO
50
100
Concentration (μM)
C
pFAK/FAK
Rottlerin
TG100-115
DMSO
50
100
Concentration (μM)
D
% Inhibition
FAK
[TG100-115] (M)

TG100-115 suppresses the channel activity of TRPM7.

To determine if TG100-115 inhibits the channel activity of TRPM7, patch clamp recordings were made using T-REx-293 cells stably expressing TRPM7. The voltage-dependent outward TRPM7 currents of the cells treated with different concentrations of TG100-115 were measured by applying voltage pulses from -120 mV to +100 mV in 10-mV increments using a whole-cell patch-clamp technique (Figure 2.12A). Consistent with previous reports (Li et al., 2006), I observed that 2-APB, a known TRPM7 channel blocker, decreases the TRPM7 current amplitude. In addition, TG100-115 causes a decrease in the current in a concentration-dependent manner (Figure 2.12B). TRPM7 currents are decreased by 41.51 ± 10.33% in the presence of 100 μM TG100-115. TG100-115 blocked TRPM7 channel activity at 100 μM concentration in time course of TRPM7 current amplitude (Figure 2.12C). These results show that TG100-115 is an inhibitor of the channel activity of TRPM7. To further confirm whether TG100-115 inhibits the channel activity of endogenous TRPM7, I performed patch clamp experiments using MDA-MB-231 cancer cells. The voltage-dependent outward TRPM7-like currents of the cells in the presence of 100 μM TG100-115 were recorded by applying voltage pulses from -100 mV to +100 mV in 10 mV increments using a whole-cell patch-clamp technique (Figure 2.12D). Like T-REx-293 cells expressing TRPM7, TG100-115 decreased TRPM7-like currents by 53.60 ± 7.44% at 100 μM concentration (Figure 2.12E). Reduced TRPM7-like currents induced by TG100-115 were rescued after wash-out. TG100-115 has reversible inhibitory activities against TRPM7-like currents, which implies that the channel inhibitory activity of TG100-115 would not result from its TRPM7 kinase-inhibitory activity because decreased TRPM7-like currents by TG100-115 were rescued after wash-out.

Figure 2.12. TG100-115 suppresses TRPM7 channel activities in both T-REx-293 cells stably expressing TRPM7 and MDA-MB-231 cells. (A) Representative traces showing the TRPM7 current-voltage relationships before and after treatment with TG100-115 in T-REx-293 cells expressing TRPM7. (B) Histograms showing the inhibitory effect of TG100-115 on TRPM7 current amplitude at +80 mV. (C) Time course of TRPM7 current amplitude at +80 mV during application of 100 μM TG100-115. (D) Representative traces showing the TRPM7-like current-voltage relationships before and after treatment with TG100-115 in MDA-MB-231 cells. (E) Histograms showing the inhibitory effect of TG100-115 on TRPM7-like current amplitude at +100 mV. Error bars represent S.D. (The n value for each statistical analysis was indicated at histograms.). The patch clamp experiments were performed by Ms. Bae, Yeonju (School of Biosystem and Biomedical Science, College of Health Science, Korea University, Republic of Korea).

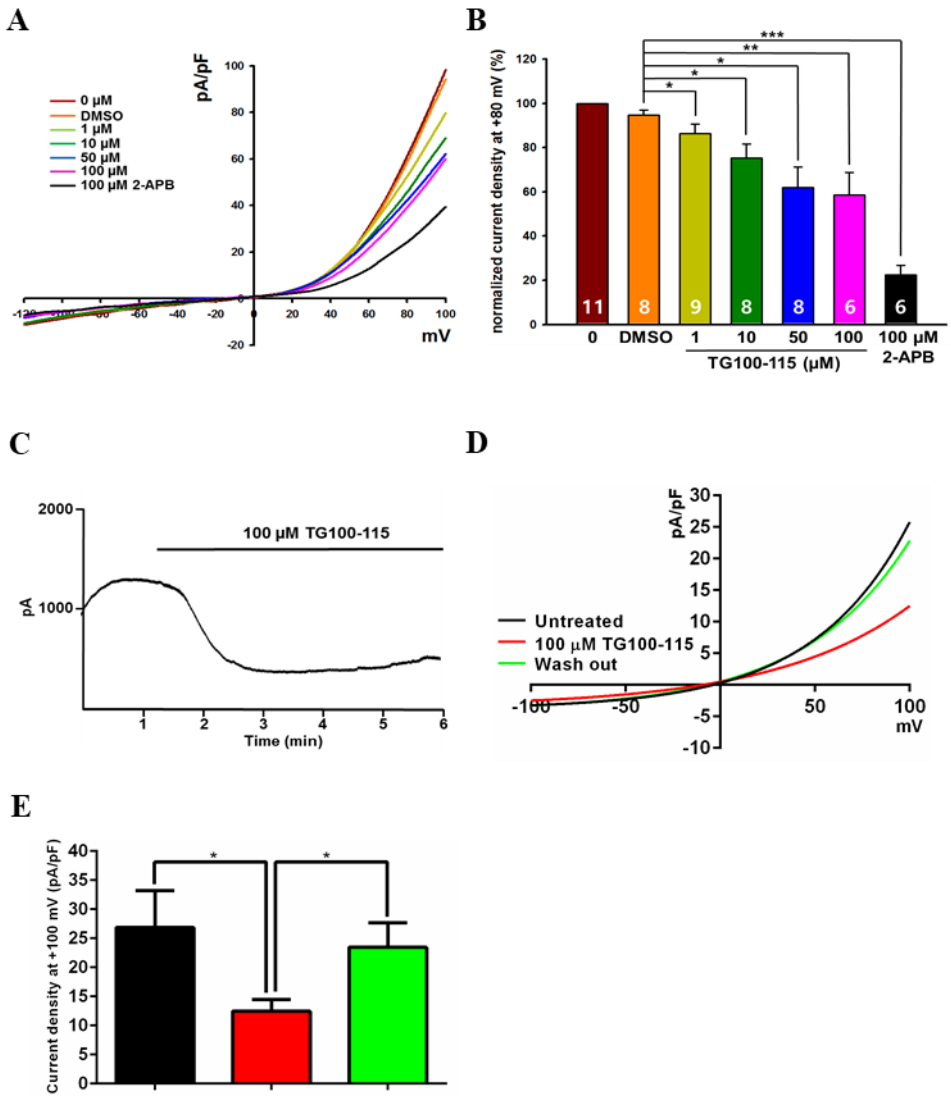
A
0 μM
DMSO
1 μM
10 μM
50 μM
100 μM
100 μM 2-APB
pA/pF
mV
B
normalized current density at +80 mV (%)
11
8
9
8
8
6
6
0
DMSO
1
10
50
100
TG100-115 (μM)
100 μM
2-APB
C
100 μM TG100-115
pA
Time (min)
D
pA/pF
Untreated
100 μM TG100-115
Wash out
mV
E
Current density at +100 mV (pA/pF)

Discussion

A HTS assay to identify inhibitors of TRPM7 ion channel has been developed previously (Castillo et al., 2010). The method relies on quenching of the fluorescence of fura-2 by Mn^{2+}. The TRPM7 kinase assay, however, is performed using radioactive isotopes (Ryazanova et al., 2004), an approach that is not suitable for HTS to uncover new TRPM7 kinase inhibitors. The approach used a LANCE *Ultra* TR-FRET based assay system, which is widely used for screening owing to its low background signals and homogeneous assay format. Because homogeneous assays do not require separation of the bound antigen-antibody from the free antigen, they are typically more easily and rapidly performed. In order to identify an ideal substrate for the *in vitro* TRPM7 kinase assay using the LANCE *Ultra* TR-FRET system, five U*Light*-labeled peptides were screened. Unexpectedly, the S/B ratios seen in the LANCE *Ultra* TR-FRET assays were too low when MBP and histone H3 peptides were used as substrates, although MBP and histone H3 were identified as substrates for TRPM7 kinase using the conventional radiolabel based *in vitro* assay (Ryazanova et al., 2004). These results might be a consequence of the different conditions employed in the two assays such as phosphorylation sites and divalent cation concentrations. It was reported that phosphorylation of MBP by TRPM7 kinase domain occurs predominantly on serine (Ryazanova et al., 2004), but a MBP peptide containing Thr232 was used in the current study. Ryazanova et al. showed that phosphorylation level of histone H3 by the TRPM7 kinase domain is low in the absence of Mn^{2+} (Ryazanova et al., 2004), but I performed the *in vitro* TRPM7 kinase assays in the absence of Mn^{2+}. Finally, the effort showed CREB peptide as an ideal substrate for the TRPM7 kinase assay. The results of studies using the CREB peptide as substrate and the FRET based assay showed that divalent cations such as Mg^{2+} and Mn^{2+} have similar effects as those reported earlier (Ryazanova et al., 2004). The observations suggest that the *in vitro* TRPM7 kinase assay using CREB peptide as a substrate give results that are similar to those arising from the conventional TRPM7 kinase assay system using radioactive isotopes.

A small molecule library screening using the LANCE *Ultra* TR-FRET assay system led to identification of five compounds that have TRPM7 kinase inhibitory activities. Among them, TG100-115 was the most potent inhibitor. TG100-115 effectively reduced the migration of MDA-MB-231, TNBC cells while it has relatively low antiproliferative activity compared to rottlerin. This finding was consistent with previous reports that down regulation of TRPM7 had no influence on the proliferation of MDA-MB-231 cells (Guilbert et al., 2013) and rottlerin inhibited proliferation of MDA-MB-231 cells through suppression of Wnt/β-catenin and mTORC1 signaling (Lu et al., 2014). Like MDA-MB-231 cells, TG100-115 and rottlerin reduce the migration and invasion of MDA-MB-468 cells, TNBC cells. Reduction of cell motility by TG100-115 may be partially due to its PI3K p110δ inhibitory activity (Doukas et al., 2006), because PIK-294, a PI3K p110δ inhibitor, also reduced migration and invasion of MDA-MB-231 cells. Likewise, reduction of cell motility by TG100-115 may result from its TRPM7 inhibitory activity, because it also reduced invasion of T-REx-293 cells expressing TRPM7. Unexpectedly, TG100-115 decreased phosphorylation of FAK, which was not anticipated based on the previous report that p-FAK was not affected by *TRPM7* knockdown in MDA-MB-231 cells (Guilbert et al., 2013). PI3K p110δ inhibitory activity (Doukas et al., 2006) of TG100-115 may contribute to decrease of p-FAK, since *p110δ* knockdown decreases migration and invasion of glioma cells via downregulation of FAK and cdc42 (Luk et al., 2012). Its inhibitory effect on cancer cell migration might be a consequence of its inhibition of TRPM7 kinase-promoted phosphorylation of myosin IIA heavy chain and FAK.

Several studies reported that TRPM7 kinase domain is essential for ion channel activity (Schmitz et al., 2003; Matsushita et al., 2005; Ryazanova et al., 2010), but its effects on the ion channel function remain controversial (Runnels et al., 2001; Schmitz et al., 2003; Kozak et al., 2005; Matsushita et al., 2005; Zhang et al., 2014). Several studies showed that kinase activity affects the channel function of TRPM7 (Runnels et al., 2001; Schmitz et al., 2003; Zhang et al., 2014), while observations made in other efforts indicated that the kinase activity of TRPM7 does

not alter the ion channel activity (Matsushita et al., 2005). This discrepancy might be caused by limitations of the heterologous expression system in cell lines. Recently, two groups reported the findings of an effort utilizing an *in vivo* mice system that show that changes in the TRPM7 kinase activity do not significantly alter the ion channel function (Kaitsuka et al., 2014; Ryazanova et al., 2014). In contrast to these reports, I observed that the TRPM7 kinase inhibitor TG100-115 reduces the ion channel activity of TRPM7 in both T-REx-293 cells expressing TRPM7 and MDA-MB-231 cells. This discrepancy could be a consequence of off-target effects or direct binding effects of TG100-115 to TRPM7 channels.

The suppressive effect on cell motility by TG100-115 was related with calcium ion. This observation is consistent with the results showing that TG100-115 inhibited TRPM7 channel activity, because TRPM7 is responsible for calcium signaling (Wei et al., 2009). The detailed molecular mechanism(s) underlying the effects of TG100-115 on ion channel activity need to be elucidated.

The results described herein suggest that TG100-115 can be used as a lead compound in further efforts aimed at designing new and more potent TRPM7 kinase inhibitors. In addition, further refinement of TG100-115 may provide new therapeutic drugs for TNBC treatment.

Part III

Enhancement of TRAIL-Induced Apoptosis by Suppression of TRPM7 in TNBC Cells

Part III of the present study has been accepted for publication as Song et al., "Suppression of TRPM7 Enhances TRAIL-induced Apoptosis in Triple-Negative Breast Cancer Cells", *J Cell Physiol*.

Abstract

TRPM7 regulates TNBC cell migration, invasion, and metastasis, but it does not modulate TNBC proliferation. However, previous studies have shown that combination treatment of non-selective TRPM7 channel inhibitors (2-aminoethoxydiphenyl borate and Gd^{3+}) with TRAIL increases antiproliferative effects and apoptosis in prostate cancer cells and hepatic stellate cells. Thus, the present work investigated the potential role of TRPM7 in proliferation and apoptosis of TNBC cells (MDA-MB-231 and MDA-MB-468 cells) with TRAIL. The findings demonstrate that suppression of TRPM7 via *TRPM7* knockdown or pharmacological inhibition synergistically increases TRAIL-induced antiproliferative effects and apoptosis in TNBC cells. Furthermore, it is shown here that the synergistic interaction might be associated with TRPM7 channel activities using combination treatments of TRAIL and TRPM7 inhibitors (NS8593 as a TRPM7 channel inhibitor and TG100-115 as a TRPM7 kinase inhibitor). It is also revealed that downregulation of c-FLIP via inhibition of Ca^{2+} influx might be involved in the synergistic interaction. This study provides both a new role of TRPM7 in TNBC cell apoptosis and potential combinatorial therapeutic strategy using TRPM7 inhibitors with TRAIL for treatment of TNBC.

Introduction

Breast cancer is thought to be the most common cancer in women and the second leading cause of cancer death in women (Siegel et al., 2019). Approximately 15−20% of all breast cancer patients in the United States has been diagnosed as TNBC (Diana et al., 2018). Due to lack of drug targets such as ER and PR at cell surface, TNBC is difficult to treat effectively. Moreover, TNBC patients treated with surgery, radiation therapy, and chemotherapy are often likely to have cancer recurrence and metastasis (Wu et al., 2016). Therefore, discovery of novel potent therapies is needed to cure TNBC patients.

TRPM7 has been reported to be involved in breast cancer cell proliferation, migration, and metastasis (Guilbert et al., 2009; Middelbeek et al., 2012; Guilbert et al., 2013; Meng et al., 2013; Davis et al., 2014). It has been found that TRPM7 regulates migration and invasion of MDA-MB-435 cells (TNBC cell line) through a MAPK signaling pathway and suppression of *TRPM7* by siRNA-mediated gene silencing and pharmacological inhibition reduces metastatic potential of MDA-MB-231 cells (TNBC cell line) (Guilbert et al., 2013; Meng et al., 2013; Song et al., 2017). While *TRPM7* knockdown attenuates migration and invasion of TNBC cells, it does not affect proliferation of TNBC cells such as MDA-MB-435 and MDA-MB-231 (Guilbert et al., 2013). If I find specific conditions where suppression of TRPM7 could affect proliferation of TNBC cells, it will be a potent therapy interfering both proliferation and metastasis of TNBC.

Tumor necrosis factor-related apoptosis-inducing ligand (TRAIL) has been shown to selectively induce apoptosis in various types of cancer cells, but not in normal cells (Ashkenazi et al., 1999; MacFarlane, 2003; Wang and El-Deiry, 2003). TRAIL has been reported to induce tumor regression in xenograft models without inducing substantial toxicity in host animals (Ashkenazi et al., 1999). Despite it being able to selectively induce tumor regression without no apparent toxicity, clinical trials with TRAIL have failed due to innate or acquired resistance (Herbst et al., 2010; Lemke et al., 2014). Nevertheless, combination therapies with TRAIL and

chemotherapeutic drugs or targeted drugs have been reported due to cancer-specific apoptosis-inducing potential of TRAIL (Alladina et al., 2005; Cristofanon and Fulda, 2012; Refaat et al., 2014; Wang et al., 2007). Interestingly, two research groups have reported that inhibition of TRPM7 enhances TRAIL-induced apoptosis in both PC-3 cells (human prostate cancer cell line) and HSC-T6 cells (rat hepatic stellate cell line) (Lin et al., 2015; Liu et al., 2012). Both research groups have observed increased apoptotic cells induced by combination treatments with TRAIL and non-selective TRPM7 channel inhibitors such as 2-APB and Gd^{3+} (Lin et al., 2015; Liu et al., 2012).

The present study investigated whether suppression of TRPM7 enhances TRAIL-induced apoptosis in TNBC cells and molecular mechanisms of synergistic effect with inhibition of TRPM7 and TRAIL. It was found that suppression of TRPM7 by siRNA-mediated gene silencing or pharmacological inhibition enhances TRAIL-induced apoptosis in TNBC cells and the synergistic effect might have associated with TRPM7 channel activities rather than TRPM7 kinase activities. Furthermore, it was examined whether Ca^{2+} and c-FLIP might be responsible for the synergistic effect.

Materials and Methods

Antibodies and reagents

NS8593 was purchased from Tocris Bioscience (UK), TG100-115 was purchased from Selleck Chemicals (USA) and 1,2-Bis(2-aminophenoxy)ethane-N,N,N′,N′-tetraacetic acid tetra-acetoxymethyl ester (BAPTA-AM) was purchased from Sigma-Aldrich (USA). Recombinant soluble human TRAIL (Super Killer TRAIL) was purchased from Enzo Life Sciences (SUI). HRP-conjugated anti-mouse IgG (SA001-500) and HRP-conjugated anti-rabbit IgG (SA002-500) were purchased from GenDEPOT (USA), antibody against β actin (SC-47778) was purchased from Santa Cruz Biotechnology (USA), antibody against TRPM7 (N74/25) was purchased from NeuroMab (USA), antibodies against PARP (9542), Caspase-3 (9662), Caspase-8 (9746), and c-FLIP (56343) were purchased from Cell Signaling Technology (USA).

Cell culture

MCF10A cells were cultured in DMEM/F12 (Welgene, Republic of Korea) supplemented with 5% (v/v) horse serum (Gibco, NZ), 20 ng/mL EGF (Sigma-Aldrich, USA), 100 ng/mL cholera toxin (Sigma-Aldrich, USA), 500 ng/mL hydrocortisone (Sigma-Aldrich, USA), 10 μg/mL recombinant human insulin (Invitrogen, USA), 100 units/mL penicillin (Welgene, Republic of Korea), and 100 μg/mL streptomycin (Welgene, Republic of Korea) in a humidified 5% CO_2 incubator at 37 °C. MDA-MB-231 cells (Korean Cell Line Bank, Republic of Korea) and MDA-MB-468 cells were cultured in RPMI 1640 media and DMEM media, respectively, supplemented with 10% (v/v) FBS, penicillin (100 units/mL) and streptomycin (100 μg/mL) in a humidified 5% CO_2 incubator at 37 °C. Cells were passaged every two or three days.

RNA interference analysis

The siRNA against *TRPM7* gene (siTRPM7) was synthesized by Bioneer (Republic of Korea) and scrambled siRNA (AccuTarget Negative Contol siRNA) was purchased from Bioneer (Republic of Korea). MDA-MB-231 or MDA-MB-468 cells were seeded on 6-well plates (Thermo, USA) at 4.0 x 10^5 cells per well, and transfected with scrambled siRNA as a control, siTRPM7 (5'-GUCUUGCCAUGAAAUACUCdTdT-3') (Guilbert et al., 2013; Hanano et al., 2004), or siFLIP (5′-GGAUAAAUCUGAUGUGUCCUCAUUA-3′) (Piggott et al., 2011) using Lipofectamine RNAiMAX (Life Technologies, USA) according to the manufacturer's instructions.

RT-PCR analysis

Total RNA in MCF10A, MDA-MB-231, or MDA-MB-468 cells was extracted using TRIZOL (Invitrogen, USA) according to the manufacturer's instructions. Reverse transcription was performed with 1 μg of total RNA using M-MLV reverse transcriptase (Promega, USA). PCR reactions were carried out using AccuPower PCR PreMix (Bioneer, Republic of Korea) with complementary DNA. Sequences of primers for RT-PCR reactions were as follows: a forward primer for β-actin; 5'-TCCTGTGGCATCCACGAAACT-3'; a reverse primer for β-actin; 5'-GAAGCATTTGCGGTGGACGAT-3'; a forward primer for *TRPM7*; 5'-CCATACCATATTCTCCAAGGTTCC-3'; a reverse primer for *TRPM7*; 5'-CATTCCTCTTCAAATCTGGAAGTT-3'; a forward primer for *c-FLIP*; 5'-CGGACTATAGAGTGCTGATGG-3'; a reverse primer for *c-FLIP*$_L$; 5'-GATTATCAG GCAGATTCCTAG-3'; a reverse primer for *c-FLIP*$_S$; 5'-AGATCAGGACAATGGGCATAG-3'. PCR products were resolved on 1.8% agarose gels and relative mRNA levels were determined by densitometry analysis using Image J software (National Institutes of Health, USA).

Cell proliferation assay

MDA-MB-231 or MDA-MB-468 cells were seeded into white-walled 96-well plates (Corning, USA) with clear bottoms at a density of 5.0 x 10^3 cells per well, and then incubated for 24 h at 37 °C in a humidified 5% CO_2 incubator. After removing the culture media, fresh media containing different concentrations of recombinant TRAIL and/or compounds were added, and incubated for 16 h at 37 °C. After 16 h, proliferative cells were determined by CellTiter-Glo assay (Promega, USA). Luminescence was measured using an Envision microplate reader (PerkinElmer, USA).

Western blot analysis

MCF10A, MDA-MB-231, or MDA-MB-468 cells (4.0 x 10^5 cells) were washed once with cold DPBS (WelGene, Republic of Korea), and lysed in ice-cold RIPA buffer (20 mM Tris-HCl, 0.5% sodium deoxycholate, 0.1% SDS, 1.0% Triton X-100, 1 mM Na_2 eEF2, 100 mM NaCl, 2 mM Na_3VO_4, 2.5 mM NaF and pH7.4) with a protease inhibitor cocktail tablet (Roche, GER) for 30 min at 4°C. Proteins from cell lysates were quantified using the BCA Assay Kit (Thermo/Pierce, USA), and equivalent amounts of proteins were loaded on sodium dodecylsulfate polyacrylamide gels. Separated proteins were transferred to a 0.45-μm nitrocellulose membrane (GE Healthcare Life Sciences, USA), and the membrane was blocked with 5% skim milk in Tris-buffered saline with Tween-20 (137 mM NaCl, 20 mM Tris-HCl, 0.1% Tween-20, and pH 7.4) for 1 h. After blocking, the membrane was incubated with primary antibodies overnight at 4 °C, and HRP-conjugated anti-mouse IgG or -rabbit IgG were used as secondary antibodies. Complex with HRP-linked secondary antibody was detected using the ECL solution (AgainBS, Republic of Korea). Densitometry analysis of Western blot data was carried out using Image J software.

Apoptosis assay

Apoptosis assay was performed using FITC Annexin V Apoptosis Detection Kit with FITC-labelled annexin V and PI (BD Biosciences, USA) according to the manufacturer's instructions. MDA-MB-231 or MDA-MB-468 cells (4.0 x 10^5 cells) were harvested, washed twice with cold DPBS, and resuspended in Annexin V Binding Buffer. Cells were stained with FITC-labelled annexin V for 15 min at RT in the dark, followed by addition of PI. Stained cells were immediately analyzed using BD Accuri C6 (BD Biosciences, USA).

Synergy analysis

Combination index (CI) of NS8593 and recombinant TRAIL was determined by the Chou-Talalay method using CompuSyn software (ComboSyn, USA) (Chou, 2010; Chou & Talalay, 1984). Cell proliferation assay data were used to evaluate the CI values of NS8593 and recombinant TRAIL. The CI values defines synergism (CI < 1), additive effect (CI = 1) and antagonism (CI > 1).

Cell morphology analysis

Morphological cell changes were observed with a Nikon Eclipse Ti microscope (Nikon Instruments, JP).

Cell cycle assay

MDA-MB-231 cells (4.0 x 10^5 cells) were harvested and fixed in 70% (v/v) ethanol and stored at -20 °C until analysis. After washing, the cells were treated with PI/RNase A staining solution (Cell Signaling Technology, USA) for 30 min at RT in the dark. Stained cells were immediately analyzed using BD Accuri C6 (BD Biosciences, USA). Percentages of the cells in G0/G1, S, and G2/M phases were

calculated by the Dean-Jett-Fox model.

Colony formation assay

MDA-MB-231 cells were seeded on 6-well plates (Thermo, USA) at 1.0 x 10^3 cells per well. The cells were incubated with the compounds for 14 days at 37 °C and 5% CO_2. During the 14-day incubation period, the culture media were replaced every 2 days. Spheroids were stained using crystal violet staining solution (0.05% crystal violet, 1% methanol, and 1% formaldehyde in DPBS) for 24 h. The samples were washed twice with DPBS, and incubated with 10% (v/v) acetic acid for 30 min. The absorbance at 570 nm was measured using the FlexStation 3 microplate reader (Molecular Devices, USA).

Intracellular Ca^{2+} assay

MDA-MB-231 cells (4.0 x 10^5 cells) were harvested and washed twice with cold DPBS. The cells were stained with 1 μM Fluo-3-AM (Invitrogen, USA) for 30 min at RT in the dark. Stained cells were immediately analyzed using BD Accuri C6 (BD Biosciences, USA).

Statistical analysis

All data were analyzed using Prism 6 software (GraphPad, USA), and presented as mean ± S.D.. Statistical significances were evaluated by either two-tailed Student's t-test when differences between two groups or one-way ANOVA with Tukey's multiple comparison test when differences among three or more groups. Statistical values of $p < 0.05$ were considered to be statistically significant. *$p < 0.05$, **$p < 0.01$, ***$p < 0.001$, and ****$p < 0.0001$. Error bars represent S.D. (n = 3).

Results

Silencing of *TRPM7* increases TRAIL-induced antiproliferative effects in TNBC cells.

It has been reported that pharmacological inhibition (Gd^{3+} and 2-APB) of TRPM7 increases TRAIL-induced antiproliferative effects in PC-3 and HSC-T6 cells and *TRPM7* gene silencing increases TRAIL-induced antiproliferative effects in PC-3 cells (Lin et al., 2015; Liu et al., 2012). Based on these reports, to examine whether TRAIL-induced antiproliferative effects are affected by silencing of *TRPM7* gene in TNBC cells, siRNA-mediated *TRPM7* gene silencing was performed. Firstly, I investigated whether *TRPM7* expression level in TNBC cells (MDA-MB-231 and MDA-MB-468 cells) is higher than that in normal breast cells (MCF10A cells) through RT-PCR (Figures 3.1A and 3.1B) and Western blot (Figures 3.1C and 3.1D). TRPM7 was predominantly expressed in MDA-MB-231 cells among the three breast cancer cell lines. I then employed a human *TRPM7*-specific siRNA (siTRPM7) to decrease expression of *TRPM7* gene. After two days following transfection with siTRPM7 in MDA-MB-231 and MDA-MB-468 cells, expression levels of *TRPM7* mRNA were reduced by 83.00 ± 4.49% and 79.93 ± 2.39% in MDA-MB-231 and MDA-MB-468 cells, respectively, as compared with the cells transfected with scrambled siRNA (Figures 3.2A and 3.2B). TRPM7 protein levels in MDA-MB-231 and MDA-MB-468 cells transfected with siTRPM7 were also decreased by 89.23 ± 2.81% and 69.30 ± 7.24% in MDA-MB-231 and MDA-MB-468 cells, respectively, compared to cells that are transfected with scrambled siRNA (Figures 3.2C and 3.2D). After confirmation of significant knockdown of TRPM7 protein, I measured proliferation of MDA-MB-231 and MDA-MB-468 cells with *TRPM7* gene silencing in the presence of recombinant TRAIL (Figure 3.3). Consistent with a previous report, *TRPM7* gene silencing did not affect proliferation of MDA-MB-231 cells in the absence of recombinant TRAIL (Guilbert et al., 2013). However, proliferation of cells transfected with siTRPM7 was significantly reduced more than that of cells transfected with scrambled siRNA in the presence of recombinant TRAIL. Treatment

of recombinant TRAIL decreased proliferation of both MDA-MB-231 and MDA-MB-468 cells in a dose-dependent manner. These results show that *TRPM7* gene silencing might increase TRAIL-induced antiproliferative effects in TNBC cells.

Figure 3.1. Expression level of TRPM7 in breast cell lines. (A) Representative RT-PCR gels of TRPM7 mRNA expression in MCF10A, MDA-MB-231, and MDA-MB-468 cell lines. (B) Densitometric analysis of RT-PCR data obtained from (A). (C) Representative Western blots of TRPM7 protein expression in MCF10A, MDA-MB-231, and MDA-MB-468 cell lines. (D) Densitometric analysis of Western blot data obtained from (C). All densitometry data were normalized to the intensity of β-actin bands. The RT-PCR and Western blot experiments were performed by Ms. Choi, Seunghye (KU-KIST Graduate School of Converging Science and Technology, Korea University, Republic of Korea).

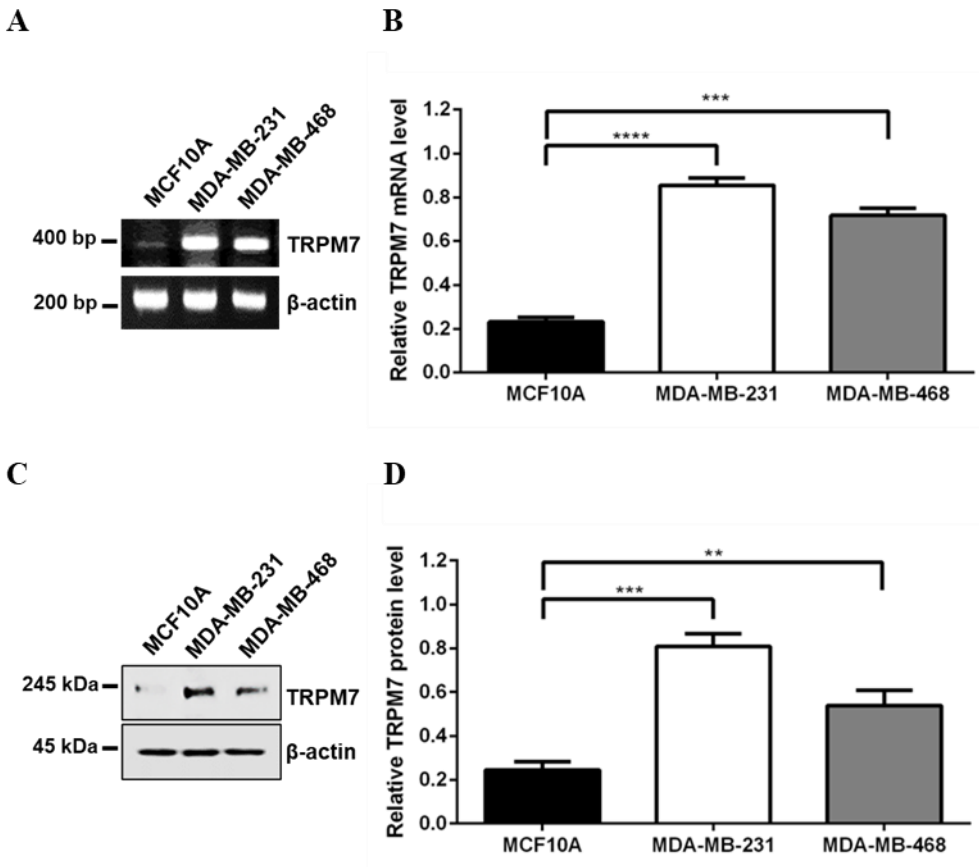
A
MCF10A
MDA-MB-231
MDA-MB-468
400 bp
200 bp
TRPM7
β-actin
B
Relative TRPM7 mRNA level
1.2
1.0
0.8
0.6
0.4
0.2
0.0
***
****
MCF10A
MDA-MB-231
MDA-MB-468
C
MCF10A
MDA-MB-231
MDA-MB-468
245 kDa
45 kDa
TRPM7
β-actin
D
Relative TRPM7 protein level
1.2
1.0
0.8
0.6
0.4
0.2
0.0
**
***
MCF10A
MDA-MB-231
MDA-MB-468

Figure 3.2. Silencing of TRPM7 in MDA-MB-231 and MDA-MB-468 cells. (A) Representative RT-PCR gels of TRPM7 mRNA expression. MDA-MB-231 and MDA-MB-468 cells were transfected with scrambled siRNA as a negative control or siTRPM7. (B) Densitometric analysis of RT-PCR data obtained from (A). (C) Representative Western blots of TRPM7 protein expression. MDA-MB-231 and MDA-MB-468 cells were transfected with scrambled siRNA as a control and siTRPM7. (D) Densitometric analysis of Western blot data obtained from (C). All densitometry data were normalized to the intensity of β-actin bands.

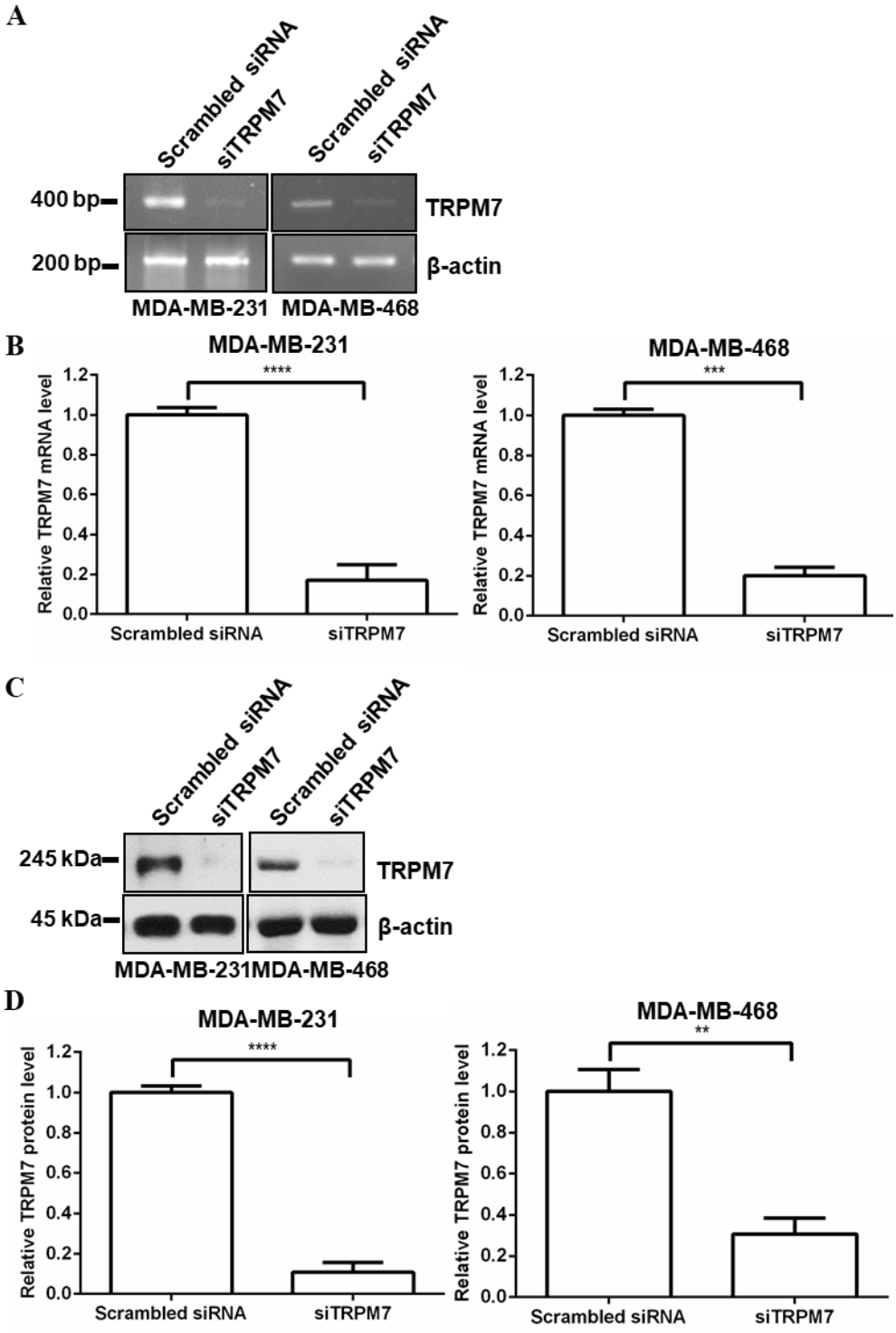
A
Scrambled siRNA
siTRPM7
Scrambled siRNA
siTRPM7
400 bp
200 bp
TRPM7
β-actin
MDA-MB-231
MDA-MB-468
B
MDA-MB-231
****
Relative TRPM7 mRNA level
1.2
1.0
0.8
0.6
0.4
0.2
0.0
Scrambled siRNA
siTRPM7
MDA-MB-468
***
Relative TRPM7 mRNA level
1.2
1.0
0.8
0.6
0.4
0.2
0.0
Scrambled siRNA
siTRPM7
C
Scrambled siRNA
siTRPM7
Scrambled siRNA
siTRPM7
245 kDa
45 kDa
TRPM7
β-actin
MDA-MB-231
MDA-MB-468
D
MDA-MB-231
****
Relative TRPM7 protein level
1.2
1.0
0.8
0.6
0.4
0.2
0.0
Scrambled siRNA
siTRPM7
MDA-MB-468
**
Relative TRPM7 protein level
1.2
1.0
0.8
0.6
0.4
0.2
0.0
Scrambled siRNA
siTRPM7

Figure 3.3. Silencing of TRPM7 increases TRAIL-induced antiproliferative effects in MDA-MB-231 and MDA-MB-468 cells. MDA-MB-231 and MDA-MB-468 cells transfected with scrambled siRNA or siTRPM7 were incubated with various concentrations of recombinant TRAIL for 16 h. Proliferation of MDA-MB-231 and MDA-MB-468 cells was measured via CellTiter-Glo assays. All densitometry data were normalized to the intensity of β-actin bands.

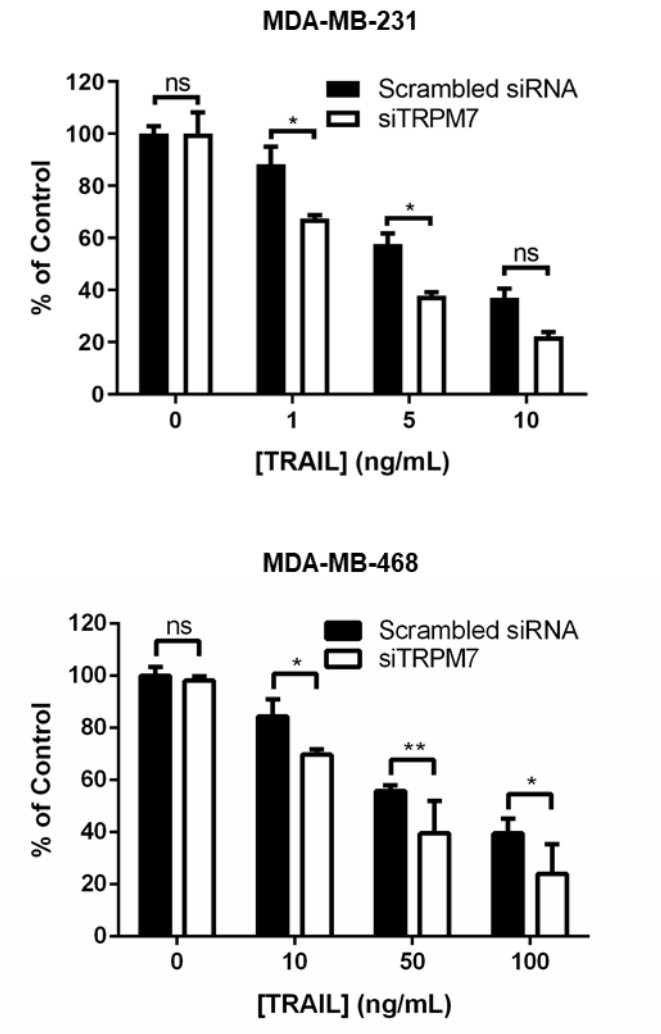
MDA-MB-231
Scrambled siRNA
siTRPM7
% of Control
120
100
80
60
40
20
0
ns
*
*
ns
0
1
5
10
[TRAIL] (ng/mL)
MDA-MB-468
Scrambled siRNA
siTRPM7
% of Control
120
100
80
60
40
20
0
ns
*
**
*
0
10
50
100
[TRAIL] (ng/mL)

Silencing of *TRPM7* promotes TRAIL-induced apoptosis in TNBC cells.

Recombinant TRAIL induces apoptosis of MDA-MB-231 cells (Piggott et al., 2011; Dufour et al., 2017). To investigate whether TRAIL-induced apoptosis is affected by *TRPM7* gene silencing in MDA-MB-231 and MDA-MB-468 cells, I measured apoptotic cells transfected with siTRPM7 in the presence of recombinant TRAIL through annexin V-FITC/PI staining (Figures 3.4A and 3.4B). Like the above proliferation results, silencing of *TRPM7* gene did not increase apoptotic cells in the absence of recombinant TRAIL, but it significantly increased apoptosis in presence of it in MDA-MB-231 and MDA-MB-468 cells. To confirm TRAIL-induced apoptosis, cleaved caspase-3 and cleaved PARP as prominent apoptotic markers were detected by Western blot analysis (Figures 3.5A, 3.5B, and 3.5C). Consistent with proliferation and flow cytometry results, protein levels of cleaved caspase-3 and cleaved PARP in MDA-MB-231 cells transfected with siTRPM7 significantly were increased about 6-fold and 5-fold higher, respectively, than those in cells transfected with scrambled siRNA at 1 ng/mL TRAIL. Likewise, protein levels of both cleaved caspase-3 and cleaved PARP in MDA-MB-468 cells transfected with siTRPM7 significantly were also increased at 10 ng/mL TRAIL. These data indicate that *TRPM7* gene silencing could increase TRAIL-induced apoptosis in TNBC cells.

Figure 3.4. Silencing of TRPM7 promotes TRAIL-induced apoptosis in MDA-MB-231 and MDA-MB-468 cells. (A) MDA-MB-231 and MDA-MB-468 cells transfected with scrambled siRNA or siTRPM7 were incubated with various concentrations of recombinant TRAIL for 16 h. Apoptosis was analyzed by annexin V-FITC/PI staining. (B) Percentages of apoptotic cells. Upper right and lower right quadrants represent apoptotic cells.

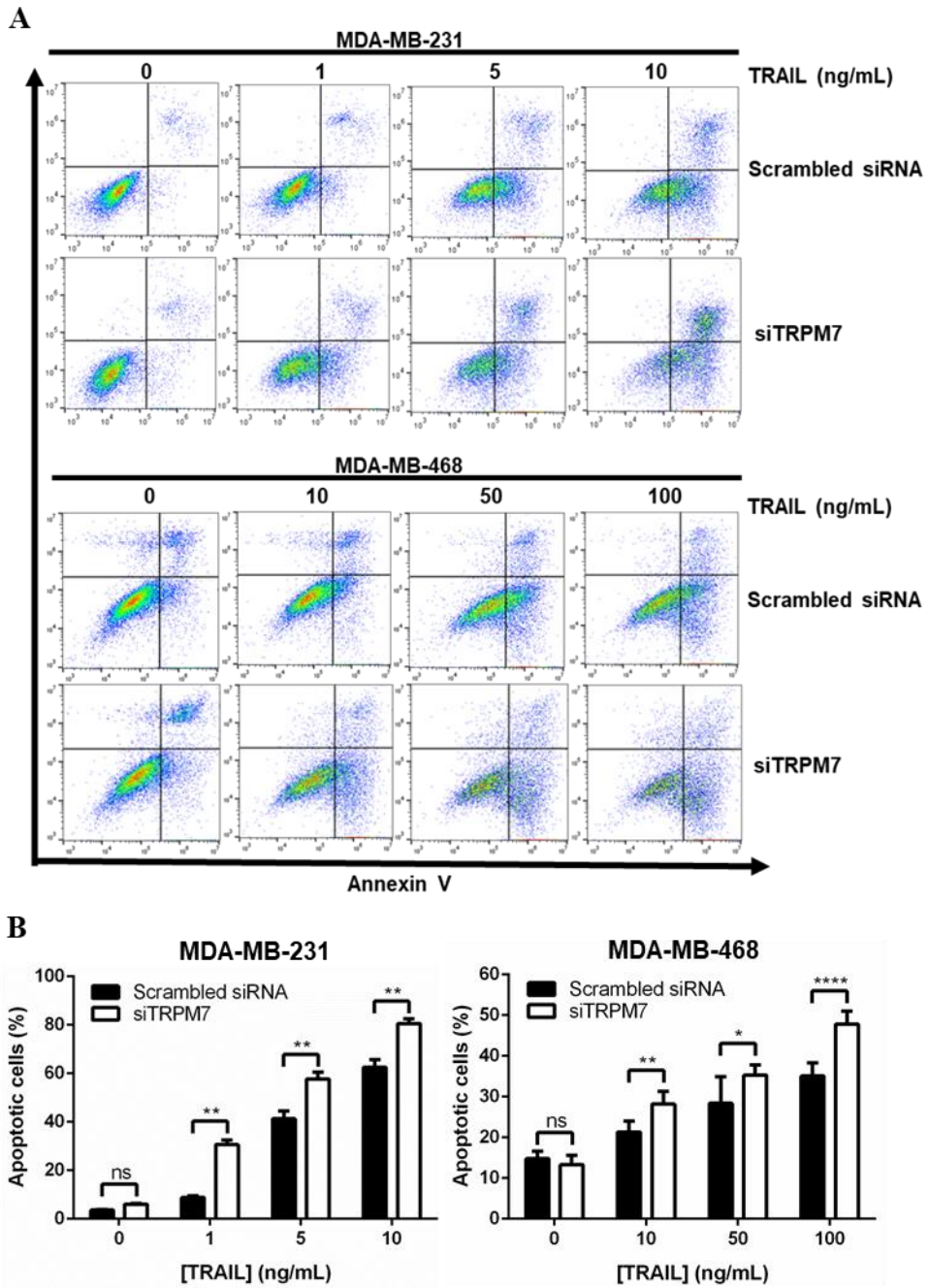
A
MDA-MB-231
0
1
5
10
TRAIL (ng/mL)
Scrambled siRNA
siTRPM7
MDA-MB-468
0
10
50
100
TRAIL (ng/mL)
Scrambled siRNA
siTRPM7
Annexin V
B
MDA-MB-231
Scrambled siRNA
siTRPM7
Apoptotic cells (%)
ns
**
**
**
[TRAIL] (ng/mL)
MDA-MB-468
Scrambled siRNA
siTRPM7
Apoptotic cells (%)
ns
**
*
****
[TRAIL] (ng/mL)

Figure 3.5. Silencing of TRPM7 increases apoptotic molecules (cleaved caspase-3 and cleaved PARP) in the presence of TRAIL in MDA-MB-231 and MDA-MB-468 cells. (A) Representative Western blots in MDA-MB-231 and MDA-MB-468 cells (B) Densitometric analysis of cleaved caspase-3 at 1 ng/mL TRAIL in MDA-MB-231 cells and at 10 ng/mL TRAIL in MDA-MB-468 cells. (C) Densitometric analysis of cleaved PARP at 1 ng/mL TRAIL in MDA-MB-231 cells and at 10 ng/mL TRAIL in MDA-MB-468 cells. All densitometry data were normalized to the intensity of β-actin bands.

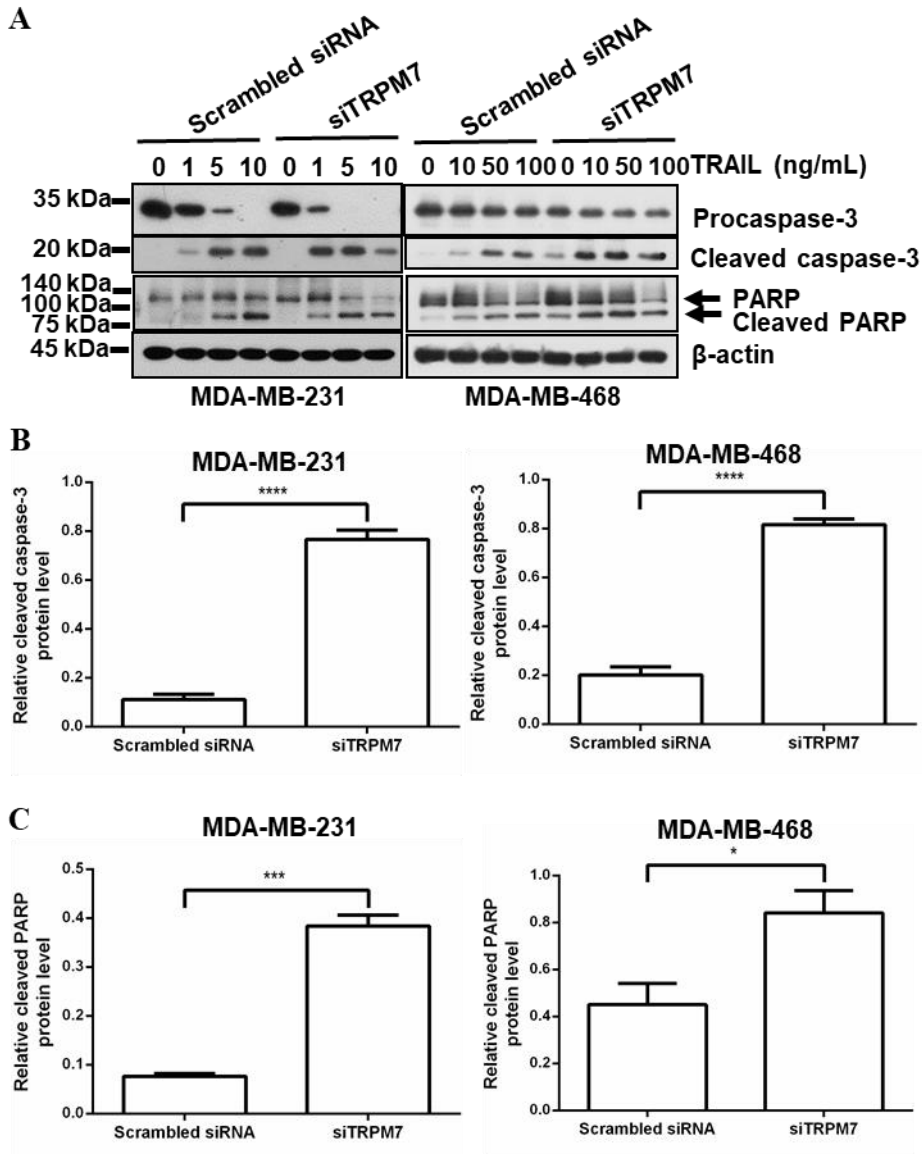
A
Scrambled siRNA
siTRPM7
Scrambled siRNA
siTRPM7
0 1 5 10 0 1 5 10 0 10 50 100 0 10 50 100 TRAIL (ng/mL)
35 kDa
20 kDa
140 kDa
100 kDa
75 kDa
45 kDa
Procaspase-3
Cleaved caspase-3
PARP
Cleaved PARP
β-actin
MDA-MB-231
MDA-MB-468
B
MDA-MB-231
MDA-MB-468
Relative cleaved caspase-3 protein level
****
Scrambled siRNA
siTRPM7
C
MDA-MB-231
MDA-MB-468
Relative cleaved PARP protein level
***
*
Scrambled siRNA
siTRPM7

NS8593 synergistically facilitates TRAIL-induced antiproliferative effects in TNBC cells.

TRPM7 is composed of an ion channel domain and a kinase domain (Nadler et al., 2001; Runnels et al., 2001). To determine which domain of TRPM7 is involved in TRAIL-induced antiproliferative effects, proliferation of MDA-MB-231 cells treated with NS8593 (a TRPM7 channel inhibitor (Chubanov et al., 2012)) or TG100-115 (a TRPM7 kinase inhibitor (Song et al., 2017)) was measured in the presence of recombinant TRAIL (Figure 3.6A). Proliferative cells treated with 10 μM NS8593 were significantly reduced by 25.57 ± 1.48%, 44.16 ± 3.13%, 71.50 ± 2.23%, and 82.40 ± 1.38% at 0, 1, 5, and 10 ng/mL TRAIL, respectively, while treatment of 10 μM TG100-115 did not significantly affect cell proliferation. To investigate if combination of NS8593 and recombinant TRAIL may have additive or synergistic effects, I determined CI values known as an indicator assessing drug combination interaction effect for two substances (Figure 3.6B) (Chou and Talalay, 1984; Chou, 2010). I found that the CI value of two substances showed a strong CI of below 0.3 at 1 ng/mL TRAIL, suggesting that NS8593 has a strong synergistic effect with recombinant TRAIL in antiproliferative effects on MDA-MB-231 cells. To further examine whether TRPM7 inhibitors affects TRAIL-induced apoptosis in MDA-MB-231 cells, I measured apoptotic cells in the presence of recombinant TRAIL through annexin V-FITC/PI staining (Figures 3.7A and 3.7B). Similar to proliferation data, combination treatment with NS8593 and recombinant TRAIL significantly induced apoptosis, whereas treatment of TG100-115 did not affect it in the presence of TRAIL. Likewise, combination treatment with NS8593 and recombinant TRAIL significantly induced apoptosis in MDA-MB-468 cells (Figures 3.8A and 3.8B). To further confirm TRAIL-induced apoptosis in the presence of NS8593, I performed Western blot analysis in MDA-MB-231 cells (Figures 3.9A, 3.9B, and 3.9C). Protein levels of cleaved caspase-3 and cleaved PARP in MDA-MB-231 cells treated with NS8593 and recombinant TRAIL significantly were increased approximately 3-fold and 4-fold higher, respectively, than those in cells treated with dimethyl sulfoxide (DMSO) as a control and recombinant TRAIL.

Similarly, combination treatment with NS8593 and recombinant TRAIL also increased protein levels of both cleaved caspase-3 and cleaved PARP in MDA-MB-468 cells (Figures 3.10A, 3.10B, and 3.10C). Moreover, I found that combination treatment with NS8593 and TRAIL affects morphology of MDA-MB-231 cells (Figure 3.11). Apoptotic cell characteristics such as cell shrinkage and detachment were observed in MDA-MB-231 cells treated with NS8593 and TRAIL. To further confirm that synergistic effects of NS8593 are associated with TRPM7, I carried out apoptosis assay through annexin V-FITC/PI staining with TRPM7 inhibitors with TRAIL in MDA-MB-231 cells transfected with siTRPM7 (Figures 3.12A and 3.12B). Both NS8593 and TG100-115 did not affect apoptosis of MDA-MB-231 cells transfected with siTRPM7 in the presence of TRAIL. These results suggest that NS8593 synergistically facilitates TRAIL-induced antiproliferative effects and apoptosis, while TG100-115 has no effect on them, indicating that TRPM7 channels might be involved in synergistic interaction of TRPM7 and recombinant TRAIL in apoptosis.

Figure 3.6. NS8593 synergistically facilitates TRAIL-induced antiproliferative effects in MDA-MB-231 cells. (A) MDA-MB-231 cells were incubated with 10 μM NS8593 or 10 μM TG100-115 in the presence of different concentrations (1, 5, and 10 ng/mL) of recombinant TRAIL for 16 h. Proliferation of MDA-MB-231 cells was measured using CellTiter-Glo assays. (B) CI values calculated by Chou-Talalay method. Cell proliferation assay data were used to evaluate the CI values of NS8593 and recombinant TRAIL.

A

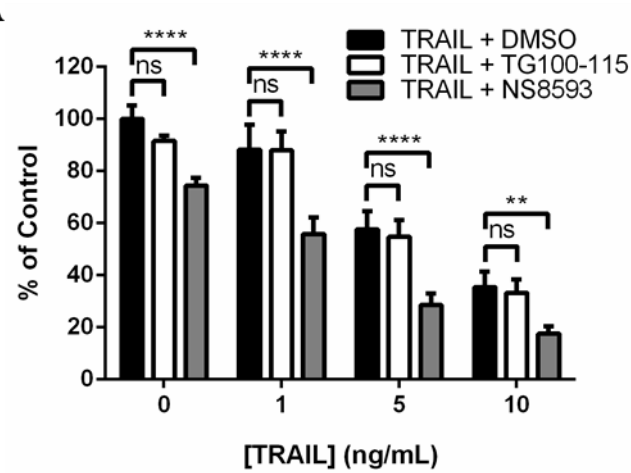

B

	TRAIL (ng/mL)		
	1	5	10
10 μM NS8593	0.25 ± 0.06	0.34 ± 0.04	0.40 ± 0.09

Figure 3.7. NS8593 increases TRAIL-induced apoptosis in MDA-MB-231 cells.
(A) Apoptosis of MDA-MB-231 cells treated with indicated compounds for 16 h was analyzed by annexin V-FITC/PI staining. (B) Percentages of apoptotic cells. Upper right and lower right quadrants represent apoptotic cells.

A

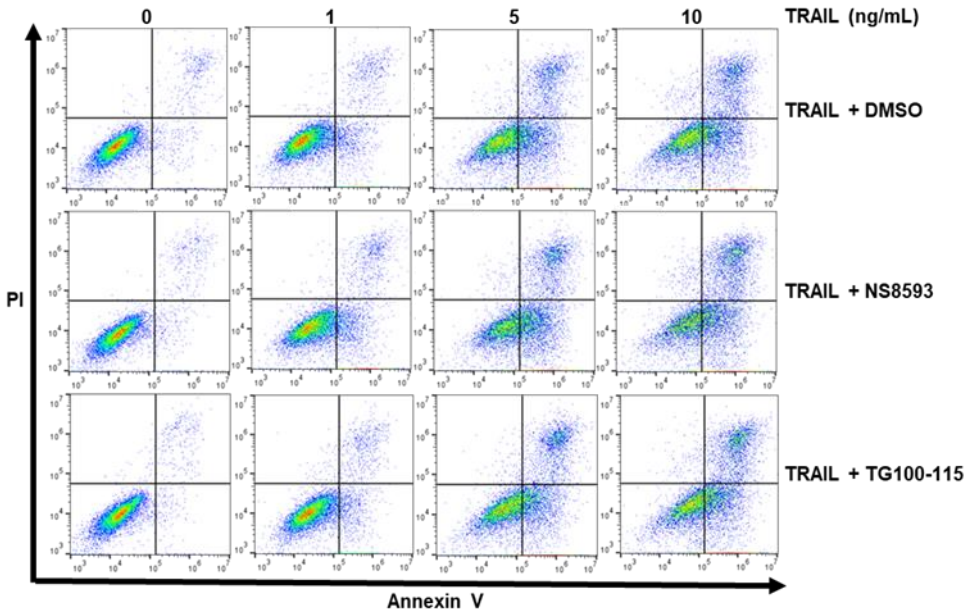
0
1
5
10
TRAIL (ng/mL)
TRAIL + DMSO
TRAIL + NS8593
TRAIL + TG100-115
PI
Annexin V

B

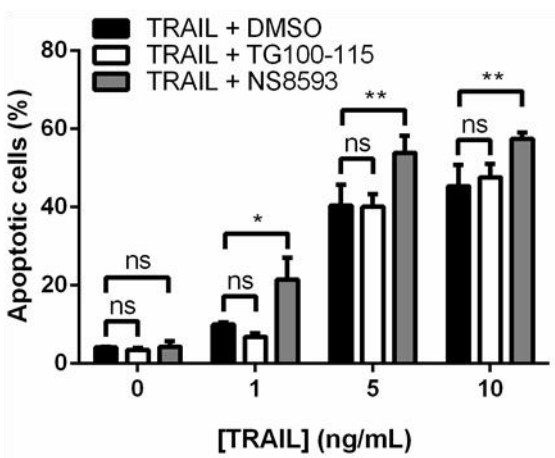
TRAIL + DMSO
TRAIL + TG100-115
TRAIL + NS8593
Apoptotic cells (%)
80
60
40
20
0
ns
ns
*
ns
**
ns
**
0
1
5
10
[TRAIL] (ng/mL)

Figure 3.8. NS8593 synergistically facilitates TRAIL-induced apoptosis in MDA-MB-468 cells. (A) Apoptosis of MDA-MB-468 cells treated with 10 μM NS8593 for 16 h was analyzed by annexin V-FITC/PI staining. (B) Percentages of apoptotic cells. Upper right and lower right quadrants represent apoptotic cells.

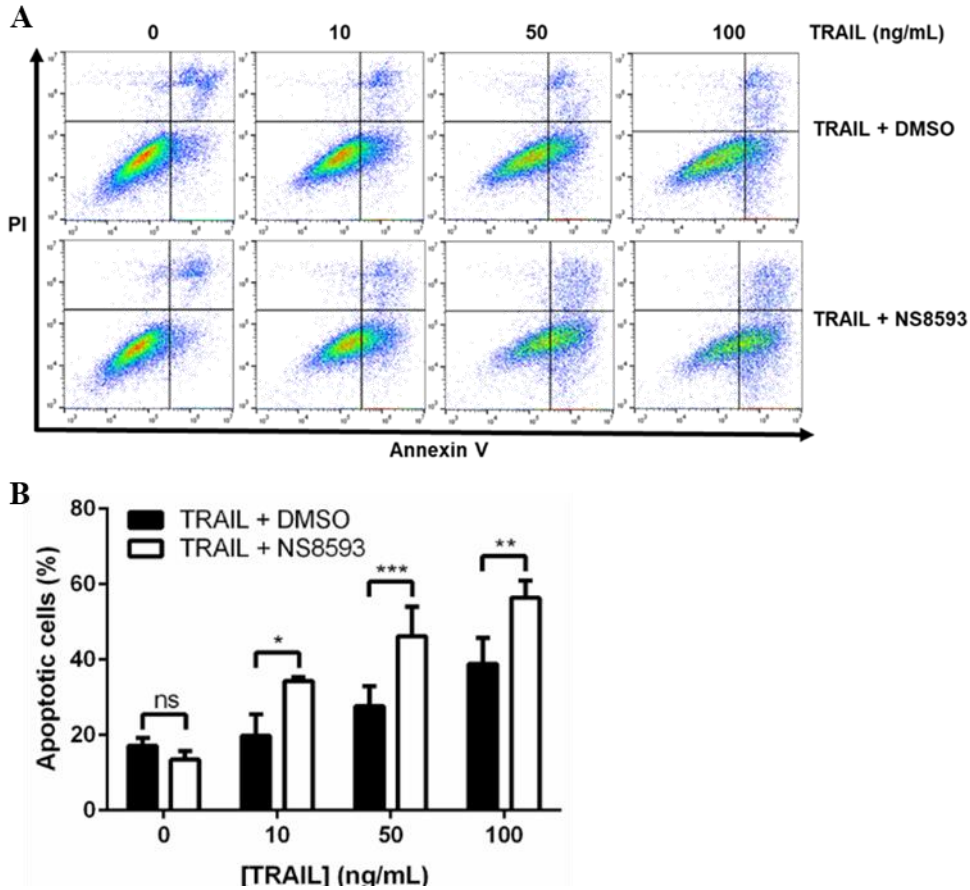
A
0
10
50
100
TRAIL (ng/mL)
TRAIL + DMSO
TRAIL + NS8593
PI
Annexin V
B
TRAIL + DMSO
TRAIL + NS8593
Apoptotic cells (%)
80
60
40
20
0
ns
*
***
**
0
10
50
100
[TRAIL] (ng/mL)

Figure 3.9. NS8593 increases apoptotic molecules (cleaved caspase-3 and cleaved PARP) in the presence of TRAIL in MDA-MB-231 cells. (A) Representative Western blots in MDA-MB-231 cells. (B) Densitometric analysis of cleaved caspase-3 at 1 ng/mL TRAIL. (C) Densitometric analysis of cleaved PARP at 1 ng/mL TRAIL. All densitometry data were normalized to the intensity of β-actin bands.

A

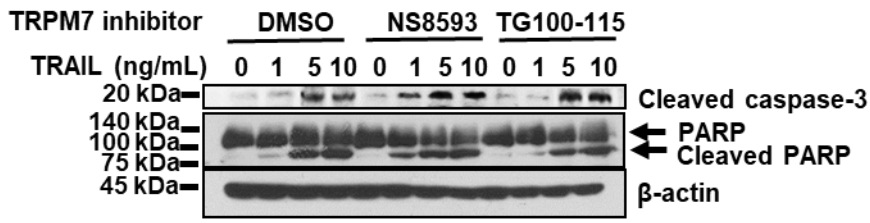
TRPM7 inhibitor
DMSO
NS8593
TG100-115
TRAIL (ng/mL)
0 1 5 10 0 1 5 10 0 1 5 10
20 kDa
140 kDa
100 kDa
75 kDa
45 kDa
Cleaved caspase-3
PARP
Cleaved PARP
β-actin

B

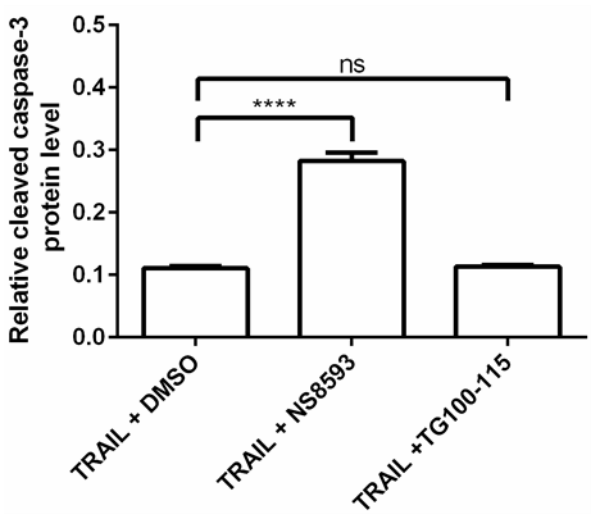
Relative cleaved caspase-3 protein level
0.5
0.4
0.3
0.2
0.1
0.0
ns
****
TRAIL + DMSO
TRAIL + NS8593
TRAIL +TG100-115

C

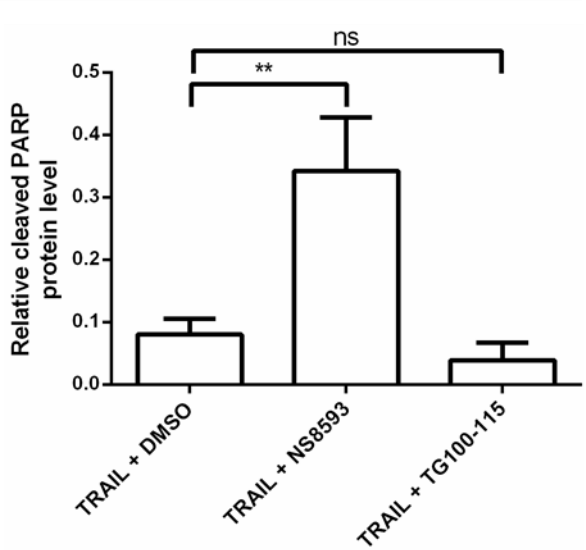
Relative cleaved PARP protein level
0.5
0.4
0.3
0.2
0.1
0.0
ns
**
TRAIL + DMSO
TRAIL + NS8593
TRAIL + TG100-115

Figure 3.10. NS8593 increases apoptotic molecules (cleaved caspase-3 and cleaved PARP) in the presence of TRAIL in MDA-MB-468 cells. (A) Representative Western blots in MDA-MB-468 cells. (B) Densitometric analysis of cleaved caspase-3 at 10 ng/mL TRAIL. (C) Densitometric analysis of cleaved PARP at 10 ng/mL TRAIL. All densitometry data were normalized to the intensity of β-actin bands.

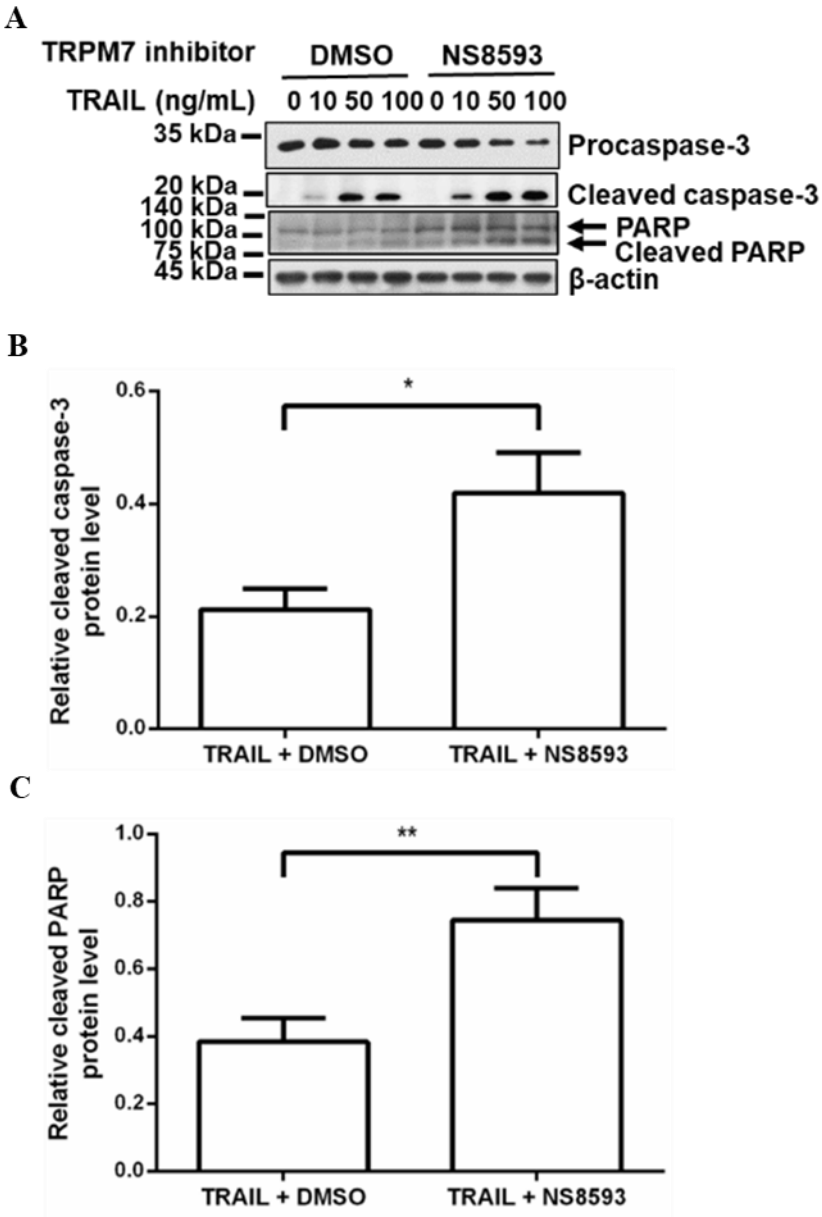
A
TRPM7 inhibitor
DMSO
NS8593
TRAIL (ng/mL)
0 10 50 100 0 10 50 100
35 kDa
Procaspase-3
20 kDa
140 kDa
Cleaved caspase-3
100 kDa
75 kDa
PARP
Cleaved PARP
45 kDa
β-actin
B
Relative cleaved caspase-3 protein level
0.6
0.4
0.2
0.0
*
TRAIL + DMSO
TRAIL + NS8593
C
Relative cleaved PARP protein level
1.0
0.8
0.6
0.4
0.2
0.0
**
TRAIL + DMSO
TRAIL + NS8593

Figure 3.11. Microscopic cell morphologies. MDA-MB-231 cells were incubated with recombinant TRAIL and 10 μM TRPM7 inhibitors for 16 h. Scale bar: 50 μm.

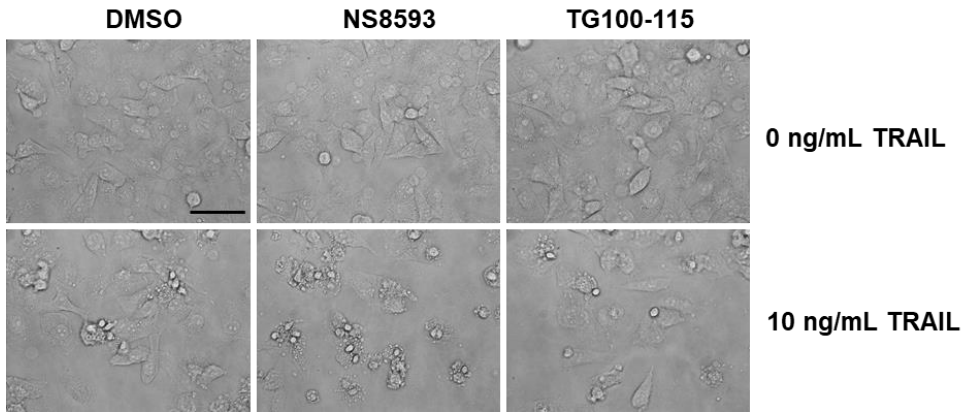
DMSO
NS8593
TG100-115
0 ng/mL TRAIL
10 ng/mL TRAIL

Figure 3.12. TRPM7 inhibitors do not promotes apoptotic cells in the presence of TRAIL during silencing of *TRPM7* in MDA-MB-231 cells. (A) MDA-MB-231 cells transfected with siTRPM7 were incubated with 10 ng/mL TRAIL and TRPM7 inhibitors for 16 h. Apoptosis of MDA-MB-231 cells was analyzed by annexin V-FITC/PI staining. (B) Percentages of apoptotic cells. Upper right and lower right quadrants represent apoptotic cells.

A

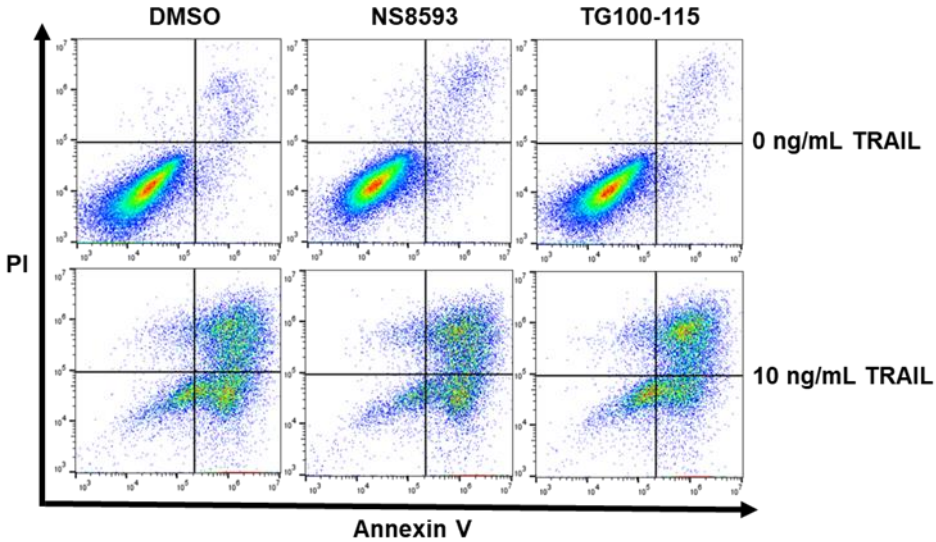
DMSO
NS8593
TG100-115
0 ng/mL TRAIL
10 ng/mL TRAIL
PI
Annexin V

B

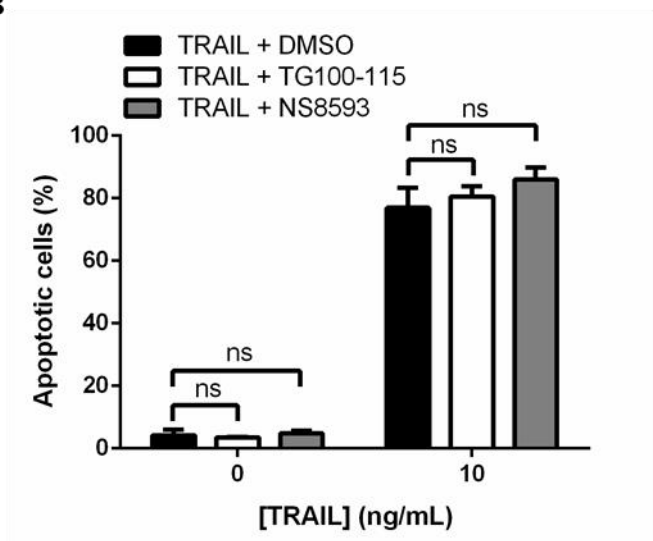
TRAIL + DMSO
TRAIL + TG100-115
TRAIL + NS8593
Apoptotic cells (%)
100
80
60
40
20
0
ns
ns
ns
ns
0
10
[TRAIL] (ng/mL)

NS8593 affects cell cycle distribution in MDA-MB-231 cells.

Recombinant TRAIL changes cell cycle distribution of MDA-MB-231 cells (Zhou et al., 2016). To examine whether cell cycle distribution is affected by treatment of TRPM7 inhibitors, I conducted cell cycle assays with NS8593 or TG100-115 in the presence of TRAIL in MDA-MB-231 cells (Figures 3.13A and 3.13B). Like a previous study (Zhou et al., 2016), TRAIL increased the cells in G0/G1 phase, but single treatments of each TRPM7 inhibitor did not significantly change cell cycle distribution. However, combination treatment with NS8593 and TRAIL increased the cells in G2/M phase from 22.33 ± 3.51% to 37.15 ± 0.35% and decreased the cells in G0/G1 phase from 55.03 ± 2.99% to 44.60 ± 2.40% compared to the cells treated with TRAIL. These data show that NS8593 induces cell cycle arrest at G2/M phase in the presence of TRAIL in MDA-MB-231 cells.

Figure 3.13. Cell cycle analysis in MDA-MB-231 cells. (A) Representative images from the cell cycle analysis. MDA-MB-231 cells were incubated with recombinant TRAIL and 10 μM TRPM7 inhibitors for 6 h. (B) Cell cycle distribution. The percentage of cells in each phase was evaluated by flow cytometry.

A

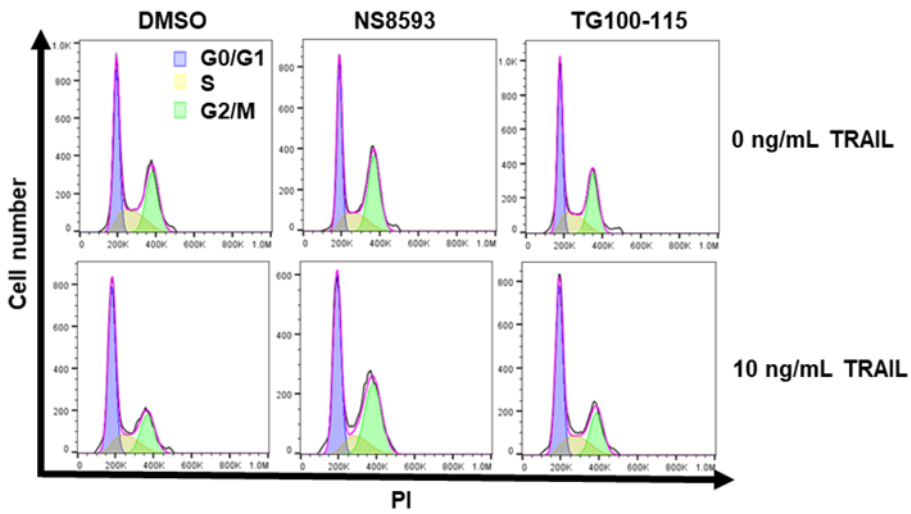
DMSO
NS8593
TG100-115
G0/G1
S
G2/M
0 ng/mL TRAIL
10 ng/mL TRAIL
Cell number
PI

B

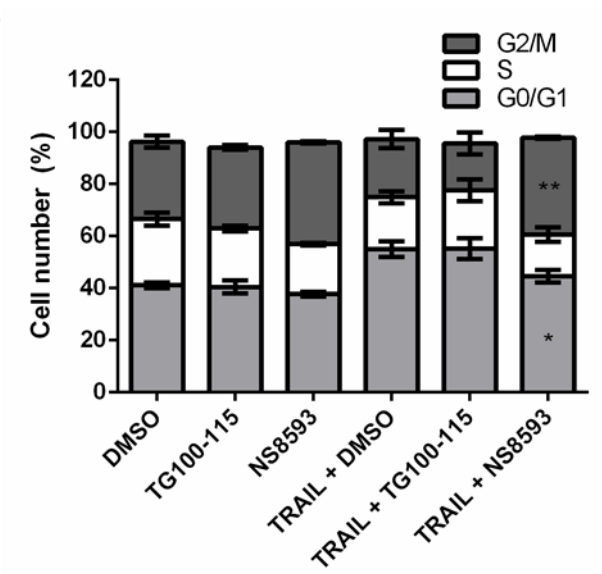
G2/M
S
G0/G1
Cell number (%)
120
100
80
60
40
20
0
**
*
DMSO
TG100-115
NS8593
TRAIL + DMSO
TRAIL + TG100-115
TRAIL + NS8593

NS8593 inhibits colony formation in MDA-MB-231 cells.

To explore whether the combinatory effects of TRAIL and TRPM7 inhibitors affects clonal proliferation of single cell, I performed colony formation assays in MDA-MB-231 cells (Figures 3.14A and 3.14B). Like the proliferation and apoptosis assay results, combination treatment with NS8593 and TRAIL significantly decreased the colony formation of the cells. These data indicate that NS8593 suppresses colony formation in the presence of TRAIL in MDA-MB-231 cells.

Figure 3.14. Colony formation assays in MDA-MB-231 cells. (A) Representative images from the colony formation assays in MDA-MB-231 cells. (B) Percentages of number of colonies. The colony formation assays were performed by Ms. Choi, Seunghye (KU-KIST Graduate School of Converging Science and Technology, Korea University, Republic of Korea).

A

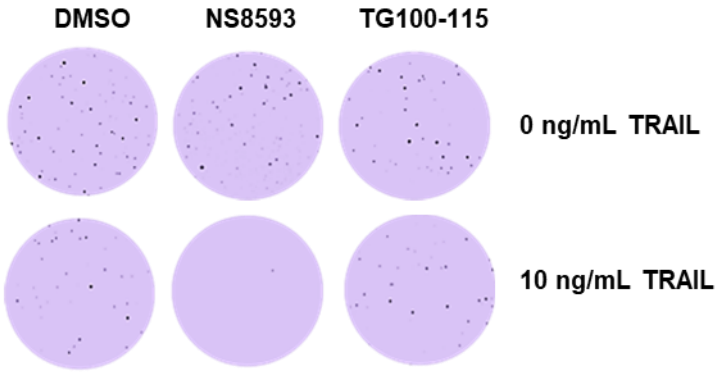
DMSO
NS8593
TG100-115
0 ng/mL TRAIL
10 ng/mL TRAIL

B

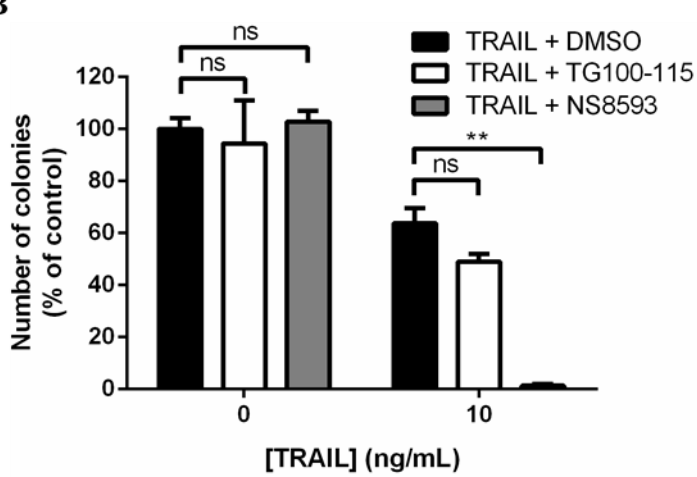
ns
ns
TRAIL + DMSO
TRAIL + TG100-115
TRAIL + NS8593
**
ns
Number of colonies
(% of control)
120
100
80
60
40
20
0
0
10
[TRAIL] (ng/mL)

Enhancement of TRAIL-induced apoptosis by suppression of TRPM7 is associated with calcium ion.

TRPM7 channels conduct divalent cations such as Ca^{2+}, which plays a critical role in cell death (Nadler et al., 2001; Runnels et al., 2001; Aarts et al., 2003; Monteilh-Zoller et al., 2003; Asrar and Aarts, 2013; Varghese et al., 2019). Therefore, I hypothesized that reduction in Ca^{2+} influx via inhibition of TRPM7 channel activity could cause increase of TRAIL-induced apoptosis. To confirm this hypothesis, annexin V-FITC/PI staining was carried out with BAPTA-AM (a cell permeable Ca^{2+} chelator) in MDA-MB-231 cells (Figures 3.15A and 3.15B). Treatment of BAPTA-AM significantly increased TRAIL-induced apoptosis at even 1 ng/mL TRAIL, but attenuated synergistic effect of NS8593 and recombinant TRAIL. Expectedly, treatment of TG100-115 did not affect TRAIL-induced apoptosis in the presence of BAPTA-AM. To further test TRAIL-induced apoptosis, Western blot analysis was performed in the presence of BAPTA-AM (Figures 3.16A, 3.16B, and 3.16C). Like annexin V-FITC/PI staining data, cleaved caspase-3 and cleaved PARP were clearly detected at even 1 ng/mL TRAIL, and significant differences among three conditions were not observed. To examine whether NS8593 decreases intracellular Ca^{2+} content, I conducted intracellular Ca^{2+} assays using Fluo-3-AM (a Ca^{2+} indicator) in MDA-MB-231 cells (Figures 3.17A and 3.17B). Like a previous study (O'Grady & Morgan, 2019), treatment of NS8593 reduced intracellular Ca^{2+} content by 49.13 ± 14.24%. These observations indicate that facilitation of TRAIL-induced apoptosis by suppression of TRPM7 might be associated with Ca^{2+}.

Figure 3.15. Enhancement of TRAIL-induced apoptosis by suppression of TRPM7 is associated with calcium ion in MDA-MB-231 cells. (A) The cells were incubated with 10 μM NS8593 or 10 μM TG100-115 in the presence of different concentrations (1, 5, and 10 ng/mL) of recombinant TRAIL and 10 μM BAPTA-AM for 16 h. Apoptosis was analyzed by annexin V-FITC/PI staining. (B) Percentages of apoptotic cells. Upper right and lower right quadrants represent apoptotic cells.

A

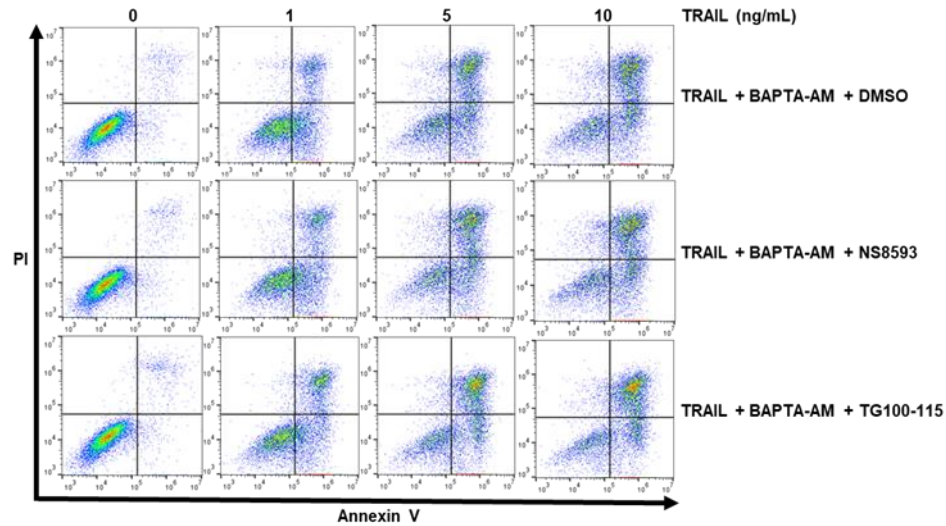
0
1
5
10
TRAIL (ng/mL)
TRAIL + BAPTA-AM + DMSO
TRAIL + BAPTA-AM + NS8593
TRAIL + BAPTA-AM + TG100-115
PI
Annexin V

B

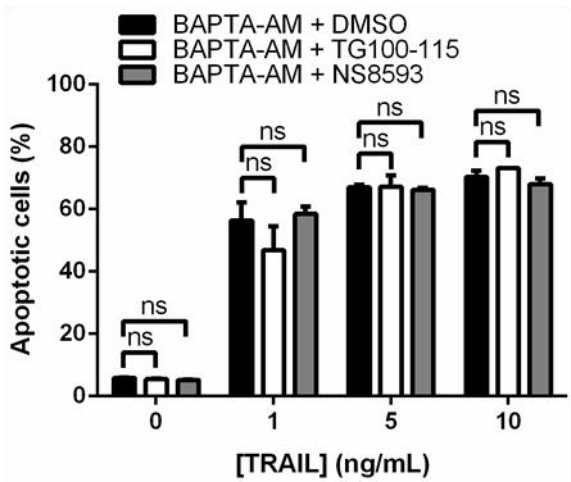
BAPTA-AM + DMSO
BAPTA-AM + TG100-115
BAPTA-AM + NS8593
Apoptotic cells (%)
100
80
60
40
20
0
ns
0
1
5
10
[TRAIL] (ng/mL)

Figure 3.16. Enhancement of TRAIL-induced apoptosis by suppression of TRPM7 is associated with calcium ion in MDA-MB-231 cells. (A) Representative Western blots for apoptotic molecules (cleaved caspase-3 and cleaved PARP) in MDA-MB-231 cells. (B) Densitometric analysis of cleaved caspase-3 at 1 ng/mL TRAIL. (C) Densitometric analysis of cleaved PARP at 1 ng/mL TRAIL. All densitometry data were normalized to the intensity of β-actin bands.

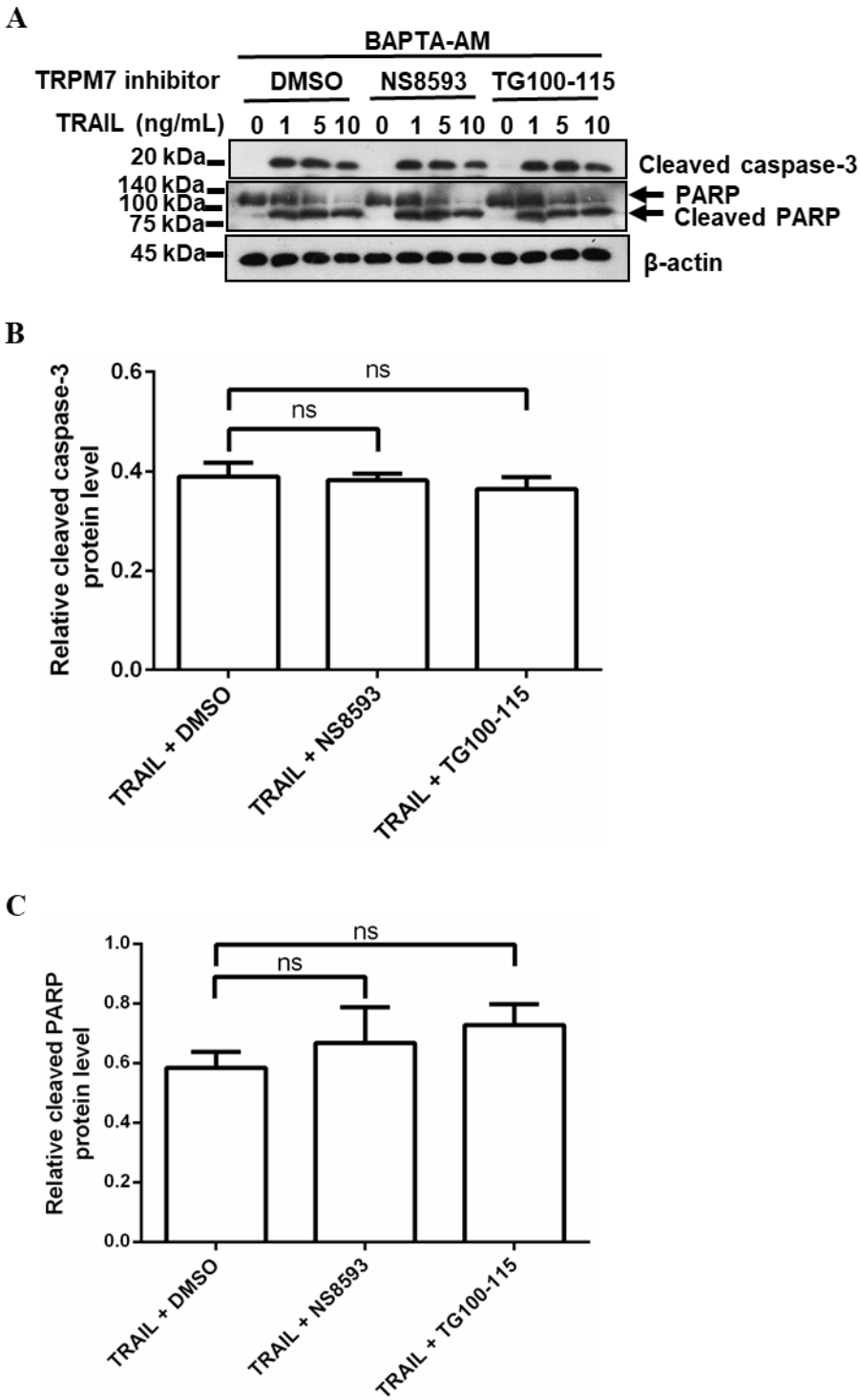
A
BAPTA-AM
TRPM7 inhibitor
DMSO
NS8593
TG100-115
TRAIL (ng/mL)
0 1 5 10 0 1 5 10 0 1 5 10
20 kDa
140 kDa
100 kDa
75 kDa
45 kDa
Cleaved caspase-3
PARP
Cleaved PARP
β-actin
B
Relative cleaved caspase-3 protein level
0.6
0.4
0.2
0.0
ns
ns
TRAIL + DMSO
TRAIL + NS8593
TRAIL + TG100-115
C
Relative cleaved PARP protein level
1.0
0.8
0.6
0.4
0.2
0.0
ns
ns
TRAIL + DMSO
TRAIL + NS8593
TRAIL + TG100-115

Figure 3.17. Intracellular Ca^{2+} content in MDA-MB-231 cells. The cells were incubated with 10 μM NS8593 for 16 h. (A) A representative image from the intracellular Ca^{2+} content analysis. It was evaluated by flow cytometry. (B) The percentage of intracellular Ca^{2+} content.

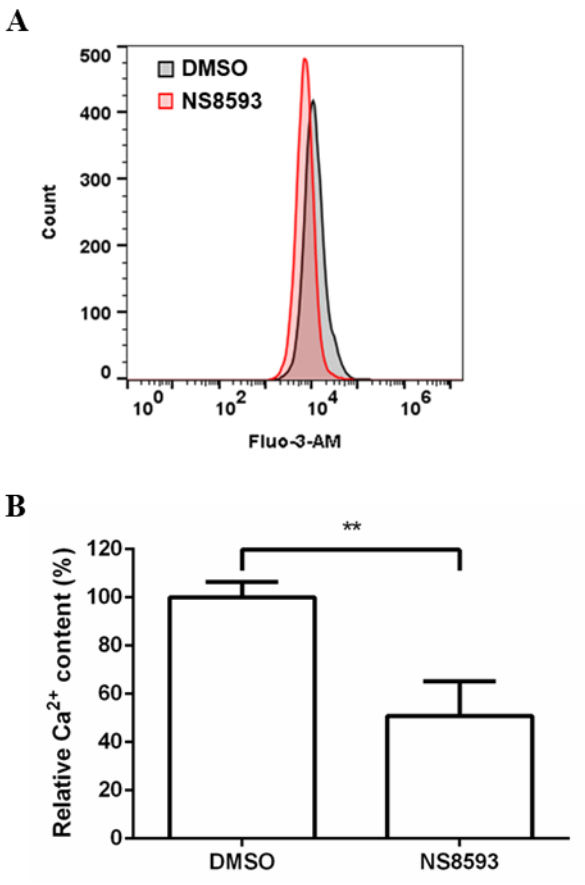
A
DMSO
NS8593
Count
500
400
300
200
100
0
10^0
10^2
10^4
10^6
Fluo-3-AM
B
**
Relative Ca^{2+} content (%)
120
100
80
60
40
20
0
DMSO
NS8593

Suppression of TRPM7 decreases protein level of c-FLIP and enhances caspase-8 activation.

Calcium ion regulates interaction of the c-$FLIP_L$ and calmodulin, and protein level of c-$FLIP_L$ is decreased by downregulation of Ca^{2+} (Pawar et al., 2008; Kaminskyy et al., 2013). Reduction in protein level of c-$FLIP_L$ promotes activation of caspase-8, which consequently enhances apoptosis and decrease of the c-$FLIP_S$ enhances TRAIL-induced DISC formation and apoptosis (Day et al., 2008; Safa, 2012). To examine whether *TRPM7* gene silencing decreases protein levels of c-$FLIP_L$ and c-$FLIP_S$ and activates caspase-8, Western blot analysis was conducted using MDA-MB-231 cells transfected with siTRPM7 in the presence of recombinant TRAIL (Figure 3.18A). Silencing of *TRPM7* gene significantly decreased protein levels of both c-$FLIP_L$ and c-$FLIP_S$ in the presence of recombinant TRAIL, and the reduction was also observed in the absence of it (Figures 3.18B and 3.18C). To investigate whether *TRPM7* gene silencing affects mRNA levels of *c-$FLIP_L$* and *c-$FLIP_S$*, I conducted RT-PCR analysis using MDA-MB-231 cells transfected with siTRPM7 (Figures 3.19A and 3.19B). Significant changes of those mRNA levels were not observed. To confirm effects of low protein level of c-FLIP on caspase-8 activation, I performed Western blot analysis with MDA-MB-231 cells transfected with siTRPM7 (Figure 3.18D). Protein level of cleaved caspase-8 in MDA-MB-231 cells transfected with siTRPM7 were significantly increased about 4-fold higher than it in cells transfected with scrambled siRNA at 5 ng/mL TRAIL. To further examine whether treatment of NS8593 affects protein levels of c-FLIP and cleaved caspase-8, Western blot analysis was carried out with MDA-MB-231 cells in the presence of NS8593 (Figure 3.20A). Similar to data obtained from *TRPM7* silencing, protein levels of both c-$FLIP_L$ and c-$FLIP_S$ were significantly reduced (Figures 3.20B and 3.20C) and protein level of cleaved caspase-8 in MDA-MB-231 cells treated with NS8593 was significantly increased approximately 4-fold higher than it in cells treated with DMSO at 5 ng/mL TRAIL (Figure 3.20D). In order to further investigate whether *TRPM7* gene silencing synergistically facilitates TRAIL-induced apoptosis during *c-FLIP* gene knockdown in MDA-MB-231 cells (Figures 3.21A and 3.21B),

I detected cleaved PARP via Western blot analysis (Figures 3.22A and 3.22B). Significant changes of cleaved PARP were not observed when double knockdowns of *TRPM7* and *c-FLIP* genes were carried out in the presence of TRAIL. These data show that suppression of TRPM7 channel activity by both siRNA-mediated gene silencing and pharmacological inhibition could reduce protein levels of c-FLIP$_L$ and c-FLIP$_S$ and activates caspase-8.

Figure 3.18. Silencing of *TRPM7* decreases protein level of c-FLIP and enhances caspase-8 activation. (A) Representative Western blots of c-FLIP and caspase-8 in MDA-MB-231 cells. MDA-MB-231 cells transfected with scrambled siRNA or siTRPM7 were incubated with different concentrations (1, 5, and 10 ng/mL) of recombinant TRAIL for 16 h. (B) Densitometric analysis of c-FLIPL. (C) Densitometric analysis of c-FLIPS. (D) Densitometric analysis of cleaved caspase-8 at 5 ng/mL TRAIL. All densitometry data were normalized to the intensity of β-actin bands.

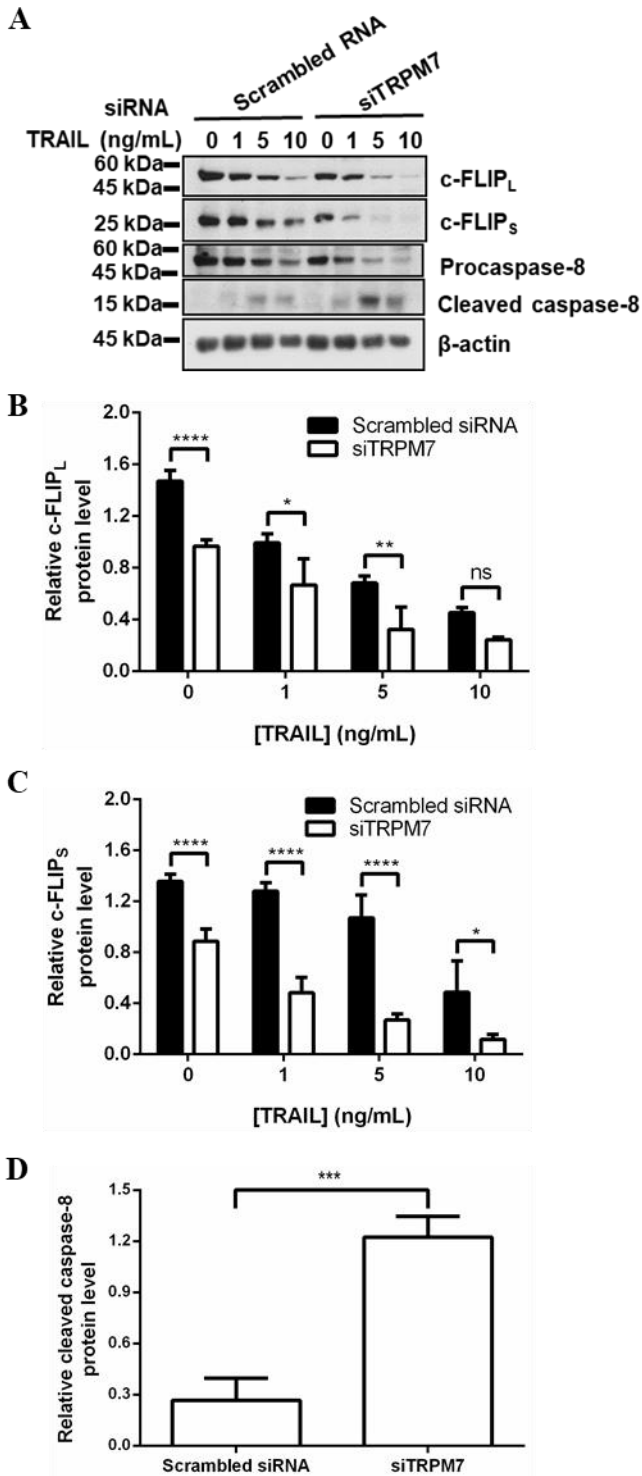
A
siRNA
Scrambled RNA
siTRPM7
TRAIL (ng/mL) 0 1 5 10 0 1 5 10
60 kDa
45 kDa
c-FLIPL
25 kDa
c-FLIPS
60 kDa
45 kDa
Procaspase-8
15 kDa
Cleaved caspase-8
45 kDa
β-actin
B
Relative c-FLIPL protein level
Scrambled siRNA
siTRPM7
****
*
**
ns
[TRAIL] (ng/mL)
C
Relative c-FLIPS protein level
Scrambled siRNA
siTRPM7
****
****
****
*
[TRAIL] (ng/mL)
D
Relative cleaved caspase-8 protein level
***
Scrambled siRNA
siTRPM7

Figure 3.19. Silencing of *TRPM7* do not affect mRNA levels in both c-FLIP$_L$ and c-FLIP$_S$. (A) Representative RT-PCR gels. MDA-MB-231 cells were transfected with scrambled siRNA as a negative control or siTRPM7. (B) Densitometric analysis of RT-PCR data obtained from (A). All densitometry data were normalized to the intensity of β-actin bands. The RT-PCR experiments were performed by Ms. Choi, Seunghye (KU-KIST Graduate School of Converging Science and Technology, Korea University, Republic of Korea).

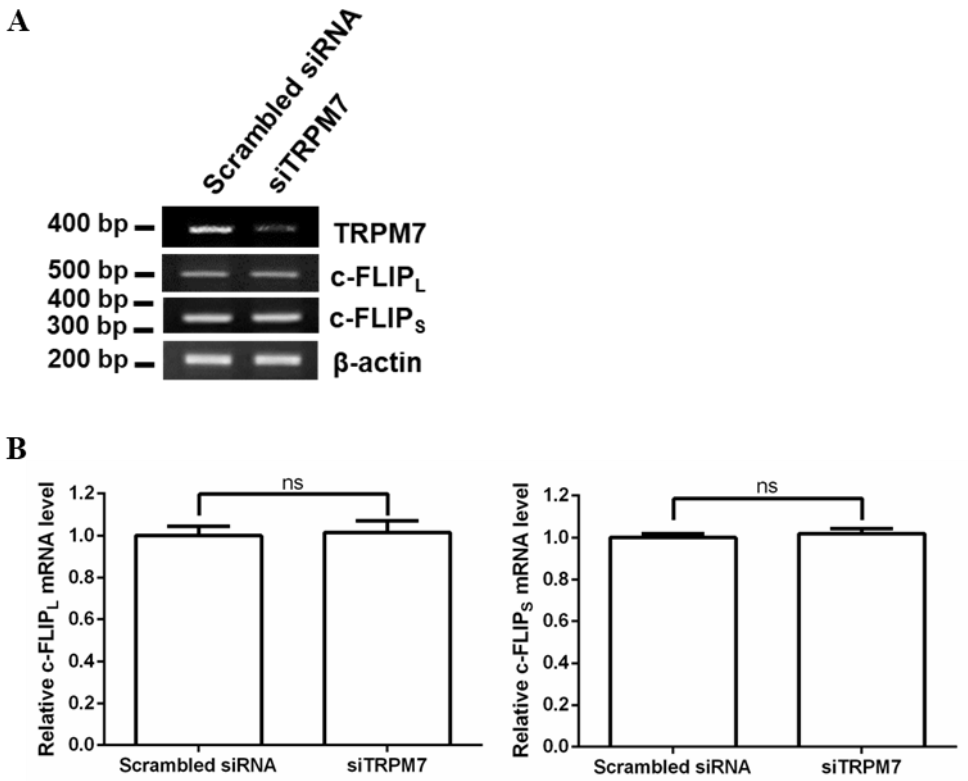
A
Scrambled siRNA
siTRPM7
400 bp
TRPM7
500 bp
c-FLIPL
400 bp
300 bp
c-FLIPS
200 bp
β-actin
B
Relative c-FLIPL mRNA level
1.2
1.0
0.8
0.6
0.4
0.2
0.0
ns
Scrambled siRNA
siTRPM7
Relative c-FLIPS mRNA level
1.2
1.0
0.8
0.6
0.4
0.2
0.0
ns
Scrambled siRNA
siTRPM7

Figure 3.20. NS8593 decreases protein level of c-FLIP and enhances caspase-8 activation. (A) Representative Western blots of c-FLIP and caspase-8 in MDA-MB-231 cells. MDA-MB-231 cells were incubated with 10 μM NS8593 in the presence of different concentrations (1, 5, and 10 ng/mL) of recombinant TRAIL. (B) Densitometric analysis of c-$FLIP_L$. (C) Densitometric analysis of c-$FLIP_S$. (D) Densitometric analysis of cleaved caspase-8 at 5 ng/mL TRAIL. All densitometry data were normalized to the intensity of β-actin bands.

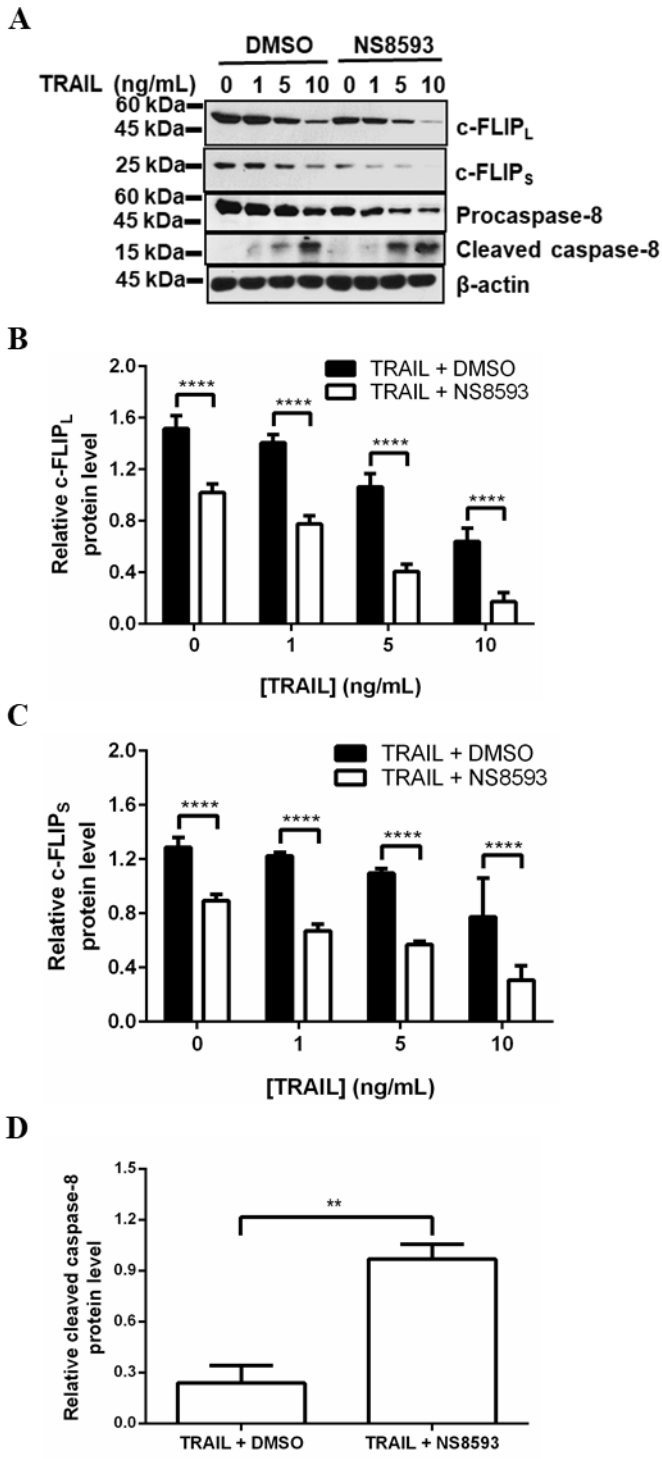
A
DMSO
NS8593
TRAIL (ng/mL) 0 1 5 10 0 1 5 10
60 kDa
45 kDa
c-FLIP$_L$
25 kDa
c-FLIP$_S$
60 kDa
45 kDa
Procaspase-8
15 kDa
Cleaved caspase-8
45 kDa
β-actin
B
TRAIL + DMSO
TRAIL + NS8593
Relative c-FLIP$_L$ protein level
2.0
1.6
1.2
0.8
0.4
0.0
****
0
1
5
10
[TRAIL] (ng/mL)
C
TRAIL + DMSO
TRAIL + NS8593
Relative c-FLIP$_S$ protein level
2.0
1.6
1.2
0.8
0.4
0.0
****
0
1
5
10
[TRAIL] (ng/mL)
D
Relative cleaved caspase-8 protein level
1.5
1.2
0.9
0.6
0.3
0.0
**
TRAIL + DMSO
TRAIL + NS8593

Figure 3.21. Silencing of *c-FLIP* in MDA-MB-231 cells. (A) Representative RT-PCR gels (up) and densitometric analysis (bottom). (B) Representative Western blots (up) and densitometric analysis (bottom). All densitometry data were normalized to the intensity of β-actin bands. The RT-PCR and Western blot experiments were performed by Ms. Choi, Seunghye (KU-KIST Graduate School of Converging Science and Technology, Korea University, Republic of Korea).

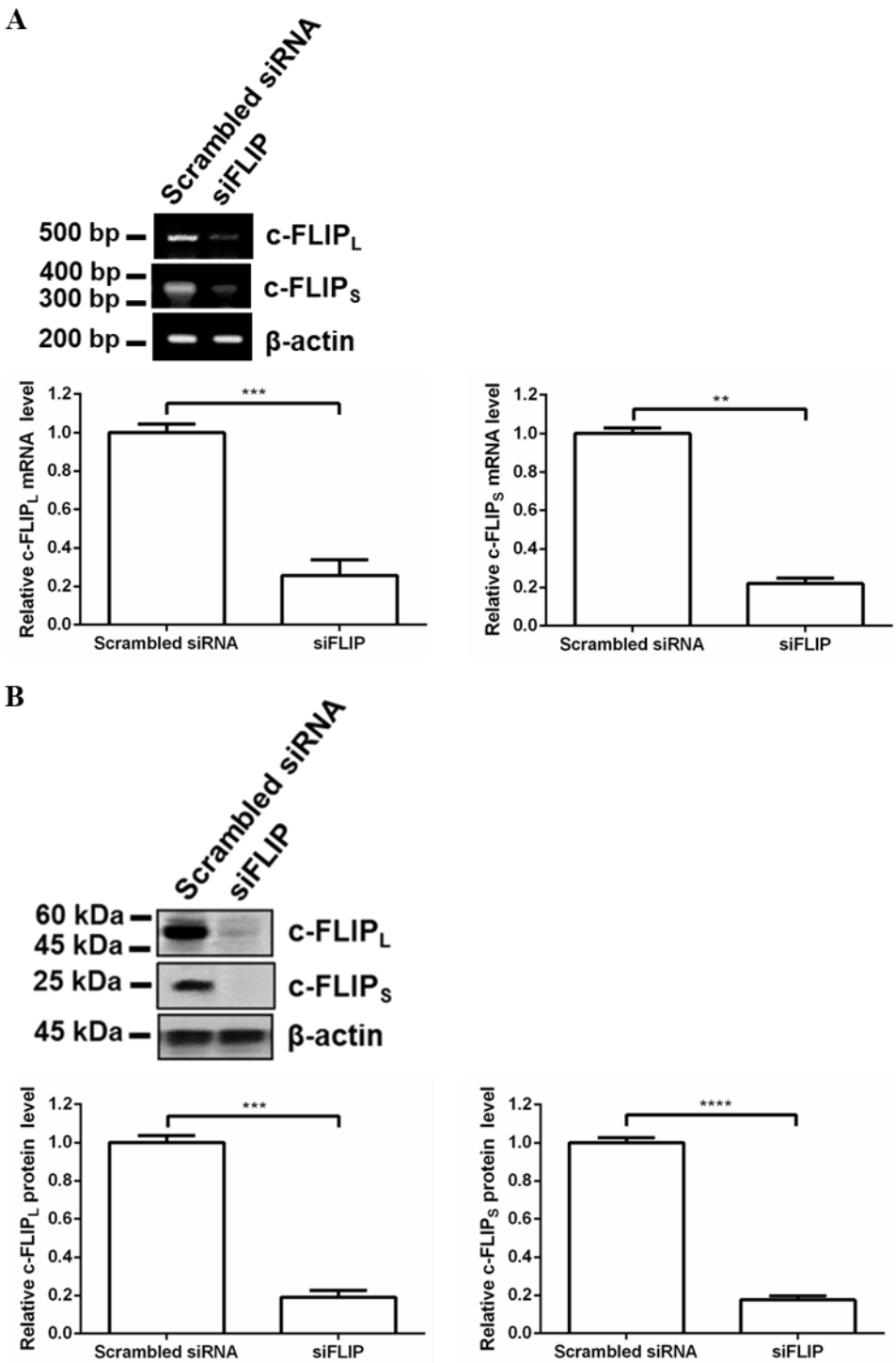
A
Scrambled siRNA
siFLIP
500 bp
400 bp
300 bp
200 bp
c-FLIPL
c-FLIPS
β-actin
Relative c-FLIPL mRNA level
Relative c-FLIPS mRNA level
***
**
Scrambled siRNA
siFLIP
B
60 kDa
45 kDa
25 kDa
45 kDa
Relative c-FLIPL protein level
Relative c-FLIPS protein level
****

Figure 3.22. Silencing of *TRPM7* do not promotes TRAIL-induced apoptosis under siRNA-mediated knockdown of *c-FLIP* in MDA-MB-231 cells. (A) Representative Western blots for cleaved PARP in MDA-MB-231 cells. MDA-MB-231 cells transfected with scrambled siRNA, siTRPM7, siFLIP, and siTRPM7/siFLIP were incubated with 10 ng/mL TRAIL for 16 h. (B) Densitometric analysis of cleaved PARP. All densitometry data were normalized to the intensity of β-actin bands. The Western blot experiments were performed by Ms. Choi, Seunghye (KU-KIST Graduate School of Converging Science and Technology, Korea University, Republic of Korea).

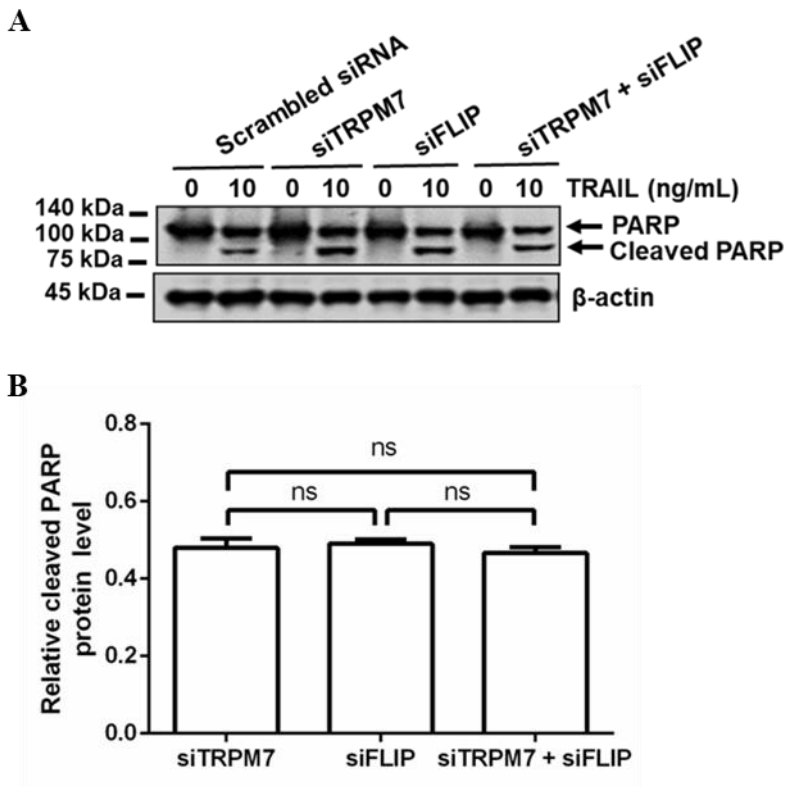
A
Scrambled siRNA
siTRPM7
siFLIP
siTRPM7 + siFLIP
0 10 0 10 0 10 0 10 TRAIL (ng/mL)
140 kDa
100 kDa
75 kDa
45 kDa
PARP
Cleaved PARP
β-actin
B
Relative cleaved PARP protein level
0.8
0.6
0.4
0.2
0.0
ns
ns
ns
siTRPM7
siFLIP
siTRPM7 + siFLIP

Discussion

TRPM7 has been shown to be involved in breast cancer cell proliferation, migration and metastasis (Guilbert et al., 2009; Middelbeek et al., 2012; Guilbert et al., 2013; Meng et al., 2013; Davis et al., 2014). However, *TRPM7* knockdown does not affect proliferation of TNBC cells such as MDA-MB-231 cells, while it decreases migration and invasion of them (Guilbert et al., 2013; Meng et al., 2013; Song et al., 2017). If I find specific substances which enable suppression of TRPM7 to affect proliferation of TNBC cells, TRPM7 inhibition will be beneficial to decrease in both proliferation and metastasis of TNBC.

Inhibition of TRPM7 by non-selective TRPM7 channel inhibitors such as 2-APB and Gd^{3+} increases TRAIL-induced apoptosis in HSC-T6 cells via reduction in both TRPM7 mRNA and protein (Liu et al., 2012). Like this report, Lin *et. al*. have also showed that inhibition of TRPM7 by 2-APB or Gd^{3+} increases TRAIL-induced apoptosis in PC-3 cells through inhibition of *TRPM7* expression (Lin et al., 2015). Based on these two reports, I hypothesized that suppression of TRPM7 could enhances TRAIL-induced antiproliferative effects and apoptosis in TNBC cells such as MDA-MB-231 and MDA-MB-468 cells. Expectedly, *TRPM7* knockdown increased both antiproliferative effects and apoptosis of TNBC cells in the presence of recombinant TRAIL. However, it did not affect both of them in cells in the absence of it, which was coincided with the previous study (Guilbert et al., 2013). Although two pharmacological studies have shown that inhibition of TRPM7 channel activities are involved in TRAIL-induced apoptosis in HSC-T6 and PC-3 cells, additional pharmacological approach is needed to clarify the involvement of each TRPM7 domain in it, because the previous studies have been performed only with non-selective TRPM7 channel inhibitors (Liu et al., 2012; Lin et al., 2015). In this study, two compounds (NS8593 (Chubanov et al., 2012) and TG100-115 (Song et al., 2017)) selectively targeting a TRPM7 channel and a TRPM7 kinase domain, respectively, were used to examine which domain of TRPM7 is involved in TRAIL-induced antiproliferative effects and apoptosis, and to investigate whether suppression of

TRPM7 by pharmacological approach can also increase both of them. Treatment of NS8593 synergistically increased TRAIL-induced antiproliferative effects and apoptosis, but treatment of TG100-115 did not. Furthermore, NS8593 dramatically inhibited colony formation of MDA-MB-231 cells. These results imply that TRPM7 channel activities might be associated with synergistic interaction of TRPM7 and TRAIL in apoptosis, which was coincided with the previous studies (Liu et al., 2012; Lin et al., 2015). However, the possibilities that TRPM7 kinase activities might be involved in the synergistic interaction should not be ignored due to lack of genetic approach regarding to a TRPM7 kinase domain.

TRPM7 channels are mostly permeable to divalent cations such as Ca^{2+}, which is involved in signaling pathway of apoptosis (Nadler et al., 2001; Runnels et al., 2001; Aarts et al., 2003; Monteilh-Zoller et al., 2003; Asrar and Aarts, 2013; Varghese et al., 2019). Ca^{2+} plays an important role in mitochondria-mediated apoptosis and Ca^{2+} dysregulation can induce endoplasmic reticulum-mediated apoptosis (Bahar et al., 2016; Varghese et al., 2019). There are some drugs inducing apoptosis via interference of calcium homeostasis in TNBC cells (Pan et al., 2014; Berzingi et al., 2016; Abdoul-Azize et al., 2018). For instance, doxorubicin (a DNA intercalator) and paclitaxel (a microtubule inhibitor) has been shown to induce apoptosis of MDA-MB-231 cells through elevation of intracellular [Ca^{2+}], and verapamil (a T-type calcium channel blocker) also has been reported to induce apoptosis of MDA-MB-231 cells (Pan et al., 2014; Berzingi et al., 2016; Abdoul-Azize et al., 2018). I investigated the hypothesis that reduction in intracellular [Ca^{2+}] via suppression of TRPM7 channel activity might be able to promote TRAIL-induced apoptosis. Expectedly, treatment of BAPTA-AM as a cell permeable Ca^{2+} chelator dramatically attenuated the synergistic effect of NS8593 and recombinant TRAIL, suggesting that Ca^{2+} might play a critical role in the synergistic interaction. Like a previous study (O'Grady and Morgan, 2019), I also confirmed that NS8593 significantly decreased intracellular [Ca^{2+}] in MDA-MB-231 cells.

c-$FLIP_L$ and c-$FLIP_S$ have been reported that they inhibit caspase-8 activation in

apoptosis, resulting in suppression of apoptosis (Krueger et al., 2001; Sharp et al., 2005). Pawar et al. have shown that Ca^{2+}–dependent interaction between c-$FLIP_L$ with calmodulin inhibits Fas-induced apoptosis (Pawar et al., 2008). Inhibition of interaction of Ca^{2+} with calmodulin by treatment of BAPTA-AM decreases protein levels of c-FLIP, and facilitates activation of caspase-8 in the presence of TRAIL, resulting in reduction of cell survival (Kaminskyy et al., 2013). Similar to the above previous reports, reduction of c-FLIP was observed when TRPM7 channel activities were suppressed by *TRPM7* knockdown or treatment of NS8593 and elevation of cleaved caspase-8 also was detected in the presence of TRAIL. Although protein levels of c-$FLIP_L$ and c-$FLIP_S$ were reduced by approximately 30% via *TRPM7* knockdown or treatment of NS8593 in the absence of TRAIL, the reduction of c-FLIP without TRAIL did not dramatically affect the proliferation and apoptosis of MDA-MB-231 cells. These findings could be explained by the previous report which has been shown that *c-FLIP* knockdown (more than 70% decrease in protein expression) decreases viability of breast cancer cells including MDA-MB-231 cells by only approximately 10 to 15% (Piggott et al., 2011). In addition, I found that the changes of c-$FLIP_S$ at low concentrations (1 and 5 ng/mL) of TRAIL was higher than them of c-$FLIP_L$. The findings might imply that c-$FLIP_S$ can play a critical role in the synergistic interaction. c-$FLIP_S$ has been reported that its protein level was regulated by ubiquitin-proteasome degradation system and JNK activation via E3 ubiquitin ligase Itch (Poukkula et al., 2005; Chang et al., 2006; Safa, 2012). Further investigations would be required to reveal the mechanisms of the synergistic interaction regarding to c-$FLIP_S$.

In summary, I demonstrated that suppression of TRPM7 synergistically increases TRAIL-induced antiproliferative effects and apoptosis in TNBC cells. Furthermore, I revealed that the synergistic interaction might be associated with TRPM7 channel activities, which modulate c-FLIP protein levels via probably inhibition of Ca^{2+} influx (Figure 3.23). The present study would provide potential combinatorial therapeutic strategy using TRPM7 inhibitors with TRAIL in treatment of TNBC.

Figure 3.23. Proposed mechanisms of cell death induced by suppression of TRPM7 with TRAIL. The combination of TRAIL and inhibition of TRPM7 channel activity via either RNA interference or NS8593 treatment promotes apoptosis of TNBC cells through reduction in Ca^{2+} influx and c-FLIP.

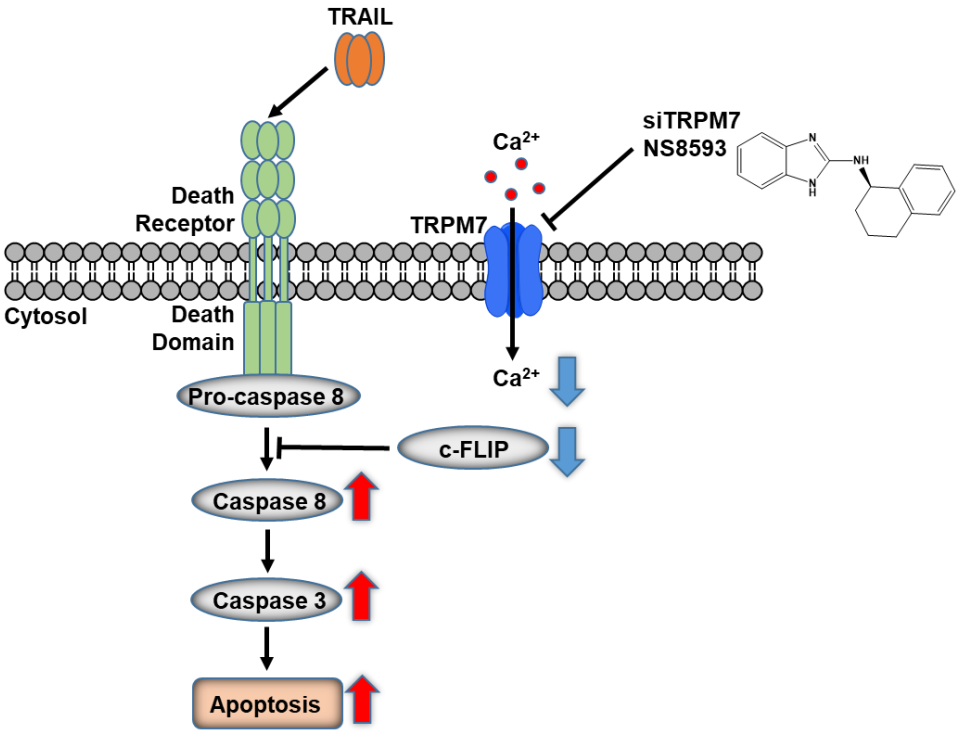
TRAIL
Death
Receptor
Cytosol
Death
Domain
Ca2+
siTRPM7
NS8593
TRPM7
Ca2+
Pro-caspase 8
c-FLIP
Caspase 8
Caspase 3
Apoptosis
N
NH
N
H

References

Aarts, M., Iihara, K., Wei, W. L., Xiong, Z. G., Arundine, M., Cerwinski, W., . . . Tymianski, M. (2003). A key role for TRPM7 channels in anoxic neuronal death. *Cell, 115*(7), 863-877.

Abdoul-Azize, S., Buquet, C., Li, H., Picquenot, J. M., & Vannier, J. P. (2018). Integration of Ca^{2+} signaling regulates the breast tumor cell response to simvastatin and doxorubicin. *Oncogene, 37*(36), 4979-4993.

Ades, F., Zardavas, D., Bozovic-Spasojevic, I., Pugliano, L., Fumagalli, D., de Azambuja, E., . . . Piccart, M. (2014). Luminal B breast cancer: molecular characterization, clinical management, and future perspectives. *J Clin Oncol, 32*(25), 2794-2803.

Alladina, S. J., Song, J. H., Davidge, S. T., Hao, C., & Easton, A. S. (2005). TRAIL-induced apoptosis in human vascular endothelium is regulated by phosphatidylinositol 3-kinase/Akt through the short form of cellular FLIP and Bcl-2. *J Vasc Res, 42*(4), 337-347.

Ashkenazi, A., Pai, R. C., Fong, S., Leung, S., Lawrence, D. A., Marsters, S. A., . . . Schwall, R. H. (1999). Safety and antitumor activity of recombinant soluble Apo2 ligand. *J Clin Invest, 104*(2), 155-162.

Asrar, S., & Aarts, M. (2013). TRPM7, the cytoskeleton and neuronal death. *Channels (Austin), 7*(1), 6-16.

Atezolizumab Combo Approved for PD-L1-positive TNBC. (2019). *Cancer Discov, 9*(5), OF2.

Bahar, E., Kim, H., & Yoon, H. (2016). ER Stress-Mediated Signaling: Action Potential and Ca^{2+} as Key Players. *Int J Mol Sci, 17*(9), 1558.

Bardia, A., Mayer, I. A., Vahdat, L. T., Tolaney, S. M., Isakoff, S. J., Diamond, J. R., . . . Kalinsky, K. (2019). Sacituzumab Govitecan-hziy in Refractory Metastatic Triple-Negative Breast Cancer. *N Engl J Med, 380*(8), 741-751.

Baselga, J., Gomez, P., Greil, R., Braga, S., Climent, M. A., Wardley, A. M., . . . Awada, A. (2013). Randomized phase II study of the anti-epidermal growth factor receptor monoclonal antibody cetuximab with cisplatin versus cisplatin alone in patients with metastatic triple-negative breast cancer. *J Clin Oncol, 31*(20), 2586-2592.

Berzingi, S., Newman, M., & Yu, H. G. (2016). Altering bioelectricit

y on inhibition of human breast cancer cells. *Cancer Cell Int, 16*, 72.

Bryant, H. E., Schultz, N., Thomas, H. D., Parker, K. M., Flower, D., Lopez, E., . . . Helleday, T. (2005). Specific killing of BR CA2-deficient tumours with inhibitors of poly(ADP-ribose) poly merase. *Nature, 434*(7035), 913-917.

Carey, L. A., Rugo, H. S., Marcom, P. K., Mayer, E. L., Esteva, F. J., Ma, C. X., . . . Winer, E. P. (2012). TBCRC 001: randomi zed phase II study of cetuximab in combination with carboplati n in stage IV triple-negative breast cancer. *J Clin Oncol, 30*(2 1), 2615-2623.

Castillo, B., Porzgen, P., Penner, R., Horgen, F. D., & Fleig, A. (201 0). Development and optimization of a high-throughput bioassay for TRPM7 ion channel inhibitors. *J Biomol Screen, 15*(5), 49 8-507.

Chang, L., Kamata, H., Solinas, G., Luo, J. L., Maeda, S., Venuprasa d, K., . . . Karin, M. (2006). The E3 ubiquitin ligase itch cou ples JNK activation to TNFalpha-induced cell death by inducin g c-FLIP(L) turnover. *Cell, 124*(3), 601-613.

Chen, H. C., Xie, J., Zhang, Z., Su, L. T., Yue, L., & Runnels, L. W. (2010). Blockade of TRPM7 channel activity and cell death by inhibitors of 5-lipoxygenase. *PLoS One, 5*(6), e11161.

Chen, J. P., Luan, Y., You, C. X., Chen, X. H., Luo, R. C., & Li, R. (2010). TRPM7 regulates the migration of human nasophary ngeal carcinoma cell by mediating Ca^{2+} influx. *Cell Calcium, 4 7*(5), 425-432.

Chen, W. L., Barszczyk, A., Turlova, E., Deurloo, M., Liu, B., Yang, B. B., . . . Sun, H. S. (2015). Inhibition of TRPM7 by carva crol suppresses glioblastoma cell proliferation, migration and in vasion. *Oncotarget, 6*(18), 16321-16340.

Chen, X., Numata, T., Li, M., Mori, Y., Orser, B. A., Jackson, M. F., . . . MacDonald, J. F. (2010). The modulation of TRPM7 currents by nafamostat mesilate depends directly upon extracell ular concentrations of divalent cations. *Mol Brain, 3*, 38.

Cheng, Y., & Prusoff, W. H. (1973). Relationship between the inhibiti on constant (K_I) and the concentration of inhibitor which cause s 50 percent inhibition (I_{50}) of an enzymatic reaction. *Biochem Pharmacol, 22*(23), 3099-3108.

Chou, T. C. (2010). Drug combination studies and their synergy quant ification using the Chou-Talalay method. *Cancer Res, 70*(2), 44 0-446.

Chou, T. C., & Talalay, P. (1984). Quantitative analysis of dose-effect relationships: the combined effects of multiple drugs or enzym e inhibitors. *Adv Enzyme Regul, 22*, 27-55.

Chubanov, V., Mederos y Schnitzler, M., Meissner, M., Schafer, S., A bstiens, K., Hofmann, T., & Gudermann, T. (2012). Natural an d synthetic modulators of SK ($K_{Ca}2$) potassium channels inhibit magnesium-dependent activity of the kinase-coupled cation cha nnel TRPM7. *Br J Pharmacol, 166*(4), 1357-1376.

Clark, K., Langeslag, M., van Leeuwen, B., Ran, L., Ryazanov, A. G., Figdor, C. G., . . . van Leeuwen, F. N. (2006). TRPM7, a novel regulator of actomyosin contractility and cell adhesion. *Embo j, 25*(2), 290-301.

Clark, K., Middelbeek, J., Lasonder, E., Dulyaninova, N. G., Morrice, N. A., Ryazanov, A. G., . . . van Leeuwen, F. N. (2008). TR PM7 regulates myosin IIA filament stability and protein localiz ation by heavy chain phosphorylation. *J Mol Biol, 378*(4), 790-803.

Corkery, B., Crown, J., Clynes, M., & O'Donovan, N. (2009). Epider mal growth factor receptor as a potential therapeutic target in t riple-negative breast cancer. *Ann Oncol, 20*(5), 862-867.

Cristofanon, S., & Fulda, S. (2012). ABT-737 promotes tBid mitochon drial accumulation to enhance TRAIL-induced apoptosis in glio blastoma cells. *Cell Death Dis, 3*, e432.

Davis, F. M., Azimi, I., Faville, R. A., Peters, A. A., Jalink, K., Putn ey, J. W., Jr., . . . Monteith, G. R. (2014). Induction of epithe lial-mesenchymal transition (EMT) in breast cancer cells is calc ium signal dependent. *Oncogene, 33*(18), 2307-2316.

Day, T. W., Huang, S., & Safa, A. R. (2008). c-FLIP knockdown ind uces ligand-independent DR5-, FADD-, caspase-8-, and caspase-9-dependent apoptosis in breast cancer cells. *Biochem Pharmac ol, 76*(12), 1694-1704.

De Vos, M., Schreiber, V., & Dantzer, F. (2012). The diverse roles a nd clinical relevance of PARPs in DNA damage repair: current state of the art. *Biochem Pharmacol, 84*(2), 137-146.

Dent, R., Hanna, W. M., Trudeau, M., Rawlinson, E., Sun, P., & Nar od, S. A. (2009). Pattern of metastatic spread in triple-negative breast cancer. *Breast Cancer Res Treat, 115*(2), 423-428.

Devkota, A. K., Tavares, C. D., Warthaka, M., Abramczyk, O., Marsh all, K. D., Kaoud, T. S., . . . Dalby, K. N. (2012). Investigati ng the kinetic mechanism of inhibition of elongation factor 2 k inase by NH125: evidence of a common in vitro artifact. *Bioch*

emistry, 51(10), 2100-2112.

Dhennin-Duthille, I., Gautier, M., Faouzi, M., Guilbert, A., Brevet, M., Vaudry, D., . . . Ouadid-Ahidouch, H. (2011). High expression of transient receptor potential channels in human breast cancer epithelial cells and tissues: correlation with pathological parameters. *Cell Physiol Biochem, 28*(5), 813-822.

Di, J., Huang, H., Qu, D., Tang, J., Cao, W., Lu, Z., . . . Zheng, J. (2015). Rap2B promotes proliferation, migration, and invasion of human breast cancer through calcium-related ERK1/2 signaling pathway. *Sci Rep, 5*, 12363.

Diana, A., Franzese, E., Centonze, S., Carlino, F., Della Corte, C. M., Ventriglia, J., . . . Orditura, M. (2018). Triple-Negative Breast Cancers: Systematic Review of the Literature on Molecular and Clinical Features with a Focus on Treatment with Innovative Drugs. *Curr Oncol Rep, 20*(10), 76.

Dorovkov, M. V., Beznosov, S. N., Shah, S., Kotlyanskaya, L., & Kostyukova, A. S. (2009). Effect of mutations imitating the phosphorylation by TRPM7 kinase on the function of the N-terminal domain of tropomodulin. *Biophysics, 53*(6), 500-504.

Doukas, J., Wrasidlo, W., Noronha, G., Dneprovskaia, E., Fine, R., Weis, S., . . . Cheresh, D. (2006). Phosphoinositide 3-kinase γ/δ inhibition limits infarct size after myocardial ischemia/reperfusion injury. *Proc Natl Acad Sci U S A, 103*(52), 19866-19871.

Dufour, F., Rattier, T., Constantinescu, A. A., Zischler, L., Morle, A., Ben Mabrouk, H., . . . Micheau, O. (2017). TRAIL receptor gene editing unveils TRAIL-R1 as a master player of apoptosis induced by TRAIL and ER stress. *Oncotarget, 8*(6), 9974-9985.

Eroles, P., Bosch, A., Perez-Fidalgo, J. A., & Lluch, A. (2012). Molecular biology in breast cancer: intrinsic subtypes and signaling pathways. *Cancer Treat Rev, 38*(6), 698-707.

Exman, P., Barroso-Sousa, R., & Tolaney, S. M. (2019). Evidence to date: talazoparib in the treatment of breast cancer. *Onco Targets Ther, 12*, 5177-5187.

Farmer, H., McCabe, N., Lord, C. J., Tutt, A. N., Johnson, D. A., Richardson, T. B., . . . Ashworth, A. (2005). Targeting the DNA repair defect in BRCA mutant cells as a therapeutic strategy. *Nature, 434*(7035), 917-921.

Foulkes, W. D., Smith, I. E., & Reis-Filho, J. S. (2010). Triple-negative breast cancer. *N Engl J Med, 363*(20), 1938-1948.

Gschwendt, M., Muller, H. J., Kielbassa, K., Zang, R., Kittstein, W., Rincke, G., & Marks, F. (1994). Rottlerin, a novel protein kina

se inhibitor. *Biochem Biophys Res Commun, 199*(1), 93-98.
Guilbert, A., Gautier, M., Dhennin-Duthille, I., Haren, N., Sevestre, H., & Ouadid-Ahidouch, H. (2009). Evidence that TRPM7 is required for breast cancer cell proliferation. *Am J Physiol Cell Physiol, 297*(3), C493-502.
Guilbert, A., Gautier, M., Dhennin-Duthille, I., Rybarczyk, P., Sahni, J., Sevestre, H., . . . Ouadid-Ahidouch, H. (2013). Transient receptor potential melastatin 7 is involved in oestrogen receptor-negative metastatic breast cancer cells migration through its kinase domain. *Eur J Cancer, 49*(17), 3694-3707.
Hanano, T., Hara, Y., Shi, J., Morita, H., Umebayashi, C., Mori, E., . . . Inoue, R. (2004). Involvement of TRPM7 in cell growth as a spontaneously activated Ca^{2+} entry pathway in human retinoblastoma cells. *J Pharmacol Sci, 95*(4), 403-419.
Helleday, T. (2011). The underlying mechanism for the PARP and BRCA synthetic lethality: clearing up the misunderstandings. *Mol Oncol, 5*(4), 387-393.
Herbst, R. S., Eckhardt, S. G., Kurzrock, R., Ebbinghaus, S., O'Dwyer, P. J., Gordon, M. S., . . . Mendelson, D. S. (2010). Phase I dose-escalation study of recombinant human Apo2L/TRAIL, a dual proapoptotic receptor agonist, in patients with advanced cancer. *J Clin Oncol, 28*(17), 2839-2846.
Hwang, S. Y., Park, S., & Kwon, Y. (2019). Recent therapeutic trends and promising targets in triple negative breast cancer. *Pharmacol Ther, 199*, 30-57.
Ikeda, H., Hideshima, T., Fulciniti, M., Perrone, G., Miura, N., Yasui, H., . . . Anderson, K. C. (2010). PI3K/p110{delta} is a novel therapeutic target in multiple myeloma. *Blood, 116*(9), 1460-1468.
Jiang, J., Li, M. H., Inoue, K., Chu, X. P., Seeds, J., & Xiong, Z. G. (2007). Transient receptor potential melastatin 7-like current in human head and neck carcinoma cells: role in cell proliferation. *Cancer Res, 67*(22), 10929-10938.
Kaitsuka, T., Katagiri, C., Beesetty, P., Nakamura, K., Hourani, S., Tomizawa, K., . . . Matsushita, M. (2014). Inactivation of TRPM7 kinase activity does not impair its channel function in mice. *Sci Rep, 4*, 5718.
Kaminskyy, V. O., Surova, O. V., Piskunova, T., Zborovskaya, I. B., Tchevkina, E. M., Andera, L., & Zhivotovsky, B. (2013). Upregulation of c-FLIP-short in response to TRAIL promotes survival of NSCLC cells, which could be suppressed by inhibition of

Ca^{2+}/calmodulin signaling. *Cell Death Dis, 4*, e522.
Kim, B. J. (2013). Involvement of melastatin type transient receptor p otential 7 channels in ginsenoside Rd-induced apoptosis in gastr ic and breast cancer cells. *J Ginseng Res, 37*(2), 201-209.
Kim, B. J., Nah, S. Y., Jeon, J. H., So, I., & Kim, S. J. (2011). Tra nsient receptor potential melastatin 7 channels are involved in ginsenoside Rg3-induced apoptosis in gastric cancer cells. *Basic Clin Pharmacol Toxicol, 109*(4), 233-239.
Kim, B. J., Nam, J. H., Kwon, Y. K., So, I., & Kim, S. J. (2013). T he role of waixenicin A as transient receptor potential melastati n 7 blocker. *Basic Clin Pharmacol Toxicol, 112*(2), 83-89.
Kim, B. J., Park, E. J., Lee, J. H., Jeon, J. H., Kim, S. J., & So, I. (2008). Suppression of transient receptor potential melastatin 7 channel induces cell death in gastric cancer. *Cancer Sci, 99*(1 2), 2502-2509.
Knight, Z. A., Gonzalez, B., Feldman, M. E., Zunder, E. R., Goldenb erg, D. D., Williams, O., . . . Shokat, K. M. (2006). A pharm acological map of the PI3-K family defines a role for p110α i n insulin signaling. *Cell, 125*(4), 733-747.
Kozak, J. A., Kerschbaum, H. H., & Cahalan, M. D. (2002). Distinct properties of CRAC and MIC channels in RBL cells. *J Gen P hysiol, 120*(2), 221-235.
Kozak, J. A., Matsushita, M., Nairn, A. C., & Cahalan, M. D. (200 5). Charge screening by internal pH and polyvalent cations as a mechanism for activation, inhibition, and rundown of TRPM7 /MIC channels. *J Gen Physiol, 126*(5), 499-514.
Krueger, A., Schmitz, I., Baumann, S., Krammer, P. H., & Kirchhoff, S. (2001). Cellular FLICE-inhibitory protein splice variants inhi bit different steps of caspase-8 activation at the CD95 death-in ducing signaling complex. *J Biol Chem, 276*(23), 20633-20640.
Lemke, J., von Karstedt, S., Zinngrebe, J., & Walczak, H. (2014). Ge tting TRAIL back on track for cancer therapy. *Cell Death Diff er, 21*(9), 1350-1364.
Li, M., Jiang, J., & Yue, L. (2006). Functional characterization of ho mo- and heteromeric channel kinases TRPM6 and TRPM7. *J G en Physiol, 127*(5), 525-537.
Lin, C. J., Lin, C. Y., Chen, Y., Huang, S. H., & Wang, S. M. (201 0). Rottlerin inhibits migration of follicular thyroid carcinoma c ells by PKCδ-independent destabilization of the focal adhesion complex. *J Cell Biochem, 110*(2), 428-437.
Lin, C. M., Ma, J. M., Zhang, L., Hao, Z. Y., Zhou, J., Zhou, Z. Y.,

. . . Liang, C. Z. (2015). Inhibition of Transient Receptor Pot ential Melastain 7 Enhances Apoptosis Induced by TRAIL in P C-3 cells. *Asian Pac J Cancer Prev, 16*(10), 4469-4475.

Liu, H., Li, J., Huang, Y., & Huang, C. (2012). Inhibition of transien t receptor potential melastain 7 channel increases HSCs apoptos is induced by TRAIL. *Life Sci, 90*(15-16), 612-618.

Lu, W., Lin, C., & Li, Y. (2014). Rottlerin induces Wnt co-receptor LRP6 degradation and suppresses both Wnt/β-catenin and mTO RC1 signaling in prostate and breast cancer cells. *Cell Signal, 26*(6), 1303-1309.

Luk, S. K., Piekorz, R. P., Nurnberg, B., & Tony To, S. S. (2012). The catalytic phosphoinositol 3-kinase isoform p110δ is require d for glioma cell migration and invasion. *Eur J Cancer, 48*(1), 149-157.

Ma, H., Deacon, S., & Horiuchi, K. (2008). The challenge of selectin g protein kinase assays for lead discovery optimization. *Expert opinion on drug discovery, 3*(6), 607-621.

MacFarlane, M. (2003). TRAIL-induced signalling and apoptosis. *Toxic ol Lett, 139*(2-3), 89-97.

Mackay, A., Weigelt, B., Grigoriadis, A., Kreike, B., Natrajan, R., A' Hern, R., . . . Reis-Filho, J. S. (2011). Microarray-based class discovery for molecular classification of breast cancer: analysis of interobserver agreement. *J Natl Cancer Inst, 103*(8), 662-673.

Matsushita, M., Kozak, J. A., Shimizu, Y., McLachlin, D. T., Yamagu chi, H., Wei, F. Y., . . . Nairn, A. C. (2005). Channel functio n is dissociated from the intrinsic kinase activity and autophosp horylation of TRPM7/ChaK1. *J Biol Chem, 280*(21), 20793-208 03.

Medina, M. A., Oza, G., Sharma, A., Arriaga, L. G., Hernandez Hern andez, J. M., Rotello, V. M., & Ramirez, J. T. (2020). Triple-Negative Breast Cancer: A Review of Conventional and Advan ced Therapeutic Strategies. *Int J Environ Res Public Health, 17* (6).

Meng, X., Cai, C., Wu, J., Cai, S., Ye, C., Chen, H., . . . Zou, F. (2013). TRPM7 mediates breast cancer cell migration and invas ion through the MAPK pathway. *Cancer Lett, 333*(1), 96-102.

Middelbeek, J., Kuipers, A. J., Henneman, L., Visser, D., Eidhof, I., van Horssen, R., . . . Jalink, K. (2012). TRPM7 is required fo r breast tumor cell metastasis. *Cancer Res, 72*(16), 4250-4261.

Monteilh-Zoller, M. K., Hermosura, M. C., Nadler, M. J., Scharenber g, A. M., Penner, R., & Fleig, A. (2003). TRPM7 provides an

ion channel mechanism for cellular entry of trace metal ions. *J Gen Physiol, 121*(1), 49-60.

Nadler, M. J., Hermosura, M. C., Inabe, K., Perraud, A. L., Zhu, Q., Stokes, A. J., . . . Fleig, A. (2001). LTRPC7 is a Mg.ATP-regulated divalent cation channel required for cell viability. *Nature, 411*(6837), 590-595.

Nakai, K., Hung, M. C., & Yamaguchi, H. (2016). A perspective on anti-EGFR therapies targeting triple-negative breast cancer. *Am J Cancer Res, 6*(8), 1609-1623.

Noordermeer, S. M., & van Attikum, H. (2019). PARP Inhibitor Resistance: A Tug-of-War in BRCA-Mutated Cells. *Trends Cell Biol, 29*(10), 820-834.

O'Grady, S., & Morgan, M. P. (2019). Deposition of calcium in an in vitro model of human breast tumour calcification reveals functional role for ALP activity, altered expression of osteogenic genes and dysregulation of the TRPM7 ion channel. *Sci Rep, 9*(1), 542.

Pan, Z., Avila, A., & Gollahon, L. (2014). Paclitaxel induces apoptosis in breast cancer cells through different calcium--regulating mechanisms depending on external calcium conditions. *Int J Mol Sci, 15*(2), 2672-2694.

Parnas, M., Peters, M., Dadon, D., Lev, S., Vertkin, I., Slutsky, I., & Minke, B. (2009). Carvacrol is a novel inhibitor of Drosophila TRPL and mammalian TRPM7 channels. *Cell Calcium, 45*(3), 300-309.

Pawar, P. S., Micoli, K. J., Ding, H., Cook, W. J., Kappes, J. C., Chen, Y., & McDonald, J. M. (2008). Calmodulin binding to cellular FLICE-like inhibitory protein modulates Fas-induced signalling. *Biochem J, 412*(3), 459-468.

Piggott, L., Omidvar, N., Marti Perez, S., French, R., Eberl, M., & Clarkson, R. W. (2011). Suppression of apoptosis inhibitor c-FLIP selectively eliminates breast cancer stem cell activity in response to the anti-cancer agent, TRAIL. *Breast Cancer Res, 13*(5), R88.

Poukkula, M., Kaunisto, A., Hietakangas, V., Denessiouk, K., Katajamaki, T., Johnson, M. S., . . . Eriksson, J. E. (2005). Rapid turnover of c-FLIPshort is determined by its unique C-terminal tail. *J Biol Chem, 280*(29), 27345-27355.

Prakriya, M., & Lewis, R. S. (2002). Separation and characterization of currents through store-operated CRAC channels and Mg^{2+}-inhibited cation (MIC) channels. *J Gen Physiol, 119*(5), 487-507.

Qin, X., Yue, Z., Sun, B., Yang, W., Xie, J., Ni, E., . . . Yue, L. (2013). Sphingosine and FTY720 are potent inhibitors of the transient receptor potential melastatin 7 (TRPM7) channels. *Br J Pharmacol, 168*(6), 1294-1312.

Refaat, A., Abd-Rabou, A., & Reda, A. (2014). TRAIL combinations: The new 'trail' for cancer therapy (Review). *Oncol Lett, 7*(5), 1327-1332.

Ross, J. S., Slodkowska, E. A., Symmans, W. F., Pusztai, L., Ravdin, P. M., & Hortobagyi, G. N. (2009). The HER-2 receptor and breast cancer: ten years of targeted anti-HER-2 therapy and personalized medicine. *Oncologist, 14*(4), 320-368.

Runnels, L. W., Yue, L., & Clapham, D. E. (2001). TRP-PLIK, a bifunctional protein with kinase and ion channel activities. *Science, 291*(5506), 1043-1047.

Ryazanova, L. V., Dorovkov, M. V., Ansari, A., & Ryazanov, A. G. (2004). Characterization of the protein kinase activity of TRPM7/ChaK1, a protein kinase fused to the transient receptor potential ion channel. *J Biol Chem, 279*(5), 3708-3716.

Ryazanova, L. V., Hu, Z., Suzuki, S., Chubanov, V., Fleig, A., & Ryazanov, A. G. (2014). Elucidating the role of the TRPM7 alpha-kinase: TRPM7 kinase inactivation leads to magnesium deprivation resistance phenotype in mice. *Sci Rep, 4*, 7599.

Ryazanova, L. V., Rondon, L. J., Zierler, S., Hu, Z., Galli, J., Yamaguchi, T. P., . . . Ryazanov, A. G. (2010). TRPM7 is essential for Mg^{2+} homeostasis in mammals. *Nat Commun, 1*, 109.

Rybarczyk, P., Gautier, M., Hague, F., Dhennin-Duthille, I., Chatelain, D., Kerr-Conte, J., . . . Ouadid-Ahidouch, H. (2012). Transient receptor potential melastatin-related 7 channel is overexpressed in human pancreatic ductal adenocarcinomas and regulates human pancreatic cancer cell migration. *Int J Cancer, 131*(6), E851-861.

Safa, A. R. (2012). c-FLIP, a master anti-apoptotic regulator. *Exp Oncol, 34*(3), 176-184.

Sawhney, R. S., Liu, W., & Brattain, M. G. (2009). A novel role of ERK5 in integrin-mediated cell adhesion and motility in cancer cells via Fak signaling. *J Cell Physiol, 219*(1), 152-161.

Schmitz, C., Perraud, A. L., Johnson, C. O., Inabe, K., Smith, M. K., Penner, R., . . . Scharenberg, A. M. (2003). Regulation of vertebrate cellular Mg^{2+} homeostasis by TRPM7. *Cell, 114*(2), 191-200.

Schrödinger Release 2015-4, Schrödinger, LLC, New York, NY. (201

5).
Sergina, N. V., Rausch, M., Wang, D., Blair, J., Hann, B., Shokat, K. M., & Moasser, M. M. (2007). Escape from HER-family tyro sine kinase inhibitor therapy by the kinase-inactive HER3. *Natu re, 445*(7126), 437-441.
Sharp, D. A., Lawrence, D. A., & Ashkenazi, A. (2005). Selective kn ockdown of the long variant of cellular FLICE inhibitory protei n augments death receptor-mediated caspase-8 activation and ap optosis. *J Biol Chem, 280*(19), 19401-19409.
Shivakumar, D., Williams, J., Wu, Y., Damm, W., Shelley, J., & Sher man, W. (2010). Prediction of Absolute Solvation Free Energie s using Molecular Dynamics Free Energy Perturbation and the OPLS Force Field. *J Chem Theory Comput, 6*(5), 1509-1519.
Siegel, R. L., Miller, K. D., & Jemal, A. (2015). Cancer statistics, 20 15. *CA Cancer J Clin, 65*(1), 5-29.
Siegel, R. L., Miller, K. D., & Jemal, A. (2019). Cancer statistics, 20 19. *CA Cancer J Clin, 69*(1), 7-34.
Small-Molecule Drug Discovery Suite 2015-4: Glide, version 6.9, Schr ödinger, LLC, New York, NY. (2015).
Song, C., Bae, Y., Jun, J., Lee, H., Kim, N. D., Lee, K. B., . . . Si m, T. (2017). Identification of TG100-115 as a new and potent TRPM7 kinase inhibitor, which suppresses breast cancer cell migration and invasion. *Biochim Biophys Acta Gen Subj, 1861* (4), 947-957.
Stevens, K. N., Vachon, C. M., & Couch, F. J. (2013). Genetic susce ptibility to triple-negative breast cancer. *Cancer Res, 73*(7), 202 5-2030.
Su, L. T., Agapito, M. A., Li, M., Simonson, W. T., Huttenlocher, A., Habas, R., . . . Runnels, L. W. (2006). TRPM7 regulates c ell adhesion by controlling the calcium-dependent protease calpa in. *J Biol Chem, 281*(16), 11260-11270.
Sun, Y., Selvaraj, S., Varma, A., Derry, S., Sahmoun, A. E., & Sing h, B. B. (2013). Increase in serum Ca^{2+}/Mg^{2+} ratio promotes pr oliferation of prostate cancer cells by activating TRPM7 channe ls. *J Biol Chem, 288*(1), 255-263.
Swain, S. M., Kim, S.-B., Cortés, J., Ro, J., Semiglazov, V., Campon e, M., . . . Baselga, J. (2013). Pertuzumab, trastuzumab, and d ocetaxel for HER2-positive metastatic breast cancer (CLEOPAT RA study): overall survival results from a randomised, double-b lind, placebo-controlled, phase 3 study. *The Lancet Oncology, 1 4*(6), 461-471.

To, C., Kim, E. H., Royce, D. B., Williams, C. R., Collins, R. M., R isingsong, R., . . . Liby, K. T. (2014). The PARP inhibitors, v eliparib and olaparib, are effective chemopreventive agents for delaying mammary tumor development in BRCA1-deficient mic e. *Cancer Prev Res (Phila), 7*(7), 698-707.

Tsai, J. H., & Yang, J. (2013). Epithelial–mesenchymal plasticity in c arcinoma metastasis. *Genes & Development, 27*(20), 2192-2206.

Vagia, E., Mahalingam, D., & Cristofanilli, M. (2020). The Landscape of Targeted Therapies in TNBC. *Cancers (Basel), 12*(4).

Varghese, E., Samuel, S. M., Sadiq, Z., Kubatka, P., Liskova, A., Be nacka, J., . . . Busselberg, D. (2019). Anti-Cancer Agents in P roliferation and Cell Death: The Calcium Connection. *Int J Mo l Sci, 20*(12).

Wang, P., Zhang, J., Bellail, A., Jiang, W., Hugh, J., Kneteman, N. M., & Hao, C. (2007). Inhibition of RIP and c-FLIP enhances TRAIL-induced apoptosis in pancreatic cancer cells. *Cell Signa l, 19*(11), 2237-2246.

Wang, S., & El-Deiry, W. S. (2003). TRAIL and apoptosis induction by TNF-family death receptors. *Oncogene, 22*(53), 8628-8633.

Wei, C., Wang, X., Chen, M., Ouyang, K., Song, L. S., & Cheng, H. (2009). Calcium flickers steer cell migration. *Nature, 457*(723 1), 901-905.

Wirapati, P., Sotiriou, C., Kunkel, S., Farmer, P., Pradervand, S., Haib e-Kains, B., . . . Delorenzi, M. (2008). Meta-analysis of gene expression profiles in breast cancer: toward a unified understan ding of breast cancer subtyping and prognosis signatures. *Breas t Cancer Res, 10*(4), R65.

Wu, X., Baig, A., Kasymjanova, G., Kafi, K., Holcroft, C., Mekouar, H., . . . Muanza, T. (2016). Pattern of Local Recurrence and Distant Metastasis in Breast Cancer By Molecular Subtype. *Cur eus, 8*(12), e924.

Yamaguchi, H., Matsushita, M., Nairn, A. C., & Kuriyan, J. (2001). Crystal structure of the atypical protein kinase domain of a TR P channel with phosphotransferase activity. *Mol Cell, 7*(5), 104 7-1057.

Yang, S., Zhang, J. J., & Huang, X. Y. (2009). Orai1 and STIM1 are critical for breast tumor cell migration and metastasis. *Cancer Cell, 15*(2), 124-134.

Yee, N. S. (2017). Role of TRPM7 in Cancer: Potential as Molecular Biomarker and Therapeutic Target. *Pharmaceuticals (Basel), 10* (2).

Yee, N. S., Zhou, W., Lee, M., & Yee, R. K. (2012). Targeted silenc ing of TRPM7 ion channel induces replicative senescence and produces enhanced cytotoxicity with gemcitabine in pancreatic a denocarcinoma. *Cancer Lett, 318*(1), 99-105.

Yee, N. S., Zhou, W., & Liang, I. C. (2011). Transient receptor pote ntial ion channel Trpm7 regulates exocrine pancreatic epithelial proliferation by Mg^{2+}-sensitive Socs3a signaling in development and cancer. *Dis Model Mech, 4*(2), 240-254.

Zhang, Z., Yu, H., Huang, J., Faouzi, M., Schmitz, C., Penner, R., & Fleig, A. (2014). The TRPM6 kinase domain determines the M g.ATP sensitivity of TRPM7/M6 heteromeric ion channels. *J Bi ol Chem, 289*(8), 5217-5227.

Zhou, W., Feng, X., Han, H., Guo, S., & Wang, G. (2016). Synergist ic effects of combined treatment with histone deacetylase inhibi tor suberoylanilide hydroxamic acid and TRAIL on human brea st cancer cells. *Sci Rep, 6*, 28004.

Zierler, S., Yao, G., Zhang, Z., Kuo, W. C., Porzgen, P., Penner, R., . . . Fleig, A. (2011). Waixenicin A inhibits cell proliferation through magnesium-dependent block of transient receptor potent ial melastatin 7 (TRPM7) channels. *J Biol Chem, 286*(45), 393 28-39335.

Zou, Z. G., Rios, F. J., Montezano, A. C., & Touyz, R. M. (2019). TRPM7, Magnesium, and Signaling. *Int J Mol Sci, 20*(8).

Abstract in Korean

서울대학교 대학원

농생명공학부 응용생명화학전공

송치만

삼중음성유방암 (Triple negative breast cancer, TNBC)은 다른 subtype의 유방암에 비해 전이 및 재발률이 높기 때문에 가장 예후가 나쁜 유방암 subtype으로 여겨진다. 다른 유방암과는 달리, TNBC는 에스트로겐 수용체 (estrogen receptor), 프로게스테론 수용체 (progesterone receptor), human epidermal growth factor receptor 2 (HER2) 등의 수용체를 보유하지 않기 때문에 아직까지 효과적인 표적 치료제가 없다. Transient receptor potential cation channel subfamily M member 7 (TRPM7)은 ion channel domain과 kinase domain을 동시에 갖는 독특한 단백질로서, kinase domain의 기능을 통해 TNBC 세포 전이를 조절한다는 것이 알려져 있다. 현재까지 TRPM7 kinase domain의 저해제로서 NH125, rottlerin이 보고되어 있지만, 낮은 저해활성을 갖는다는 한계가 있다. 본 연구에서는 172종의 kinase 저해제 라이브러리에 대한 스크리닝을 통해 신규 TRPM7 kinase 저해제인 TG100-115 (IC_{50} = 1.07 μM)를 발굴하였다. Docking study와 ATP 농도 의존적 kinase 저해능을 통해, TG100-115가 TRPM7 kinase domain에 ATP 경쟁적으로 작용함을 밝혔다. Migration assay, invasion assay를 통해, TG100-115가 농도의존적으로 TNBC 세포인 MDA-MB-231, MDA-MB-468의 전이를 억제함을 관찰하였다. Western blot을 통해 TG100-115가

myosin IIA heavy chain과 focal adhesion kinase 인산화를 농도의존적으로 저해함을 확인하였다. TRPM7 과발현 T-REx-293 세포주와 MDA-MB-231 세포주에 대한 patch clamp 실험을 통해, TG100-115가 가역적으로 TRPM7 channel domain의 기능을 고농도 (53.60%inhibition at 100 μM)에서 농도의존적으로 저해함을 관찰하였다. 결과적으로, 기존보다 약 70배 이상 높은 저해활성을 갖는 신규 TRPM7 kinase 저해제인 TG100-115를 발굴하였고, TRPM7 kinase domain의 약리학적 저해를 통한 TNBC 세포 전이 억제 가능성을 확인하였다. TRPM7이 TNBC 세포 전이에 관여한다는 기존 연구들과는 달리, TRPM7은 TNBC 세포 성장에는 특별한 영향을 미치지 않는다고 알려져 있다. 그러나 본 연구에서는 RNA silencing을 통한 TRPM7의 저해를 통해, TNBC 세포에 대한 Tumor necrosis factor-related apoptosis-inducing ligand (TRAIL) 유도 세포 사멸이 강화되는 것을 관찰하였다. NS8593 (TRPM7 channel domain 저해제)과 TG100-115 (TRPM7 kinase domain 저해제)를 활용하여 TRAIL 유도 세포 사멸을 확인한 결과, TRPM7 kinase domain보다는 TRPM7 channel의 기능이 해당 현상에 관여함을 밝혔다. BAPTA-AM (Ca^{2+} chelator)의 처리를 통해, TRAIL 유도 세포 사멸에 대한 TRPM7 저해의 시너지 효과에 Ca^{2+}이 연관됨을 확인하였다. Ca^{2+}은 cellular FLICE-inhibitory protein (c-FLIP)의 발현수준을 조절함으로써 apoptosis에 관여한다고 보고되어 있는데, 본 연구에서는 Western blot을 통해 TRPM7의 약리학적/분자생물학적 기능 저해가 c-FLIP의 발현수준을 감소시키고, apoptosis의 대표적 marker인 caspase 8과 caspase 3을 활성화시킴을 확인하였다. 요약하면, TRPM7 channel의 약리학적 저해를 통해 TNBC 세포에 대한 TRAIL 유도 세포 사멸 효과를 강화시킬 수 있

음을 확인하였다. 결과적으로, 본 연구는 TRPM7의 kinase domain과 channel domain의 약리학적 저해를 통해, TNBC 세포의 전이능 억제 및 TRAIL 유도 세포 사멸 강화 가능성을 확인하였고, 해당 현상에 대한 작용기전을 규명하였다.

주요어: TRPM7, 삼중음성유방암, TG100-115, c-FLIP, TRAIL, 암전이, 아폽토시스

학번: 2014-30385